The Roles of Viral and Host Proteins in Influenza A Virus Assembly and Budding in Infected Cells

By

Sukhmani Kaur Bedi

A dissertation submitted in partial fulfillment
of the requirements for the degree of
Doctor of Philosophy
(Microbiology and Immunology)
in the University of Michigan
2019

Doctoral Committee:

Professor Akira Ono, Chair
Associate Professor Adam Lauring
Professor Bethany Moore
Professor Joel Swanson
Associate Professor Andrew Tai

Sukhmani K. Bedi

sukhbedi@umich.edu

ORCID iD: 0000-0002-4316-1774

Acknowledgements

This work would not have been possible without the help and guidance of many wonderful people in my life. First, I would like to thank my parents and brother for their unwavering support towards every endeavor I have undertaken in the 30 years of my life. They were my pillars even when they were thousands of miles away. Second, I would like to thank my partner, Krishanu Mathur, for believing in me even when I found it difficult to believe in myself. I will always value his patience and perseverance with me. Third, a big thank you to my Ann Arbor family: Matangi Marthi, Ruba Fauzan, Adeel Ajaz, Megan Lafferty, Adarsh Appukuttan, Prashanth Venkataramani, Doug Bowman, Theresa Mau, Ada Hagan, Nandini Ravi, and Aniruddha Ray, for making my time in Ann Arbor cherishable. Fourth, I would like to thank the members of the Ono lab: Dishari Thornhill, Christopher Sumner, and Dr Tomoyuki Murakami for not only being excellent colleagues but also loving friends. No matter where I go, a part of me will always belong to the Ono lab. Special thank you to the administrative staff in the Department of Microbiology and Immunology for always making things seem easier than they really are.

Lastly and most importantly, I would like to thank all my mentors. Dr Akira Ono has been a guiding light for me for the past five years. His perseverance towards science and commitment to mentoring have helped shape me into the scientist I am today. I would not be in graduate school without the help of Dr Malini Raghavan, who believed in me and took me on as a research assistant even when I had very little prior research experience. A special thanks to my

committee members: Drs Bethany Moore, Joel Swanson, Adam Lauring, and Andrew Tai. Over the years, I have highly valued their support and guidance in steering my thesis project.

The work published in this thesis would have been impossible without the help of many people. I would like to acknowledge Akira for his suggestions and valuable feedback with all published and unpublished work.

Part of the literature review in chapters 1 and 4 was previously published:

Bedi, S.; Ono, A. 2019. Friend or Foe: The Role of the Cytoskeleton in Influenza A Virus Assembly. *Viruses 11*, 46.

The work in chapter 2 was also previously published:

Bedi S, Noda T, Kawaoka Y, Ono A. 2018. A defect in influenza A virus particle assembly specific to primary human macrophages. *mBio* 9:e01916-18.

I would like to thank my co-authors Drs Takeshi Noda and Yoshihiro Kawaoka for providing us with plasmids to generate virus. In addition, thank you to them for their helpful suggestions to the manuscript. I would also like to thank Drs Adam Lauring and Christopher Brooke for providing technical assistance with this project.

The work in chapter 3 would not have been possible without plasmid construction and cell line generation by Amanda Haag. All the microscopy analysis performed in chapters 2 and 3 were done with the help of the staff at BRCF Microscopy core, University of Michigan.

Table of Contents

List of Tables

List of Figures

Abstract

Influenza A Virus (IAV) assembly at the plasma membrane of infected cells is a complicated process that is orchestrated by at least five viral components: hemagglutinin (HA), neuraminidase (NA), matrix (M1), the ion channel M2, and viral ribonucleoprotein complexes (vRNPs). While the roles of these individual viral components during IAV assembly have been described before, the precise nature and sequence of interactions between viral proteins during IAV assembly are not completely understood. In addition, very few host factors that are involved in IAV assembly have been identified. The goal of this thesis is to better define the role of viral and host factors in IAV assembly. To do so, a strategy that involves comparison between cell types that support IAV assembly (permissive) and cell types that do not (non-permissive) has been employed. This comparison allows for identification of viral-viral and viral-host interactions that regulate IAV assembly in host cells.

In this thesis, the primary human monocyte-derived macrophages (MDM) has been identified as a cell type that is non-permissive to IAV assembly. In comparison with a cell type that is permissive to IAV assembly, MDM are efficient at supporting the early steps of the IAV life cycle but fail to support assembly of nascent particles. A more thorough analysis of the IAV assembly process revealed that MDM are defective at supporting a discrete step in IAV assembly: association between the viral proteins HA and M2 at the plasma membrane. In addition, the association between HA and M2 likely precedes particle assembly in cells and hence, is an essential step for initiation of virus particle assembly.

As for the host factors involved in IAV assembly, IAV particle assembly is restored in MDM upon disruption of the actin cytoskeleton. Hence, the actin cytoskeleton plays a negative role in IAV assembly in a cell-type-dependent manner. In addition, the actin cytoskeleton suppresses IAV assembly in MDM likely by restricting the association of M2 with HA. Data in this thesis further indicate that both linear and branched actin filaments contribute to suppression of HA-M2 association in MDM.

Overall, in this thesis, key viral and host factors that regulate assembly of nascent IAV particles have been identified. This information will potentially aid in development of new antiviral strategies that specifically target IAV assembly.

Chapter 1

Introduction

Influenza A Virus (IAV) belongs to the Orthomyxovirus family of viruses. The Orthomyxovirus family consists of seven genera, out of which three genera: Influenza A, Influenza B and Influenza C cause disease in humans. Among these three genera, IAV is the most widespread with respect to its host range. While the natural reservoir of IAV are wild birds, the virus can infect pigs, horses, minks, seals, whales, dogs, cats, bats as well as humans [1]. In humans, seasonal outbreaks of IAV infection occur every year and affect 3-5 million people worldwide. Severe disease and complications leading to death occur in susceptible populations including children, individuals older than 65 years, individuals with chronic medical conditions as well as individuals with immunosuppressive conditions such as HIV/AIDS. A recent study estimated that 291,243-645,832 seasonal influenza-associated respiratory deaths (4·0-8·8 per 100,000 individuals) occur annually worldwide [2]. In addition to these seasonal outbreaks, IAV has been the cause of disease pandemics affecting millions worldwide. These pandemics are caused by the introduction and adaptation of new viral strains in humans from an animal source. The deadliest influenza pandemic in recent history is the Spanish Flu, which began in 1918 and killed 40-50 million people [3]. The most recent 2009 H1N1 pandemic affected about 60 million people worldwide but the mortality rates were relatively low because of advancements in medicine as well as higher infection rates in children and young and middle-aged adults than in older individuals [4]. The emergence of new IAV strains within the human population, via the

introduction of new viral strains from other animals (antigenic shift) and/or adaptation of existing strains (antigenic drift), continues to be a threat.

Composition of IAV

IAV is an enveloped virus with an eight-segmented negative sense RNA genome. On the surface of the virus are present three transmembrane proteins: hemagglutinin (HA), neuraminidase (NA) and the ion channel protein (M2). On the cytoplasmic side of the viral membrane, the matrix (M1) protein oligomerizes to coat the inside of the virus particle [5]. The viral RNA segments incorporated into the virus particle are present as a viral ribonucleoprotein (vRNP) complex between the RNA, nucleoprotein (NP) and three polymerase subunits: PA, PB1, and PB2 [6]. The virus also encodes for two NS proteins: NS1 and NS2, which play non-structural roles during virus replication. Recently, five additional proteins expressed by the PA and PB1 segment of IAV have been identified: PB1-F2 [7], PB1-N40 [8], PA-X [9], PA-N155 and PA-N182 [10]. With exception to the identification of PB1-F2 as a virulence factor inducing cell death [7], the functions of the remaining four proteins are not well understood.

IAV life cycle

The IAV life cycle begins with binding of IAV to the target cell via interactions between HA on the viral membrane and sialic acids on the host cell membrane [11,12]. Following this interaction, the virus is internalized via the host cell's endocytic pathway. The acidic pH of the endosome causes a conformational change in HA, exposing a fusion peptide that allows for fusion of the endosomal membrane with the viral membrane [13], following which the vRNPs can be released in the cytosol and imported into the nucleus. Viral RNA replication and transcription of mRNAs take place in the nucleus, followed by viral protein translation in the cytoplasm. Assembly of

new virus particles requires trafficking of at least four viral structural proteins, HA, NA, M1, and M2 as well as vRNPs to the plasma membrane [14,15]. After incorporation of the viral genome into budding virus particles, the M2 protein mediates scission and thus, release of the nascent particles from the cell [16]. The IAV life cycle is depicted in Figure 1.1.

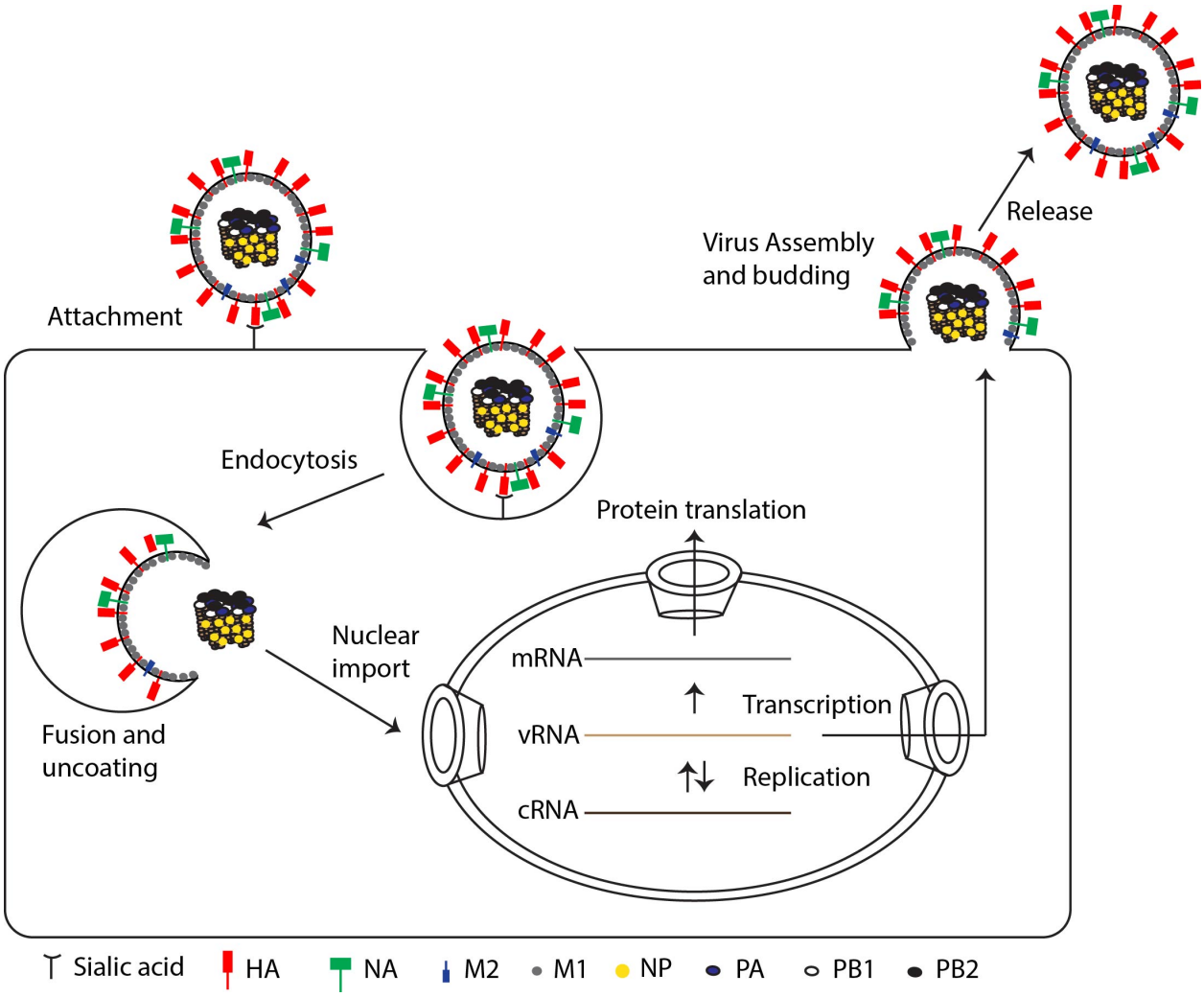

Figure 1.1: An overview of IAV lifecycle. The virus lifecycle is initiated upon binding of virus-associated HA to cell-associated sialic acid groups. The early stages of the lifecycle are: fusion, uncoating, nuclear import of viral genome, viral gene replication and transcription, and protein translation. Viral RNA (vRNA) is replicated via complementary RNA (cRNA). vRNA is also transcribed into messenger RNA (mRNA), which is used to produce viral proteins. The late stages of the virus lifecycle are: protein trafficking to plasma membrane, virus particle assembly and budding, and particle release.

IAV Assembly

IAV is thought to assemble in cholesterol-enriched microdomains, or membrane rafts, of the plasma membrane of host cells [14,15,17-20]. HA and NA accumulate and co-cluster at these microdomains and form sites of virus assembly known as budozones [17,18,21-24], while the third transmembrane protein, M2, is suggested to localize at the edge of the budozone [16,18,25,26]. M1, which is predominantly cytosolic, associates with membranes containing HA, NA and M2, either at the ER-Golgi or at the plasma membrane [27-30]. Expression of HA, NA, M1 and M2 in cells is sufficient to drive assembly and budding of virus-like particles at the plasma membrane [21,31]. A subset of the M1 population is also imported into the nucleus [32-35], where it mediates the export of vRNPs via the Crm1 pathway along with NS2 [36,37]. After nuclear export, vRNPs are thought to co-opt the cellular recycling compartment to traffic to assembly sites at the plasma membrane [38-41]. Arrival of vRNPs at virus assembly sites further promotes assembly and budding of virus particles [42-44]. While HA, NA and, likely, M1 induce and stabilize membrane curvature [21,31,45], membrane scission and release of virus buds requires M2. M2 is enriched at the neck of the virus bud [16,25,26] and is thought to induce positive membrane curvature, which may be sufficient for membrane scission [16,46]. NA prevents retention of nascent particles that have undergone scission by cleaving cell-surface sialic acid moieties, which could otherwise bind virus-associated HA [47,48]. The different steps of IAV assembly are depicted in Figure 1.2.

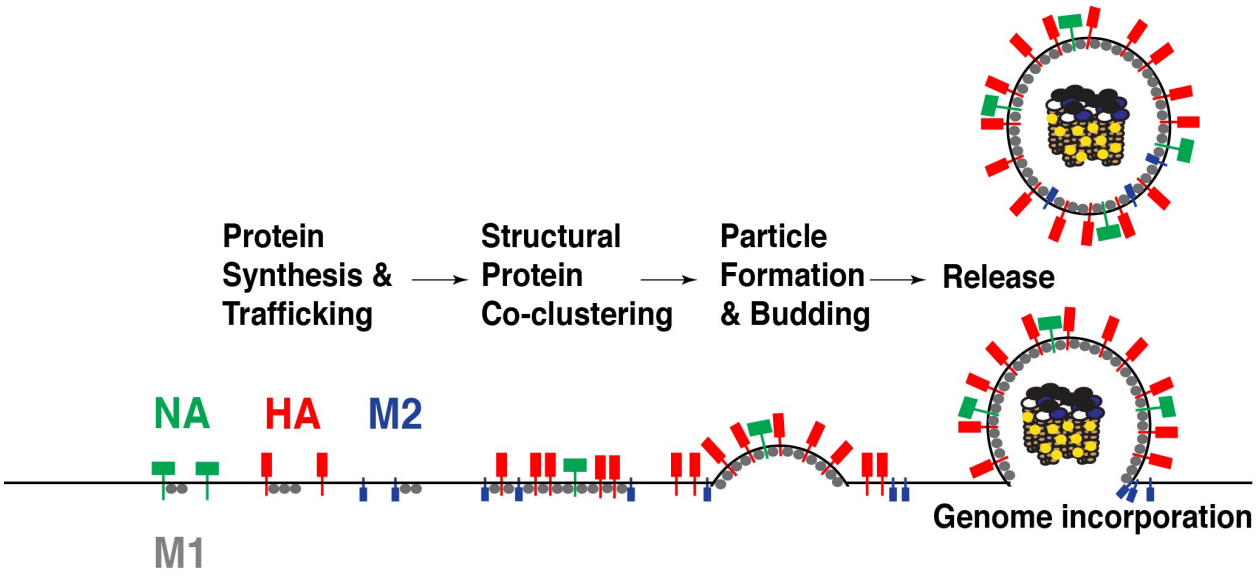

Figure 1.2: Overview of IAV assembly. IAV assembly is initiated at the plasma membrane after arrival of three transmembrane proteins, HA, NA and M2, and the cytoplasmic protein M1 through the cytoplasm. Clustering of these viral proteins drives assembly of the virus particle. Assembling virus particles can have a spherical or filamentous morphology. For the sake of simplicity, only the spherical morphology is depicted in this figure. vRNPs are transported across the cytoplasm on Rab11-positive vesicles and are incorporated into the assembling virus particle. NA allows for release of nascent particles that have undergone the scission by cleaving cell-surface sialic acid moieties.

Different morphologies of IAV

IAV is pleomorphic, possessing two distinct morphologies: spherical virions that are ~100 nm in diameter and filamentous particles that are ~100 nm in diameter and up to 20 um in length [49-52]. Most commonly used laboratory-adapted strains, such as A/Puerto Rico/8/1934 (H1N1) (PR8) and A/WSN/1933 (H1N1) (WSN), are solely spherical [53]; however, *in vivo* human infection produces both spherical and filamentous virions [49,51]. In addition, virions having filamentous morphology emerge after passaging of spherical viral strains in guinea pigs, suggesting the selective advantages of this morphology [52]. The key genetic determinant of virion morphology is the M1 protein, since specific mutations in the M1 protein confer the

ability to form filamentous virions [52,54-58], although M2 [57,59,60] and NP [44] also play some roles.

Viral proteins important for IAV assembly and budding

The roles of individual viral components that contribute to IAV assembly are briefly described below. In addition, a schematic describing the functional domains of individual viral proteins involved in IAV assembly is shown in Figure 1.3.

i. HA: HA is a homotrimeric glycoprotein with a 27 residue transmembrane domain. The HA ectodomain, which is 529 residues long, is involved in virus binding and entry and hence, serves as a target for most anti-HA antibodies. The motifs that mediate association of HA with lipid rafts are found in the transmembrane domain and the 10 amino acid long cytoplasmic tail [17,22,61-63]. These motifs are also involved in the targeting of HA to the apical plasma membrane [23,64], indicating that lipid-raft association and apical targeting of HA are linked. The role of HA in particle assembly is not fully understood. In early studies using transfection systems, expression of HA without expression of any other viral proteins showed that HA alone cannot form virus-like particles [65,66]. However, it was later shown that expression of HA alone is sufficient for assembly and release of virus-like particles [21]. A recent study showed that while HA (along with NA) can induce curvature in the plasma membrane, the expression of additional proteins such as M1 and/or M2 is required for stabilization of this curvature and hence, formation of virus-like particles [31]. In terms of virus infection, viruses lacking HA are still able to bud from infected cells [61], suggesting that other viral proteins such as NA, M1 and M2 can drive virus assembly in the absence of HA. Similarly, even when HA is intentionally targeted to the basolateral membrane of the cell, virus assembly still takes place at the apical membrane [67,68]. Therefore, the current understanding in the field is that HA can initiate

membrane curvature at the plasma membrane; however, it is not essential for assembly or budding of virus particles. In addition to its role in induction of membrane curvature, HA helps in recruitment of other viral structural components such as M1 [27-30,45] and vRNPs [69,70] to virus assembly sites.

ii. NA: NA is a type II transmembrane glycoprotein that, like HA, associates with lipid rafts in a manner dependent on its transmembrane (29 amino acids) and cytoplasmic (5 amino acids) domains [22,71-73]. Similarly to HA, the exact role of NA during virus particle assembly is not fully understood. While NA is thought to be able to induce membrane curvature [21], particle assembly relies on additional viral components such as HA, M1 and M2 [31,65,66]. The cytoplasmic tail of NA plays an important role in IAV assembly since mutations in this domain alter the shape and morphology of assembling virus particles [29,73]. Like in the case of HA, the cytoplasmic domain of NA is also important for recruitment of M1 to virus assembly sites [27-30]. Apart from its role in particle assembly, NA plays a key role in cleaving sialic acid residues on the cell surface before the assembled virus particle can be released from the cell. This enzymatic activity of NA is encoded by the extracellular domain (436 amino acids) of the protein [47].

iii. M1: M1 is a 252 amino acid protein that contains three domains: N-domain, Middle(M)-domain and the C-domain. The N- and M- domains play key roles in the oligomerization [74-76], membrane binding [74,75], and vRNP binding [32,74,77,78] of M1. The C-domain has been suggested to be involved in vRNP binding [34] and M1-M1 interactions [74,76]. Nevertheless, all three domains of M1 protein are important for virus assembly and contribute to the morphology of virus particles [55,56,74]. When expressed alone, M1 is predominantly localized to the cytosol. However, it associates with detergent resistant membranes and is incorporated into virus-like

particles in the presence of HA and/or NA [27-29,69]. Even though earlier studies showed that M1 possesses intrinsic membrane binding ability [34,79,80] and can initiate virus-like particle formation by itself [65,66], later studies showed that HA, NA and/or M2 and not M1 initiate particle assembly [21,81]. Based on these studies, the current model is that interactions between M1 and the cytoplasmic tails of HA, NA or M2 allow for initial targeting of M1 to the plasma membrane, following which interactions with negatively charged lipids stabilize membrane-association of M1. Upon membrane binding, M1 multimerizes to provide structure to the virus particle [5]. The importance of M1 in IAV assembly is further evident by its role in conferring the ability to form filamentous virus particles [52,54-57,82,83].

iv. M2: M2 is a homotetrameric transmembrane protein, which is also encoded by the M segment of the viral genome through alternate splicing. The transmembrane domain (19 amino acids) of M2 forms the pore of the ion channel, the activity of which is important for uncoating of the virus particle core during virus entry [84,85]. The cytoplasmic tail (54 amino acids) of M2 plays important roles in virus assembly and budding [16,59,86-88]. While the membrane proximal 17 amino acids of the M2 cytoplasmic tail form an amphipathic helix, which has been proposed to induce positive membrane curvature for scission of the virus bud [16,26,46,89], the membrane distal amino acids are involved in binding and recruitment of M1 and/or vRNPs to virus assembly sites [59,60,86-88,90,91]. Some complementarity has been observed for the roles of M1 and M2 during particle assembly [92,93], suggesting a direct link between the two viral proteins. With respect to spherical IAV particle assembly, M2 is not important for initiating particle assembly *per se* but is important for membrane scission and pinching off of the assembled bud [16,26,59,88]. In contrast, filamentous particle assembly is highly dependent on the function(s) of

M2 [25,26,60,88,92,93], indicating that, in addition to M1, M2 also plays an important role in IAV morphogenesis.

v. vRNP: While incorporation of vRNPs into assembling virus particles is required for generation of infectious virus particles, the arrival of vRNPs at virus assembly sites also promotes IAV assembly [42,43]. Consistent with the role of vRNP recruitment in IAV particle assembly, mutations in NP also confer the ability to form filamentous virus particles [44]. However, the exact mechanism by which vRNPs regulates particle assembly is not known. Since NP associates with both M1 and M2 [59,60,74,87,90], it is likely that the role of vRNPs in particle assembly is at least partially dependent on its association with M1 and/or M2. In addition, transport of vRNPs and cholesterol to the plasma membrane are linked [42] and hence, vRNP recruitment may drive particle assembly in a cholesterol-dependent manner.

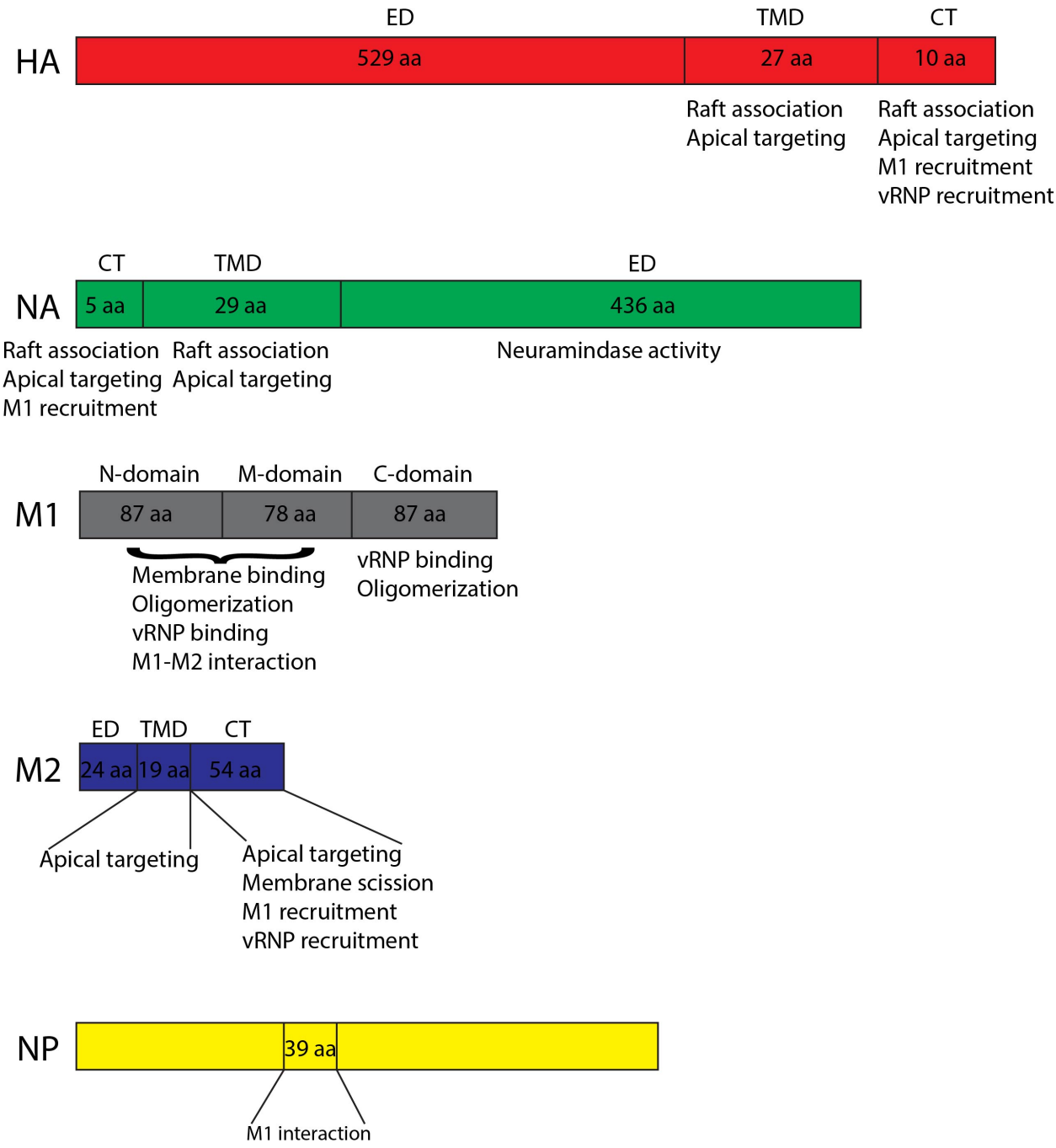

Figure 1.3: Functional domains of viral proteins involved in IAV assembly. The five viral structural proteins (HA, NA, M1, M2, and NP) that play important roles during IAV assembly are shown. Note that HA and M2 are type I transmembrane proteins while NA is a type II transmembrane protein. The functional domains of individual viral proteins as well as the specific functions of these domains during IAV assembly are shown. ED, Ectodomain; TMD, Transmembrane domain; CT, Cytoplasmic tail; aa, amino acids.

Host factors regulating IAV assembly

Genome-wide approaches have identified numerous host cellular proteins that play important roles during IAV infection [94-103]. However, the functional significance of many of the identified proteins still needs to be determined. Host cellular proteins could either serve as virus cofactors or restriction factors for replication of viruses. Released IAV particles incorporate several host cellular proteins that are known to associate with plasma membrane lipid rafts such as cytoskeletal proteins, annexins, glycolytic enzymes, and tetraspanins [104,105]. However, the exact roles (positive or negative) are understood for only a subset of these proteins. In this section, I provide a brief description of the host cellular proteins known to play positive or negative roles during different steps of IAV assembly. The roles of these individual proteins during IAV assembly are further summarized in Table 1.1.

Host proteins important for trafficking of vRNPs:

i. Rab11: Trafficking of the newly replicated genome to sites of virus assembly at the apical plasma membrane and its packaging into assembling virus particles is mediated by Rab11-positive vesicles [39,40,106-112]. While these vesicles were thought to be derived from the endocytic recycling compartment (ERC) in earlier studies [39,40,43,107,112-114], a more recent study suggested that they are derived from the ER [41]. Rab11 also localizes in the Golgi and post-Golgi vesicles, where it may serve as a link between the endocytic and exocytic pathways [115]. The ubiquitous localization of Rab11 in the cell makes it difficult to understand the exact nature of the compartment driving vRNP transport in the cell. While their origin is yet to be determined, the Rab11-positive vesicles, which are enriched in cholesterol [42], are proposed to promote IAV particle assembly [42,116]. Rab11-dependent transport is also important for bundling of vRNPs so that eight unique segments can be incorporated into assembling virus particles [107,108].

ii. HRB: Human immunodeficiency virus (HIV) Rev-binding protein (HRB) is a cytoplasmic protein, which has been shown to be important for trafficking of vRNPs to the cell periphery [117]. In addition to its association with vRNPs, HRB also interacts with Crm1 [118] and NS2 [37,117], which are both key drivers of vRNP nuclear export. While HRB has no obvious effect on nuclear export of vRNPs, the lack of functional HRB impairs vRNP transport to the plasma membrane [117]. The localization of HRB in the cytoplasm as well as its ability to interact with the nuclear export machinery may allow it to serve as a potential link between nuclear export and trafficking of vRNPs in the cytoplasm. However, the molecular mechanisms behind HRB-mediated transport of vRNPs are not completely understood.

iii. STAU1: Staufen 1 (STAU1) is an RNA-binding protein that regulates the transport and localization of mRNA in cells [119,120]. In terms of IAV infection, STAU1 is required for efficient particle assembly and release. STAU1 is important late during the IAV life cycle and associates with vRNPs to likely drive their trafficking and/or packaging into assembling virus particles [121].

iv. YB-1: Y-box-binding protein 1 (YB-1) is a predominantly cytoplasmic RNA- and DNA-binding protein, which translocates to the nucleus in response to IAV infection [122]. While YB-1 likely first interacts with vRNPs in the nucleus [122], its role in vRNP trafficking has been mainly described in the cytoplasm [42,122]. YB-1 anchors microtubules at the microtubule organizing center (MTOC) and bridges the interactions between vRNPs and microtubules. However, since the role of microtubules in vRNP trafficking to the plasma membrane is still debatable [39,106,110], the exact mechanism by which YB-1 drives vRNP transport in the cytoplasm is not clear.

v. hCLE: hCLE is a human transcription factor, which was previously shown to promote the activity of the IAV polymerase [123-125]. However, recently, hCLE was also shown to be upregulated in IAV-infected cells and associate with vRNPs in the cytoplasm as well as in released virus particles [126]. However, the exact role(s) of hCLE during vRNP transport is not known.

Host proteins important for trafficking of transmembrane proteins:

i. COPI: The IAV transmembrane proteins HA, NA and M2 traffic from the ER to the plasma membrane via the anterograde transport pathway. COPI, which is expressed on vesicles transporting contents between the Golgi and the ER, is important for efficient membrane protein expression and trafficking of the transmembrane proteins M2 and NA to the plasma membrane [127].

ii. Cdc42: Cdc42, a Rho GTPase that is involved in regulation of the cell cycle, is activated in response to IAV infection. The active form of Cdc42 promotes the transport of NA to the plasma membrane by increasing the efficiency of anterograde transport in cells [128].

iii. UBR4: Ubiquitin N-recognin domain-containing E3 ligase 4 (UBR4) is a predominantly nuclear protein, which translocates to the cytoplasm in response to IAV infection. It associates with M2 in the perinuclear ER region and promotes the trafficking of not just M2 but also HA and NA to the plasma membrane. While the binding of UBR4 to M2 prevents the degradation of M2 and thus increases its expression at the plasma membrane, it is not clear how UBR4 promotes the trafficking of HA and NA [100].

iv. Rab11: In addition to its role in vRNP trafficking, Rab11 also promotes trafficking of M2 to the plasma membrane [16]. However, it is not known whether Rab11-dependent trafficking of M2 occurs by mechanisms similar to those for vRNP trafficking.

v. TRAPPC6AΔ: The transport protein particle (TRAPP) complex is a multisubunit tethering complex that is involved in protein transport between different cellular organelles. TRAPPC6AΔ, a subunit of TRAPP complex, interacts with M2 and slows down the trafficking of M2 to the plasma membrane [129]. While TRAPPC6AΔ associates with M2 in cytoplasmic vesicles, the exact identity of these vesicles as well as their role in regulating M2 transport are not known.

vi. Cyclin D3: Cyclin D3 is a key regulator of the cell cycle that restricts IAV assembly in a manner independent of its regulatory role during the cell cycle. In response to IAV infection, Cyclin D3 redistributes from the nucleus to the cytoplasm, where it binds to M2. Binding of Cyclin D3 to M2 impairs binding of M1 to M2 and reduces the efficiency of M2 trafficking to the plasma membrane [130].

Host proteins important for particle assembly

i. CD81: CD81 is a tetraspanin that is expressed on the plasma membrane and endosomal membranes. It is incorporated into IAV particles [104] and plays important roles during both IAV entry and assembly [131]. With respect to IAV assembly, the efficiency of virus bud formation is not altered in the absence of CD81; however, the buds are elongated and have a higher propensity to remain attached to the host cell. With respect to the mechanism by which CD81 promotes IAV assembly, it localizes to the growing tip as well as the neck of the assembling particle and is thought to promote pinching-off of the virus bud [131].

ii. Rack1: The scaffolding protein receptor for protein C kinase 1 (Rack1) interacts with the N-domain of M1. In the absence of Rack1, M1 is still recruited to the plasma membrane and virus particle assembly can be initiated. However, the assembled virus particles are unable to pinch off and be released from the cell [132].

iii. F1Fo ATPase: The F1Fo ATPase is an enzyme complex, which consists of a catalytic portion (F1) and a proton channel (Fo). It is found in the inner membrane of the mitochondria and at the plasma membrane. The β subunit of plasma membrane-associated F1Fo ATPase interacts with NS2 and this interaction allows for clustering and polymerization of the ATPase close to virus assembly sites. At virus assembly sites, F1Fo ATPase localizes at the bottom edge of assembling virus particles and promotes particle assembly [133].

iv. Annexin A6: Annexin A6 is a calcium-dependent membrane-binding protein that associates with M2 at the plasma membrane and negatively regulates IAV budding. Upon overexpression of Annexin A6 in IAV-infected cells, particle assembly is still initiated; however, membrane scission and release of virus particles are significantly reduced [134].

v. Viperin: Viperin is an evolutionarily conserved protein that is inducible by interferon and blocks the infection of many different viruses [135]. In the case of IAV, expression of Viperin inhibits IAV budding. While particle assembly is initiated, assembled virus particles are not able to pinch off and be released from the cell. Viperin interacts with a key enzyme in the isoprenoid biosynthesis pathway to block its activity and thereby, affects lipid raft formation. Consistent with its role in lipid raft disruption, expression of Viperin increases the diffusion rate of plasma membrane-associated HA [136].

vi. Actin cytoskeleton: The role of the actin cytoskeleton in IAV assembly depends on the morphology of the assembling virus particle. Disruption of the actin cytoskeleton has no obvious effects on spherical particle assembly. Interestingly, in some cases, disruption of the actin cytoskeleton modestly increases spherical virus release [82,137]. In contrast, filamentous particle assembly is highly dependent on an intact actin cytoskeleton. Both stabilization and disruption of F-actin impedes filamentous particle formation at the apical surface [82,137]. In **chapter 2**, I

describe a host cell-type-dependent role for the actin cytoskeleton in assembly of spherical IAV particles.

Since I focus on the role of the actin cytoskeleton during IAV assembly in later chapters, I provide an overview of the structure and function of the actin cytoskeleton in the following section(s). In addition, I provide a summary of the currently known roles of the actin cytoskeleton at different steps of IAV assembly.

Overview of the Actin Cytoskeleton

The actin cytoskeletal system is composed of actin monomers (G-actin) that polymerize to form helical filaments (F-actin) [138,139]. Actin filaments are asymmetric in nature with a barbed end that grows faster and a pointed end that loses actin monomers faster. Actin filaments can form more complex structures such as branched networks, bundled networks, and non-aligned networks. These different conformations of F-actin require different actin-nucleating proteins [140,141]. While the Arp2/3 complex nucleates branched F-actin structures, formins nucleate unbranched actin filaments and serve as elongation factors for the growing actin filament. In addition to nucleating factors, organization of F-actin is dependent on cofilin, an actin-binding protein that severs filaments to generate free ends for addition of G-actin [142]. Actin filaments do not grow outwards from an organizing center but polymerize and depolymerize locally in response to different stimuli. The actin cytoskeleton functions in cell migration, providing structure and strength to the plasma membrane, trafficking of cargo within the cell, organization of organelles, and regulation of cytokinesis during cell division. The cortical actin cytoskeleton, a network of actin filaments that underlies and interacts with the plasma membrane, plays an important role in maintaining the structure of the plasma membrane [143-145]. These functions of F-actin are carried out with the help of myosin motors, which play key roles in regulating the

dynamics of F-actin networks [146]. The Rho family of small GTPases also regulates actin assembly and disassembly. The most well characterized Rho GTPases are RhoA, Rac, and Cdc42. RhoA stimulates the activity of formins and promotes assembly of linear F-actin bundles. On the other hand, Rac and Cdc42 promote branching of the actin cytoskeleton by activating the Arp2/3 complex [147].

Relationships between IAV growth and actin cytoskeleton

Various lines of evidence support multifaceted relationships between the actin cytoskeleton and the IAV life cycle. First, actin is incorporated into released IAV particles [104,105]. Second, viral components, specifically M1 and proteins comprising the vRNPs, associate with actin in host cells [148-151]. Third, IAV infection alters the levels, structures and functions of F-actin in host cells. Several studies show an enhancement in total actin [152,153] levels upon infection, with the exception of one study that showed no difference in cellular actin levels [154]. In addition to total actin levels, IAV infection can also modulate the levels or activities of proteins involved in regulation of F-actin dynamics. While some key proteins involved in F-actin dynamics such as cofilin-1 [153,155], ERM proteins [153], talin [153], and the regulatory light chain of myosin II motor [153] are upregulated in response to IAV infection, others such as Arp2/3 [154], formins [154], cortactin [156] and myosin Vb [154] are downregulated. RhoA, which regulates functions of the actin cytoskeleton, was downregulated in infected epithelial cells [157]. In addition, the activity of RhoA [153,157] and another Rho GTPase, Rac1 [158], is reduced upon IAV infection but the activity of a third Rho GTPase, Cdc42 [128], is enhanced upon infection. Therefore, there seems to be some specificity with which IAV infection modulates expression or activity of proteins engaged in F-actin dynamics.

Fourth, disruption of actin cytoskeletal dynamics has either a negative or a positive effect on viral replication. Disruption of F-actin dynamics, by drugs inhibiting polymerization (cytochalasin D), enhancing depolymerization (latrunculin A), or stabilizing actin filaments (jasplakinolide), leads to increase in released viral titers in non-polarized cells [82,137]. In epithelial cells, the effects of these drugs on viral replication differ between different studies. In the Madin-Darby Canine Kidney (MDCK) cell line, disruption of F-actin dynamics has no [82], a positive [137], or a negative [159,160] effect on released viral titers. In polarized rhesus monkey kidney cells, which are inefficient in supporting infection of a laboratory adapted IAV strain, inhibition of F-actin polymerization [161] drastically increases released viral titers. Cofilin-1 [155] and cortactin [156], which can promote disassembly and assembly of F-actin, respectively, are both thought to play positive roles during IAV infection.

Among those listed above, studies that show infection-induced changes in actin cytoskeletal proteins or their association with viral proteins or particles are consistent with a role for the cytoskeleton in IAV infection. Obviously, however, studies conducted using specific inhibitors or genetic ablation should provide more definitive evidence on the role of specific actin cytoskeletal components in the virus life cycle. Nonetheless, some studies using these strategies show contradictory data even as to whether the actin cytoskeleton of interest plays a positive role or not [39,82,110,114,137,155,159,161,162]. This could partially be attributed to the use of viral titers as read-out for IAV infection. Measurement of viral titers may not allow for identification of the role(s) of the actin cytoskeleton at different stages of the IAV life cycle, especially if the actin cytoskeleton plays opposing roles in the early and late stages of IAV infection. Even with studies focusing on the late stages of the virus life cycle, disruption of F-actin can have contradictory effects on particle assembly [82,137,159,163]. This could be because

F-actin can play negative and positive roles at different steps in IAV assembly. Depending on the conditions, such as host cell types, viral strains, and the time points at which analyses are performed, cumulative effects of F-actin disruption may lead to different final outcomes on virus production. Therefore, to advance our understanding of the roles played by cytoskeletons in virus growth, it is necessary to determine the effects of cytoskeleton disruption on each of single defined steps of the virus life cycle in addition to the overall viral titers. In the following sections, I describe the individual steps of the IAV assembly process as well as the role of actin cytoskeleton during these steps.

Roles played by the actin cytoskeleton at specific steps of IAV assembly

F-actin could regulate at least the following steps in the IAV assembly process: trafficking of viral transmembrane proteins to the plasma membrane, trafficking of cytoplasmic viral components to the assembly sites, association between viral components at the plasma membrane, and morphogenesis of nascent particles. The different steps of IAV assembly and the roles (positive or negative) of the actin cytoskeleton during these steps are depicted in Figure 1.4. In addition, the roles of specific actin cytoskeletal components at different steps of IAV assembly are summarized in Table 1.2.

Trafficking of viral transmembrane proteins to the apical membrane:

As mentioned above, IAV assembles at the apical surface of polarized epithelial cells, which requires targeting of virus components to the apical plasma membrane [64,72,73,164-173]. F-actin disruption has no obvious effect on apical targeting of transmembrane proteins HA and NA or spherical virus assembly in polarized MDCK cells [160,174]. In one study, impairment in glycosylation of HA and NA was observed upon F-actin disruption; however, this did not have an effect on apical targeting of the proteins [160]. Cdc42, the Rho GTPase that regulates F-actin

branching, promotes the apical trafficking of NA [128]. However, it is not clear whether this positive role of Cdc42 in IAV assembly is via its effect on F-actin dynamics or via its other regulatory roles during the cell cycle.

Trafficking of viral cytoplasmic components to the assembly sites:

In addition to viral transmembrane protein trafficking, M1 protein trafficking to the plasma membrane is also thought to at least partially rely on the ER-Golgi transport pathway, since M1 associates with HA- and NA-enriched membranes both at the ER-Golgi and the plasma membrane [27,28]. In the cytoplasm, M1 may also associate with F-actin, since it remains insoluble after a detergent treatment that disrupts M1-lipid interactions but still allows M1-actin interactions [148]. However, it is not clear whether this association of M1 with F-actin mediates the trafficking of M1 to HA- and/or NA-enriched membranes or is involved in the cytoplasmic transport of the M1-vRNP complex.

Trafficking of the viral genome or vRNPs to the apical membrane is also a key step in the assembly of infectious IAV particles. Upon export from the nucleus, vRNPs associate with both the actin cytoskeleton [149] and microtubules [122,175]. While the association with F-actin is proposed to govern the intracellular localization of vRNPs [149] and partially drive their movement in the cytoplasm [113], their association with microtubules appears to be a key driver for vRNP trafficking [106,113,114,122,175]. Overall, the findings from previous studies support a minimal role for the actin cytoskeleton in apical targeting of IAV components.

Association between viral components at the plasma membrane:

Viral proteins have been shown to co-cluster in microdomains of the plasma membrane [18,163,176]. However, it is not known whether these associations between viral proteins are initiated during ER-Golgi transport or occur post arrival at the plasma membrane. Since HA and NA accelerate each other's apical trafficking [23], they are likely to co-traffic and associate with

each other prior to their arrival at the plasma membrane. In contrast, it is not clear whether M2 co-traffics with HA and/or NA to the apical membrane. While earlier studies suggested that HA and M2 traffic together through the ER-Golgi [177-179], a more recent study suggests that the two proteins use distinct pathways for trafficking to the plasma membrane [23]. Hence, we currently do not know the exact sequence of association between the transmembrane proteins as well as their association with M1 and vRNPs. In addition, very little is known about the host cell mechanisms that regulate these associations.

The cortical actin cytoskeleton is likely to be involved in the regulation of co-clustering of viral transmembrane proteins through its ability to regulate the structure of plasma membrane microdomains. In fact, the concentration of cortical actin is apparently increased close to the plasma membrane in response to IAV infection, and this reorganization of F-actin is proposed to be important for efficient virus assembly and budding [155]. The cortical actin lowers the mobility of HA at the plasma membrane and enhances the clustering of HA molecules [180]. While HA movement is restricted to regions of the plasma membrane with an underlying F-actin network, HA mobility negatively correlates with the density of the underlying F-actin [180]. A role for the actin cytoskeleton in modulating HA clustering is further supported by the presence of HA aggregates at the plasma membrane when the activity of myosin II motors is inhibited [159]. Association or co-clustering between HA with M2 is also regulated by the actin cytoskeleton. Thaa et al. used fluorescence resonance energy transfer (FRET) approaches, where fluorescent probes were fused to the cytoplasmic domains of HA and M2, and observed that cytochalasin D treatment reduces FRET between fluorescent protein fusions of HA and M2. Hence, these data indicate that the actin cytoskeleton plays a positive role in the association between the two proteins in the absence of any other viral proteins [181]. However, it is not clear

whether the actin cytoskeleton promotes HA-M2 association during the transport of the proteins in the ER-golgi or after their arrival at the plasma membrane.

Morphogenesis of nascent particles at the plasma membrane:

In addition to regulating association between viral proteins, the actin cytoskeleton also plays direct roles in particle morphogenesis. As described above, the effect of F-actin disruption on particle morphogenesis varies depending on the virus morphology with no obvious effects of F-actin disruption observed for IAV strains that assemble solely spherical particles (WSN or PR8) [137,160]. However, one caveat of previous studies with epithelial cells is that they were all performed using epithelial cell lines and not primary epithelial cells. It is becoming increasingly clear that some steps in the IAV particle assembly process are more stringently regulated in primary human cells than in cells lines [91,163], hence, highlighting the need for more studies looking at the role of actin cytoskeleton in primary cells.

In case of an IAV strain that forms filamentous particles (A/Udorn/72 [H3/N2]), particle morphogenesis is highly dependent on F-actin. Both stabilization and disruption of F-actin impedes filamentous particle formation at the apical surface [82,137]. The mechanisms by which the actin cytoskeleton supports filamentous IAV assembly are not well understood. The actin cytoskeleton may provide mechanical support at the base of, or inside the viral filament. Of note, while proteomic studies showed incorporation of actin molecules into released virions [104,105], F-actin has been observed to localize only at the base of the viral filament [137]. In such locations, it is possible that the actin cytoskeleton interacts with one or more viral structural proteins and drives their incorporation into the growing filamentous particle. This role of the actin cytoskeleton might not be as important for spherical particle assembly since there are fewer copies of the structural proteins such as HA, NA, M1 and M2 to be incorporated into spherical particles relative to filamentous particles [5]. Of note, the role of F-actin in particle

morphogenesis has thus far been examined for only a limited number of the laboratory strains; whether the observations above hold true for morphogenesis of a broad range of IAV strains with varied tendency to form filamentous versus spherical particles remains to be tested.

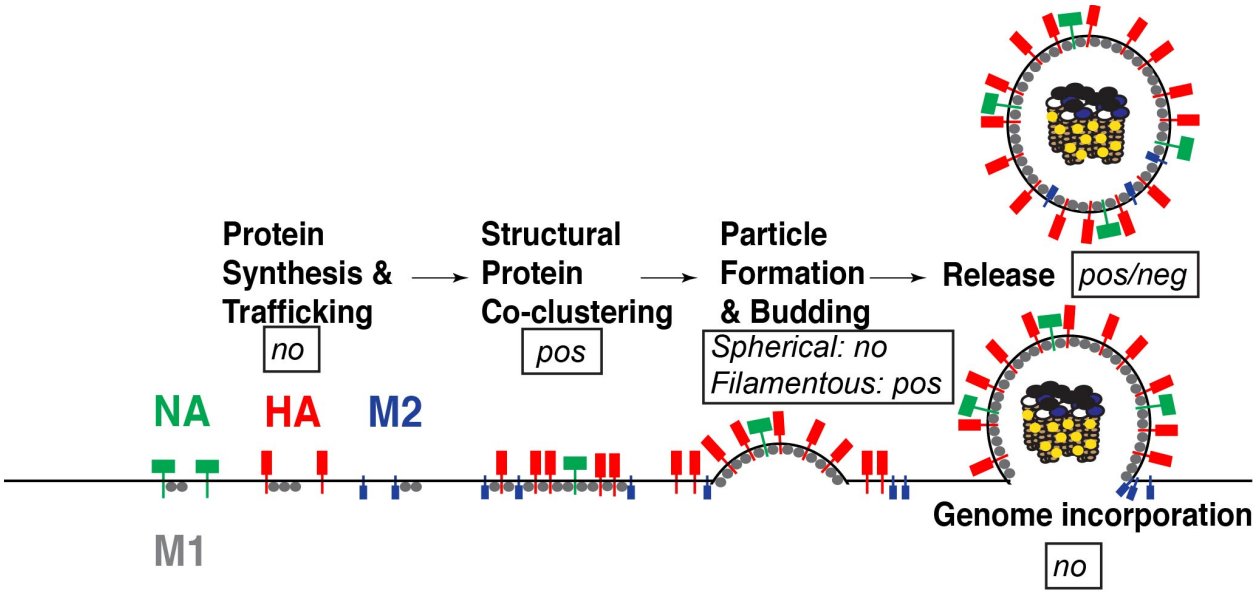

Figure 1.4: Roles of the actin cytoskeleton at different steps of IAV Assembly. Whether the actin cytoskeleton promotes (pos), suppresses (neg) or has no (no) roles during individual IAV assembly steps is depicted.

Overview of the thesis

IAV assembly is driven by five viral components: HA, NA, M1, M2 and vRNPs. As highlighted in this chapter, previous studies have described the role(s) of these individual viral components in IAV particle assembly and budding. However, limited information is available in terms of the nature as well as the sequence of interactions between these viral components that drive assembly of virus particles at the plasma membrane. In addition, very few host cellular proteins that play a role during IAV assembly and budding have been identified. Of the identified cellular proteins, the mechanism by which they contribute to virus assembly has been fully described for only a handful of them. Since IAV assembly is not a target for anti-IAV drugs that are either

available in clinics or are undergoing clinical trials, an understanding of the viral and host proteins that are involved in this stage will potentially reveal targets for future anti-IAV drugs. The potential of virus assembly as a target for antiviral drugs is evident in the case of other viruses such as human immunodeficiency virus (HIV-1) [182] and hepatitis C virus (HCV) [183], where several drugs targeting virus assembly are currently under development.

My dissertation focuses on studying the viral-viral and viral-host protein interactions that drive IAV assembly in host cells. To better facilitate identification of interactions important for IAV assembly, I have compared cells that support IAV assembly (permissive) to cells that are unable to do so (non-permissive). In **chapter 2**, I characterize the primary human monocyte-derived macrophage as a cell type that is non-permissive to IAV assembly. In addition, using this cell type, I show that association between HA and M2 is a discrete step in IAV assembly, which is susceptible to suppression by the host cell's actin cytoskeleton in a cell-type-specific manner. In **chapter 3**, I elucidate the molecular mechanisms by which the actin cytoskeleton restricts IAV particle assembly in a cell-type-dependent manner.

In **chapter 4,** I summarize the results of **chapters 2 and 3** and highlight the questions that need to be addressed in the future. In addition, I present the implications of my work for understanding and targeting IAV assembly in host cells.

Table 1.1: Roles of host cellular proteins at different steps of IAV Assembly.

IAV Assembly Step	Host cellular protein	Role of host cellular protein	Reference
vRNP trafficking	Rab11	Positive	[39,40,106-112]
	HRB	Positive	[117]
	STAU1	Positive	[121]
	YB-1	Positive	[42,122]
	hCLE	Positive	[126]
Transmembrane protein trafficking	COPI	Positive	[127]
	Cdc42	Positive	[128]
	UBR4	Positive	[100]
	Rab11	Positive	[16]
	TRAPPC6AΔ	Negative	[129]
	Cyclin D3	Negative	[130]
Particle assembly/budding	CD81	Positive	[131]
	Rack1	Positive	[132]
	F1Fo ATPase	Positive	[133]
	Annexin A6	Negative	[134]
	Viperin	Negative	[136]
	Actin cytoskeleton	Positive	[82,137]

Table 1.2: Roles of specific actin cytoskeletal components at different steps of IAV Assembly.

IAV Assembly Step	Actin cytoskeletal component	Role of cytoskeletal component	Reference
HA trafficking	F-actin	No role	[160]
NA trafficking	Cdc42	Positive	[128]
vRNP trafficking	Myosin II	No role	[159]
HA clustering	F-actin	Positive	[180]
	Myosin II	Positive	[159]
HA-M2 coclustering	F-actin	Positive	[181]
Spherical particle assembly	F-actin	No role	[137,160]
Filamentous particle assembly	F-actin	Positive	[82,137]
Release of nascent particles	F-actin	Moderately negative/ positive	[82,137,159]

Chapter 2

A Defect In Influenza A Virus Particle Assembly Specific To Primary Human Macrophages

Abstract

Influenza A virus (IAV) propagates efficiently in epithelial cells, its primary target in the respiratory tract. In contrast, productive infection of most IAV strains is either blocked or highly inefficient in macrophages. The exact nature of the defect in IAV replication in human macrophages remains unknown. In this study, we showed that even when compared to a monocytic cell line differentiated to macrophage-like cells, primary human monocyte-derived macrophages (MDM) are inefficient in IAV production, despite comparable levels of expression of viral glycoproteins at the plasma membrane. Correlative fluorescence scanning electron microscopy revealed that formation of budding structures at the cell surface is inefficient in MDM even though clustering of a viral glycoprotein, hemagglutinin (HA), is observed, suggesting that a step in IAV particle assembly is blocked in MDM. Using an *in situ* proximity ligation assay, we further determined that HA associates with neuraminidase (NA) but fails to associate with another viral transmembrane protein M2 at the MDM plasma membrane. Notably, the defects in HA-M2 association and particle assembly in MDM were reversed upon cytochalasin D treatment that inhibits actin polymerization. These results suggest that HA-M2 association on the plasma membrane is a discrete step in IAV production, which is susceptible to suppression by actin cytoskeleton in MDM. Virus release remained inefficient in MDM upon cytochalasin D treatment, suggesting the presence of additional defect(s) in virus release in this

cell type. Overall, our study revealed the presence of multiple cell-type-specific mechanisms negatively regulating IAV production at the plasma membrane in MDM.

Introduction

Influenza A virus (IAV) is a negative strand RNA virus that mainly infects and replicates in epithelial cells in the respiratory tract. However, the virus has also been shown to infect other cell types such as macrophages, dendritic cells, and mast cells *ex vivo* [184-186]. Host-cell-specific differences have been observed for various properties of IAV including morphology and replication [for example, [82,187-190]]. These differences could be due to differences in expression levels or functions of host cellular proteins between cell types. In cases where cell-type-specific differences affect productive infection of a virus, detailed comparison between permissive and non-permissive cell types often leads to identification of virus cofactors [189,191-194] or host factors that restrict replication of viruses [190,195-198]. This approach, which often determines the specific function of the host factor of interest even prior to the identity of the factor, can serve as a complementary approach to genome-wide approaches [94-103].

Ex vivo infection studies have shown that in comparison to epithelial cells, macrophages are less permissive or non-permissive to productive infection of seasonal IAV strains [199-205]. Murine macrophages are non-permissive to IAV replication [199,201,205,206]. Primary human blood-derived or alveolar macrophages do support seasonal IAV replication at detectable levels although they are still much less permissive to virus growth than human epithelial cells [200,202,203,206]. As for the defective stages of the IAV life cycle, a block at the entry stage of infection has been identified in murine macrophages for most H1N1 strains [199,201,205]. In addition, the presence of a defect(s) at a later stage has been known for IAV infection in murine macrophages [201,205]. However, there are apparently conflicting data as to whether the defect is

at pre- or post-translation stage [201,205]. Moreover, the mechanism in either case has yet to be determined. In contrast to murine macrophages, human macrophages support early stages of replication of all tested IAV strains yet are unable to complete the virus life cycle [205]. While the defect appears to be post-translational, the exact nature of this defect in human macrophages and the molecular mechanism behind it are not known.

Determining the nature of the human macrophage-specific defect in IAV replication is likely to advance our understanding of the roles played by cellular functions in late phases of the IAV life cycle and potentially facilitate identification of human host factors involved in this process. In the current study, we used primary human monocyte-derived macrophages (MDM) in order to identify the defective step in IAV replication in human macrophages. We show that MDM support early stages of the IAV assembly process, i.e. trafficking of the viral glycoproteins hemagglutinin (HA), neuraminidase (NA), and the ion channel protein M2 to the plasma membrane, but are inefficient at virus particle formation and subsequent virus release. This defect in virus particle formation and release is specific to primary MDM, since a monocytic cell line THP1 differentiated into macrophage-like cells supports efficient virus particle production. Notably, we observed that the association of HA with M2 on the plasma membrane, as determined by the close proximity of <40 nm, is highly inefficient in MDM relative to the differentiated THP1 cells. In contrast, HA and NA associate efficiently on the surface of MDM. The defective association between HA and M2 is rescued in MDM upon treatment with an actin polymerization inhibitor, cytochalasin D, whereas this defect is recreated in differentiated THP1 cells by treatment with jasplakinolide, which promotes actin polymerization. Consistent with the restoration of HA-M2 association in MDM, treatment with cytochalasin D also increases formation of budding structures in this cell type. However, virus

release is not restored in MDM upon cytochalasin D treatment, suggesting the presence of an additional block in IAV assembly/release in this cell type. Overall, this study has identified virus particle formation, more specifically association between HA and M2, as a step defective in IAV life cycle in primary human macrophages and revealed that this macrophage-specific block of IAV assembly requires actin polymerization.

Materials and Methods

Cells and reagents: Monocytes were isolated by plate adhesion from peripheral blood mononuclear cells, which were obtained from buffy coats derived from unidentified healthy donors (New York Blood Center, NY). Cells were cultured in RPMI 1640 (Gibco) supplemented with 10% fetal bovine serum (FBS, Hyclone) for 7 days before they were used for experiments. THP1 (ATCC® TIB202™) cells were cultured in RPMI 1640 supplemented with 10% FBS, 1 mM Sodium Pyruvate (Gibco) and 0.05 mM 2-mercaptoethanol. To generate differentiated THP1 cells (dTHP1), THP1 cells were cultured in the medium containing 0.1 μM phorbol 12-myristate 13-acetate (PMA; Sigma) and 0.1 μM Vitamin D3 (Sigma) for 2-3 days. Madin-Darby canine kidney (MDCK) cells were provided by Dr. Arnold S. Monto (University of Michigan) and were cultured in DMEM (Gibco) supplemented with 10% FBS and 25 mM HEPES. Human lung carcinoma cell line A549 was provided by Dr. Mike Bachman (University of Michigan) and was cultured in DMEM (Gibco) supplemented with 10% FBS and 25 mM HEPES. Human embryonic kidney-derived 293T cell line (ATCC) was cultured and maintained in DMEM (Lonza) supplemented with 10% FBS.

The following antibodies were used for immunofluorescence microscopy: mouse anti-HA monoclonal antibody (clone C179 [207]; Takara), mouse anti-M2 monoclonal antibody (clone

14C2 [93]; Thermofisher), mouse anti-vRNP monoclonal antibody (clone 61A5 [114]; a kind gift from Dr. Fumitaka Momose, Kitasato University), goat anti-HA antiserum (BEI NR-3148), mouse anti-transferrin receptor (TfR) monoclonal antibody (clone M-A712; BD Biosciences). Rabbit anti-NA antiserum was a kind gift from Dr. Christopher Brooke (University of Illinois). Mouse anti-actin (ACTN05) was purchased from Thermofisher. All secondary antibodies used for immunofluorescence and Alexa Fluor 488-labeled phalloidin were purchased from Thermofisher. Cytochalasin D and jasplakinolide were purchased from Sigma and re-constituted in DMSO and 100% Ethanol, respectively.

Plasmids and virus stocks: A/WSN/1933 (H1N1) virus was generated by reverse genetics [208] using the 8 pPolI plasmids encoding different segments of IAV genome and the 4 pCAGGS plasmids that express the PA, PB1, PB2, and NP proteins. The titers of the stocks were determined using the plaque assay with MDCK cells. A/Wyoming/03/2003 (H3N2) [Wyoming (H3N2)], A/Panama/2007/1999 (H3N2) [Panama (H3N2)], and A/California/04/2009 (H1N1) [California (H1N1)] viruses were kind gifts from Dr. Arnold S. Monto (University of Michigan) and were received as low passage stocks (less than 5 passages in MDCK cells) of virus isolated from clinical specimen. Virus infection was performed and monitored using the plaque assay and flow cytometry as described in Supplementary Information.

Measurement of vRNA levels: Virus-containing cell culture supernatants were centrifuged at 3000 rpm for 5 minutes in a microfuge, filtered through a 0.45-μm filter, and subjected to ultracentrifugation at 30,800 rpm (AH650 swinging bucket rotor, Thermofisher) for 90 minutes to prepare virus pellets. Virus and cell-associated vRNA was measured using a previously described protocol [209]. Briefly, total RNA was extracted from virus pellets and cell lysates using TRIzol reagent (Ambion) according to the manufacturer's protocol. Complementary DNA

was generated using random hexamer priming and the SuperScript III First-Strand Synthesis System (Invitrogen). Quantitative PCR was performed on a CFX96 Real Time PCR system (Biorad) using Platinum SYBR Green pPCR SuperMiX-UDG (Thermo Scientific Fisher). Serial ten-fold dilutions of pPolI plasmids containing specific viral gene of WSN were used to generate a standard curve for quantification of cDNA copy number based on cycle threshold (Ct) values. The primer sequences are shown in Supplementary Information.

Correlative fluorescence and scanning electron microscopy (CFSEM): CFSEM experiments were performed as described before [210]. Briefly, cells cultured on gridded coverslips (Bellco Biotechnology) were infected with WSN at MOI 0.1. Cells were fixed with 4% PFA in PBS at 20 hpi. After rinsing in PBS, quenching of PFA with PBS containing 0.1 M glycine (Sigma), and blocking with PBS containing 3% bovine serum albumin (BSA, Sigma), cells were immunostained with mouse anti-HA and fluorescently labeled secondary antibody. Cells were imaged using a Leica Inverted SP5X Confocal Microscope with a 40× PL APO objective and 10-20× scanning zoom. After fluorescence imaging, cells were fixed with PBS containing 2.5% glutaraldehyde (Electron Microscopy Sciences), stained with 1% OsO_4,dehydrated in a series of ethanol washes, rinsed in hexamethyldisilazane (Electron Microscopy Sciences) and allowed to dry overnight. Coverslips were affixed to specimen mounts and sputter coated with gold for 90 s (Polaron). Cells were identified by their location on the gridded coverslip and imaged on an Amray 1910FEG scanning electron microscope at 5-10 kV. Fluorescence and SEM images were roughly brought into registration by scaling and rotating images in Adobe Illustrator, similarly to other correlative fluorescence/SEM studies [210]. Landmarks used for registration included cell edges. Cell surface structures visible in SEM were manually classified as virus-like buds if they appeared spherical and near 100 nm in diameter. To identify HA clusters in fluorescence images

unambiguously, we removed uniform non-puncta HA signal from the images. To do this, we calculated a 20-pixel radius median filter and subtracted the median filtered image from the original using the *Image Calculator* function in ImageJ. Number of HA-positive puncta was measured in the background-subtracted fluorescence images using the *Analyze particle* function in ImageJ. Since MDM have substantial membrane folds on the cell surface especially towards the center of the cell, we focused on areas towards the edge of the cells, which have a flatter topology, for quantification of efficiency of virus bud formation.

***In situ* Proximity Ligation Assay (PLA):** PLA was performed using Duolink® PLA fluorescence kit following the manufacturer's instruction (Sigma). Cells fixed with 4% PFA (non-permeabilized) were incubated with following primary antibody combinations: goat anti-HA and mouse anti-M2 for PLA and rabbit anti-NA for identification of infected cells; mouse anti-HA and rabbit anti-NA for PLA and goat anti-HA for identification of infected cells; or goat anti-HA and mouse anti-TfR for PLA and rabbit anti-NA for identification of infected cells. Detection of PLA signals and identification of infected cells were performed using PLA probes specific to goat, mouse or rabbit IgG and AlexaFluor-488-labeled secondary antibody recognizing anti-NA or anti-HA, respectively. Cells were observed using a Leica Inverted SP5X Confocal Microscope System with a 63X objective. Z-stacks extending from the focal plane corresponding to the middle plane of the nucleus (identified by DAPI staining) to the bottom of cells were acquired for each cell, and the maximum intensity projection for each cell was constructed using ImageJ. The PLA signal in projection images was thresholded to eliminate weak and hazy background signal in the nucleus, and the number of PLA-positive spots was counted using the *Analyze particle* function in ImageJ.

Actin fractionation assay: Actin fractionation was performed as previously described [211]. Briefly, dTHP1 cells were treated with 0.5% ethanol (vehicle) or 1 μM jasplakinolide for 4 hours. Cells were incubated with cytoskeleton stabilization buffer (4M glycerol, 25 mM Pipes pH 6.9, 1mM EGTA, 1mM $CaCl_2$) containing 0.1% TritonX-100 for 2-3 minutes. Cells were centrifuged for 5 minutes at 7,500 g at 4°C. The pellet was re-suspended in the cytoskeleton stabilization buffer. Supernatant (S) and pellet (P) fractions were run on a reducing and denaturing polyacrylamide gel and analyzed by immunoblotting.

Statistical analysis: Statistical analyses were performed using GraphPad Prism version 7. Two-tailed paired student *t* test was used to calculate p-values in Figures 2.1-2.5, 2.8, 2.10, and 2.12. Two-tailed unpaired student *t* test was performed in Figures 2.6, 2.7, 2.9, 2.11, 2.13, and 2.15.

Results

MDM are inefficient in supporting productive IAV infection relative to differentiated THP1 cells

To determine the extent to which human epithelial cells and macrophages differ in their ability to support productive IAV infection, we compared infectious IAV release from three different human cell types: the lung-derived epithelial cell line A549, the monocytic cell line THP1, which has been differentiated to adopt macrophage-like morphology (dTHP1), and primary monocyte-derived macrophages (MDM). The dTHP1 cells were obtained via treatment of THP1 cells with phorbol 12-myristate 13-acetate (PMA) and vitamin D3 for 2-3 days. A549, dTHP1, and MDM were infected with the laboratory strain A/WSN/1933 (H1N1) (WSN) at MOI 0.01 based on the plaque forming units of virus stocks determined using MDCK cells. At 11 hours post infection (hpi), we observed that virus titers in MDM culture supernatants were up to 100-fold reduced in comparison to that in A549 culture supernatants. Unexpectedly, virus titers

in culture supernatants were similar between A549 and dTHP1 cells (Figure 2.1A). Since dTHP1 cells support influenza virus replication efficiently unlike MDM and yet belong to the same cellular lineage, to facilitate the analyses of MDM-specific defect(s), we chose to compare IAV replication in MDM with that in dTHP1 cells in subsequent experiments. We noticed that while MDM isolated from the vast majority of the tested human donors showed a defect in productive IAV infection relative to dTHP1 at 24 hpi (denoted as Group 1 in Figure 2.1B), MDM from some donors (denoted as Group 2 in Figure 2.1B; ~20%) showed no significant difference. The differences between the two groups of MDM could be due to differences in the genetic background and/or the infection history of the donors. Therefore, to identify the MDM-specific defect, the subsequent experiments were performed using MDM from the donors in Group 1. In particular, in the mechanistic experiments (Figures 2.6, 2.7, 2.9, and 2.11), we verified in each experiment that MDM used show 10-20 fold reduction in the supernatant virus titers or released vRNA relative to dTHP1 cells at the indicated time point of the corresponding assays (data not shown).

To assess whether other IAV strains also replicate inefficiently in MDM relative to dTHP1 cells, we compared productive infection in dTHP1 cells and MDM of three previously or currently circulating IAV strains, in addition to WSN: A/Wyoming/03/2003 (H3N2) [Wyoming (H3N2)], A/Panama/2007/1999 (H3N2) [Panama (H3N2)], and A/California/04/2009 (H1N1) [California (H1N1)]. Infectious virus titers of all tested IAV strains, as measured by the plaque assay, were reduced by 10-50-fold in MDM in comparison to dTHP1 cells (Figure 2.1C). These data suggest that MDM are highly inefficient at producing infectious IAV particles in comparison to dTHP1 cells.

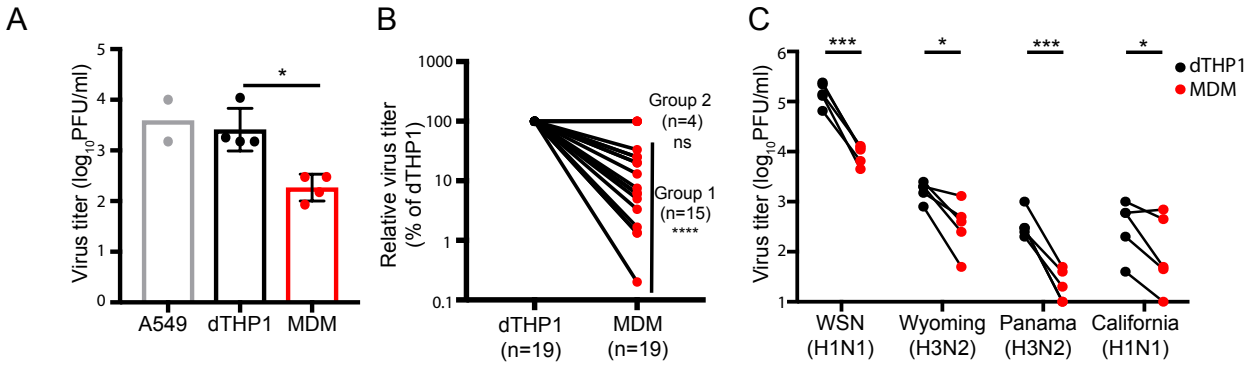

Figure 2.1: MDM are defective in productive IAV infection. (A) A549 cells, dTHP1 cells and MDM were infected with WSN at MOI 0.01. Infectious virus titers in culture supernatants were measured at 11 hpi. (B) Infectious virus titers in culture supernatants were measured for WSN-infected dTHP1 cells and MDM at 24 hpi. For all tested donors, the relative virus titers in MDM cultures were calculated in comparison to the titer in dTHP1 cell cultures tested in parallel within the same experiment. Two groups of donors (Groups 1 and 2) were denoted based on the reduction in the titers or lack thereof. For Group 1, the values for virus titers were in the range 1.9-5.07 $\log_{10}$ PFU/ml. For Group 2, the values were identical to those of corresponding dTHP1 cultures and in the range 4.39-5.17 $\log_{10}$ PFU/ml. (C) dTHP1 and MDM (Group 1) were infected with the given IAV strains at MOI 0.01, and infectious virus titers in culture supernatants at 24 hpi were determined by plaque assays using MDCK cells that have been passaged 20-30 times. Each circle represents an independently prepared culture. A black and a red circle connected by a line represent each independent experiment. For panel A, data are shown as mean +/- SD. *, P<0.05; ***, P<0.001; ****, P<0.0001; ns, non-significant.

Both efficiency of virus release and infectivity of released particles are impaired in infected MDM relative to infected dTHP1 cells

The results shown above and the results of time-course experiments suggest that infectious virus release is reduced in MDM relative to dTHP1 cells even though flow cytometry using anti-vRNP antibody (clone 61A5 [114]) showed that similar fractions of cells in the cultures are infected (Figures 2.1 and 2.2). We sought to address whether the reduction in viral titers in MDM culture supernatants is due to a reduction in infectivity of released particles or whether it is due to a reduction in release of physical particles. To this end, we used viral RNA (vRNA) release as a surrogate to measure release of physical particles from dTHP1 cells and MDM. Number of vRNA copies released from MDM were 7-8-fold reduced in comparison to that from dTHP1

cells for all eight vRNA segments. However, there were no significant decrease in cell-associated vRNA levels in MDM relative to dTHP1 cells, indicating that MDM support viral RNA replication and earlier steps as efficiently as dTHP1 cells. vRNA release efficiency was calculated as the ratio of number of vRNA copies in virus pellets from cell culture supernatants to the total number of vRNA copies (cell + virus). For all eight vRNA segments, we observed a 5-10-fold reduction in vRNA release efficiency in MDM relative to dTHP1 cells (Figure 2.3A). We also measured vRNA release efficiency in dTHP1 cells and MDM after a single round of virus replication (Figure 2.3B). To block virus entry after the first round on infection, cells were treated with media containing 10 μg/ml C179, a neutralizing antibody that binds to the HA stem [207,212], at 2 hpi. At 12 hpi, we observed a 2-3 fold reduction in vRNA release efficiency in MDM relative to dTHP1 cells. These data suggest that efficiency of physical viral particle release from MDM is reduced in comparison to that from dTHP1 cells in the context of both single and multiple rounds of virus replication. Notably, virus spread, as determined by the increase in number of infected cells over time, is still supported in MDM as efficiently as in dTHP1 cells (Figure 2.2), suggesting that MDM allow for virus spread by mechanisms independent of cell-free infectious viruses.

Importantly, the reduction in vRNA release (7-8-fold) from MDM does not entirely account for reduction in infectious virus release (up to 50-fold) (Figure 2.3C). The ratio of released PFU (representing infectious virions) to released vRNA (representing total number of particles) was calculated as the infectivity per particle. Infectivity per particle for virus particles released from MDM was 5-6-fold reduced versus that released from dTHP1 cells (Figure 2.3C). Overall, our data suggest that the total number of virus particles released as well as the infectivity of released virus particles is reduced in MDM relative to dTHP1 cells.

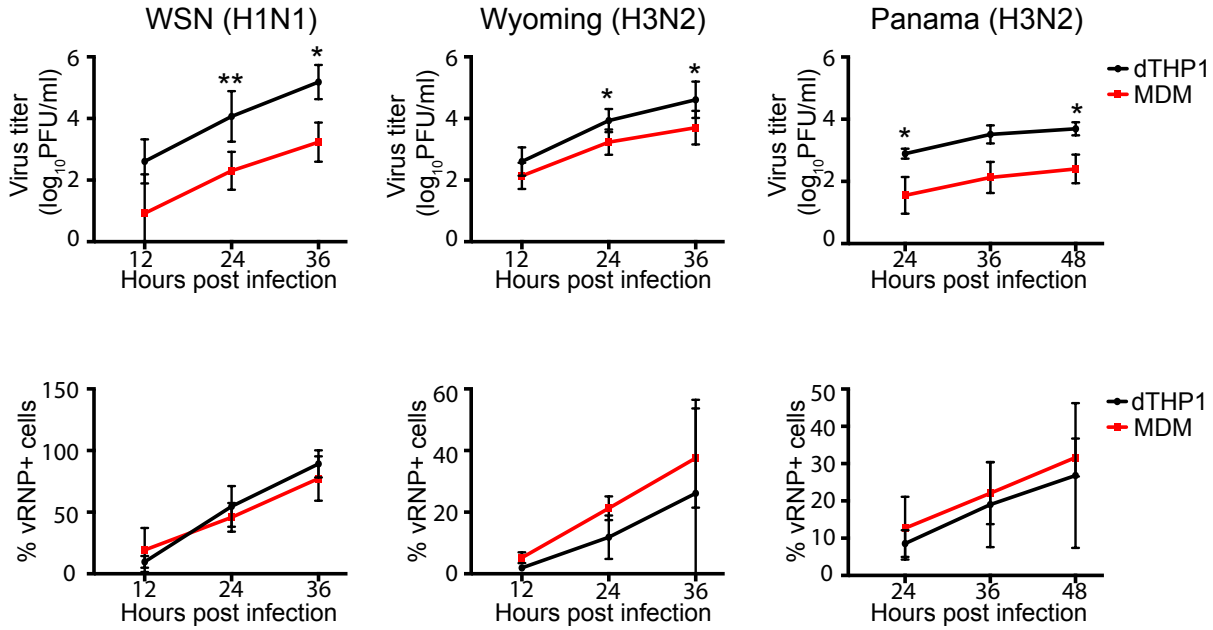

Figure 2.2: Infectious virus release is reduced in MDM cultures relative to dTHP1 cells despite similar number of infected cells in both cultures. dTHP1 cells and MDM were infected with given IAV strains at MOI 0.01. At the indicated time points post infection, culture supernatants and cells were collected and assessed for virus titer (top panels) and % vRNP+ cells (lower panels), respectively. Data from at least three independent experiments are shown as mean +/- SD. *, P<0.05; **, P<0.01.

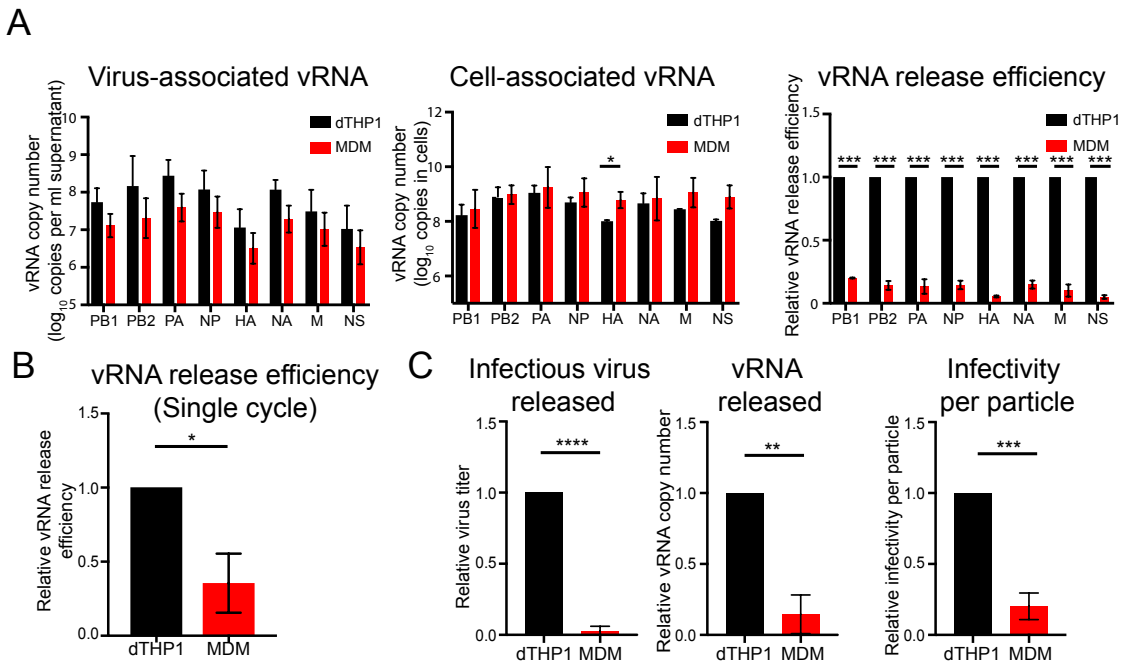

Figure 2.3: Both efficiency of virus release and infectivity of released particles are reduced in MDM than in dTHP1 cells. dTHP1 cells and MDM were infected with WSN at MOI 0.1. (A) vRNA copy numbers were measured in lysates of virus pelleted from cell culture supernatants and cell lysates at 20 hpi. vRNA release efficiency was calculated as the ratio of number of vRNA copies in virus lysates versus total number of vRNA copies (cell + virus) for each vRNA segment. Note that differences between dTHP1 cells and MDM were not significant for virus-associated and cell-associated vRNA levels when compared as pooled data in most cases (except for cell-associated HA vRNA). However, vRNA release efficiency calculated for individual experiments showed a significant reduction in MDM cultures relative to dTHP1 cell cultures. (B) vRNA release efficiency was measured for infected dTHP1 cells and MDM at 12 hpi. To prevent the second cycle of infection, 10 µg/ml C179 was added to the cultures at 2 hpi. (C) PB2 vRNA copy number and virus titer were measured in dTHP1 and MDM culture supernatants at 16 hpi. Infectivity per particle was calculated as the ratio of virus titer to PB2 vRNA copy number in culture supernatants. Data are from experiments done with MDM from at least three independent donors and shown as mean +/- S.D. *, P<0.05; **, P<0.01; ***, P<0.001, ****, P<0.0001.

Formation of budding structures is inefficient in MDM relative to dTHP1 cells despite similar levels of viral glycoprotein expression at the plasma membrane

We observed using flow cytometry that total expression levels of vRNP, HA, and M1 are comparable between dTHP1 cells and MDM in both the size of positive cell populations and the expression levels per cell (Figure 2.4), indicating that protein translation and earlier steps are unlikely to be impaired in MDM. Henceforth, we focused on steps post viral protein translation:

virus assembly, budding and release. Virus assembly is initiated by targeting of the glycoproteins HA and NA to the plasma membrane [17,18,21]. The third transmembrane protein M2 is also recruited to the assembly sites at the plasma membrane and allows for completion of the virus budding process [16,18]. To determine whether trafficking of the three glycoproteins occurs similarly in dTHP1 cells and MDM, we next compared levels of HA, NA and M2 proteins on the surface of WSN-infected cells. We found that sizes of cell populations positive for surface expression of the three proteins are comparable between MDM and dTHP1 cells (Figures 2.5A and 2.5B). The mean fluorescence intensity (MFI) for the three viral proteins in positive cell populations was also similar between MDM and dTHP1 cells (Figure 2.5C), indicating that trafficking of viral glycoproteins to the plasma membrane is comparable between MDM and dTHP1 cells.

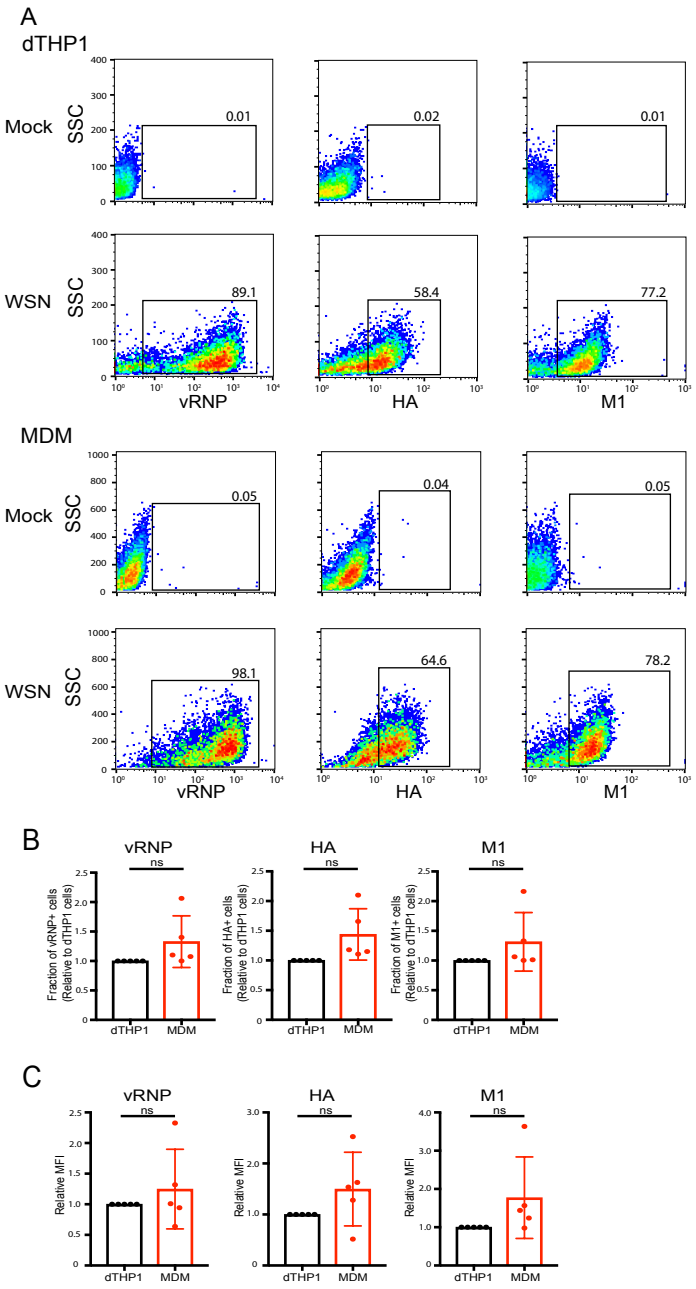

Figure 2.4: MDM express viral proteins as efficiently as dTHP1 cells. dTHP1 cells and MDM were infected with WSN at MOI 0.01 for 24 hours. Infected cells were fixed, permeabilized and analyzed for cellular levels of vRNP, HA and M1 by flow cytometry. (A) Representative flow plots for mock- and WSN-infected cells are shown. Gates for positive cell populations were set in comparison to mock-infected cells. Due to differences in the side scatter (SSC) profile between dTHP1 cells and MDM, the Y-axis (SSC) range is different between the two cell types. (B) Percentages of cells positive for vRNP, HA, and M1 are compared between dTHP1 and MDM. (C) MFIs (normalized to dTHP1 cells) for all three viral components are shown for positive cell populations (gated in panel A). Data are from at least three independent experiments and are shown as mean +/- SD. ns, non-significant.

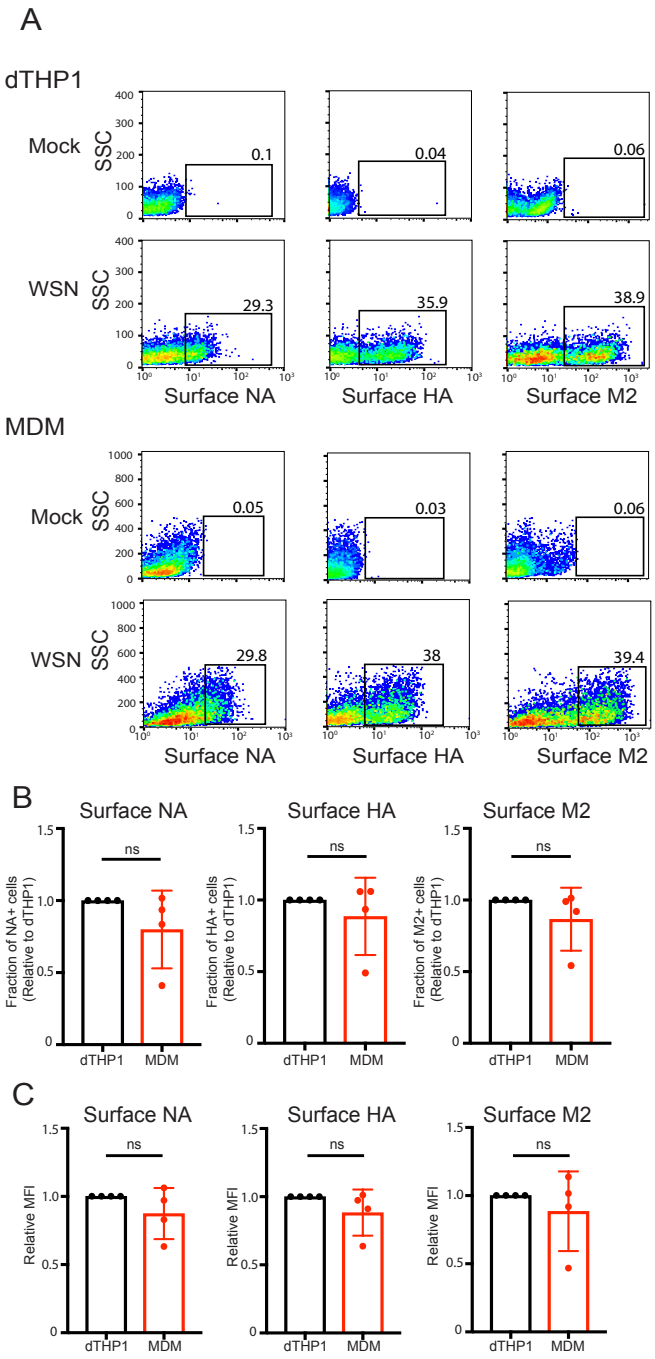

Figure 2.5: MDM are efficient at trafficking of viral glycoproteins to the cell surface. dTHP1 cells and MDM were infected with WSN at MOI 0.1. (A) Infected cells were analyzed for cell surface expression of HA, NA, and M2 by flow cytometry at 16 hpi. Representative flow plots for mock-infected (top row) and virus-infected (bottom row) cells are shown. Percentages of cells positive for viral proteins (boxed) are shown. Due to differences in the side scatter (SSC) profile between dTHP1 cells and MDM, the Y-axis (SSC) range is different between the two cell types. (B) Percentages of cells positive for surface expression of NA, HA, and M2 are compared between dTHP1 and MDM. (C) Relative MFIs for surface signal of indicated proteins for positive cell populations (gated in panel A) are shown. Data are shown as mean +/- SD and are from at least three independent experiments. ns, non-significant.

We next asked whether dTHP1 cells and MDM expressing HA on the cell surface support virus particle formation. To address this question in a single cell basis, we performed correlative fluorescence and scanning electron microscopy (CFSEM) in which we first identify cells with surface HA expression using fluorescence microscopy and then examine formation of virus particle-like buds on the surface of the same cells using scanning electron microscopy (SEM). Fluorescence microscopy showed that HA is uniformly distributed on the surface of both dTHP1 cells and MDM with some local accumulation. These HA-enriched clusters or puncta, which likely represent sites of virus assembly, were clearly distinguished on the surface of infected cells after the median filter was applied to the confocal images to remove signal for uniformly distributed non-punctate HA. These HA-enriched sites often corresponded to budding structures with a diameter of approximately 100 nm on the surface of WSN-infected dTHP1 cells (Figure 2.6A). Very few budding structures with the similar size were observed on the surface of mock-infected cells. MDM also form ~100-nm virus particle-like buds on the surface in HA-positive cells, albeit the number of buds observed in MDM were markedly lower than in dTHP1 cells (Figure 2.6A). To assess the formation of budding structures quantitatively, we counted the number of HA-positive puncta and the number of virus particle-like buds within the same sized area (100 μm^2 in size) of each cell. Even though MDM showed higher numbers of HA-positive puncta on the cell surface than dTHP1 cells, the numbers of virus buds were drastically reduced in MDM relative to dTHP1 cells (Figure 2.6B). Overall, these results indicate that virus particle assembly/budding are inefficient in MDM despite efficient trafficking of HA, NA and M2 to the plasma membrane.

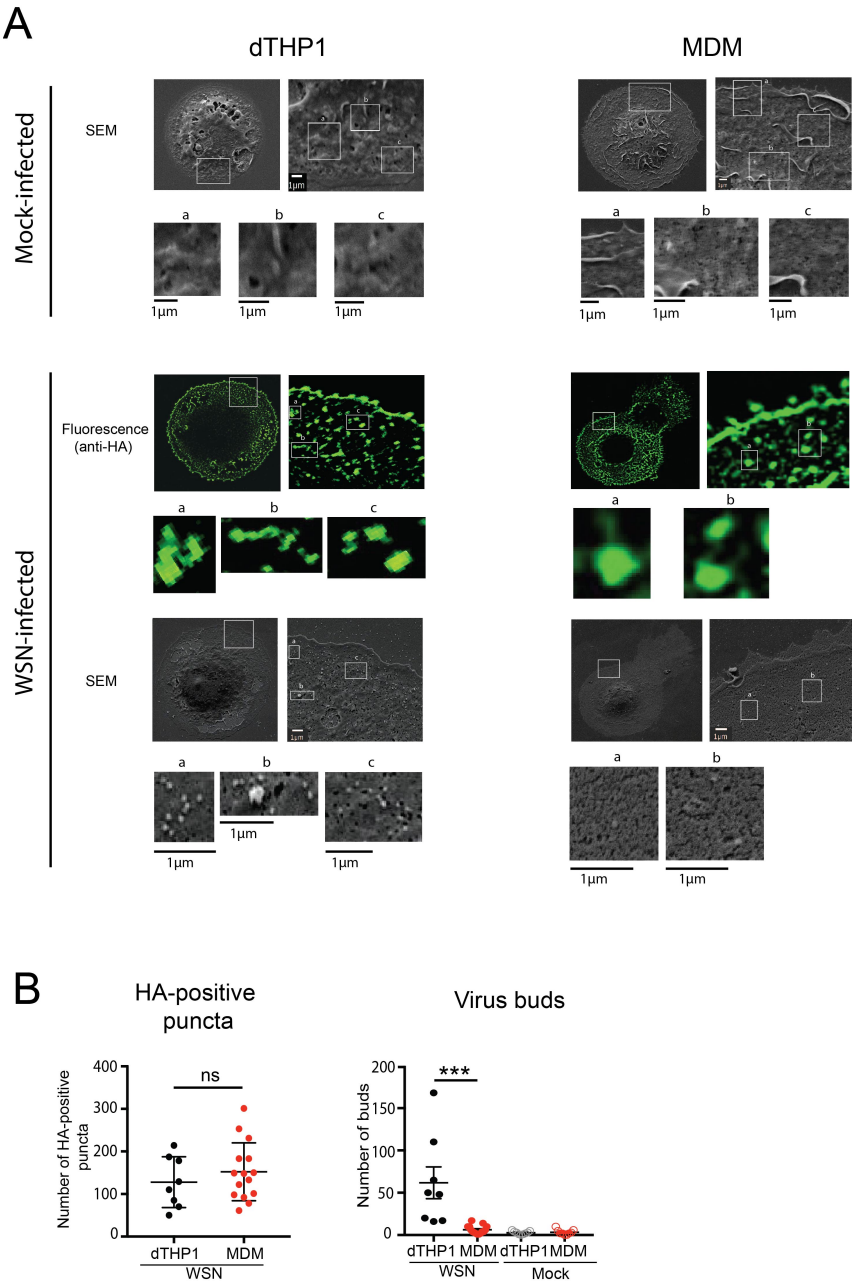

Figure 2.6: MDM are defective in virus bud formation despite expression of HA on the cell surface. dTHP1 cells and MDM grown on gridded coverslips were infected with WSN at MOI 0.1 for 20 hours. Cells were fixed and immunostained with anti-HA. After identification of HA-positive cells by confocal microscopy, cells were prepared for SEM. The same cells were identified based on grid positions and analyzed by SEM. (A) Representative SEM images for mock-infected and WSN-infected HA-positive cells are shown in the top and bottom rows, respectively. For WSN-infected cells, fluorescence images corresponding to the SEM images of WSN-infected cells are shown. Boxed areas are magnified and shown below the original images. Alphabetic labels are used to distinguish between individual boxed areas. (B) The number of HA-positive puncta identified in fluorescence images (left panel) and ~100-nm buds identified in SEM images (right panel) were counted within the same sized area (100 μm^2 in size) in each cell. Data are shown for 8-15 cells from two independent experiments. Error bars represent standard error of mean. ***, P<0.0001; ns, non-significant.

Association between HA and M2 is impaired in MDM but not in dTHP1 cells

Based on results shown above, we hypothesize that local co-enrichment of HA, NA and M2, which leads to formation of virus assembly sites, is not efficient in MDM relative to dTHP1 cells. To compare formation of the putative assembly sites between dTHP1 cells and MDM, we used *in situ* proximity ligation assay (PLA). PLA allows for detection of two proteins localized within 40-nm distance of each other and has been used to visualize IAV assembly sites on the plasma membrane [42]. In addition to measuring PLA signal between the given pair of proteins, we also co-stained cells for cell surface NA to identify infected cells. As a negative control, we performed PLA between HA and transferrin receptor (TfR). TfR does not associate with lipid rafts [213], the plasma membrane microdomains associated with IAV assembly sites [18,22]. Infected dTHP1 cells showed high PLA signal for HA-M2 association. In contrast, infected MDM showed very few PLA spots between HA and M2 (Figures 2.7A and 2.7C). As expected, no PLA signal was observed between HA and M2 in mock-infected cells or between HA and TfR in infected cells (Figure 2.7A). The majority (80-90%) of surface NA-positive MDM and dTHP1 cells express HA and M2 on their surface at comparable levels (Figure 2.8). Therefore, the significant reduction in HA-M2 PLA signal in MDM relative to dTHP1 cells is not due to the lack of expression of HA and/or M2 in NA-positive cells.

To determine whether the defect in association between transmembrane proteins in MDM is specific to HA and M2 or whether association between other pairs of viral transmembrane proteins is defective as well, we next measured PLA signal between HA and NA. In this case, to identify infected cells, we co-stained cells for cell surface HA using an antibody different from the one used for PLA. PLA signal between HA and NA was similar for dTHP1 cells and MDM, suggesting that HA and NA associate with each other as efficiently on the surface of MDM as on

dTHP1 cells (Figures 2.7B and 2.7C). Overall, our data indicate that association between HA and M2 is a virus assembly step specifically impaired in MDM.

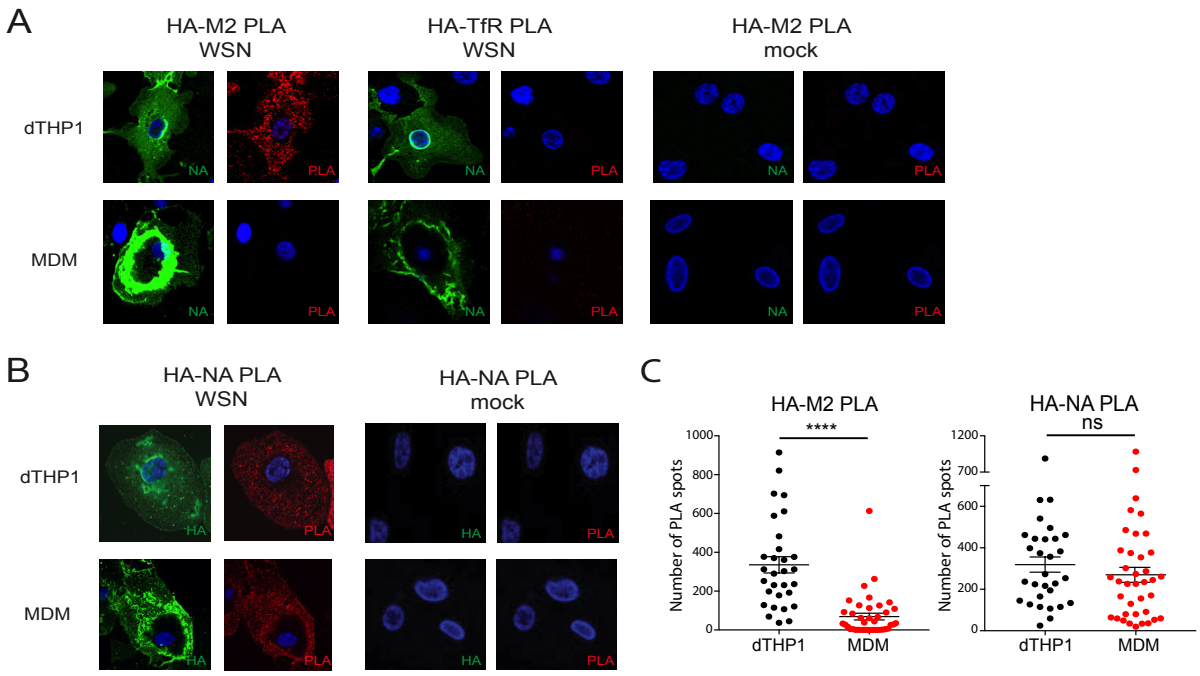

Figure 2.7: Association between HA and M2 is defective in MDM relative to dTHP1 cells. dTHP1 cells and MDM were infected with WSN at MOI 0.1 for 16 hours. (A) Cells were examined by PLA using goat anti-HA and mouse anti-M2 or goat anti-HA and mouse anti-TfR antibodies. To identify infected cells, surface NA was also detected by rabbit anti-NA. Nuclei were stained with DAPI (blue). Representative maximum intensity projection images, which were reconstructed from z-stacks corresponding to the focal planes ranging from the middle plane of the nucleus to the bottom of the cells, are shown. (B) Cells were examined by PLA using mouse anti-HA and rabbit anti-NA antibodies. Goat anti-HA was used for detection of infected cells. Representative maximum intensity projection images are shown as in panel A. Note regions of intense NA (in A) and HA (in B) signal on the surface of MDM due to the presence of membrane ruffles. (C) Number of PLA spots were counted for each cell. Data are shown for three independent experiments, and 8-10 cells were analyzed per experiment. These experiments were performed in parallel with the experiments shown in Figure 3 using MDM from the same donors. Error bars represent standard error of mean. ****, $p < 0.0001$; ns, non-significant.

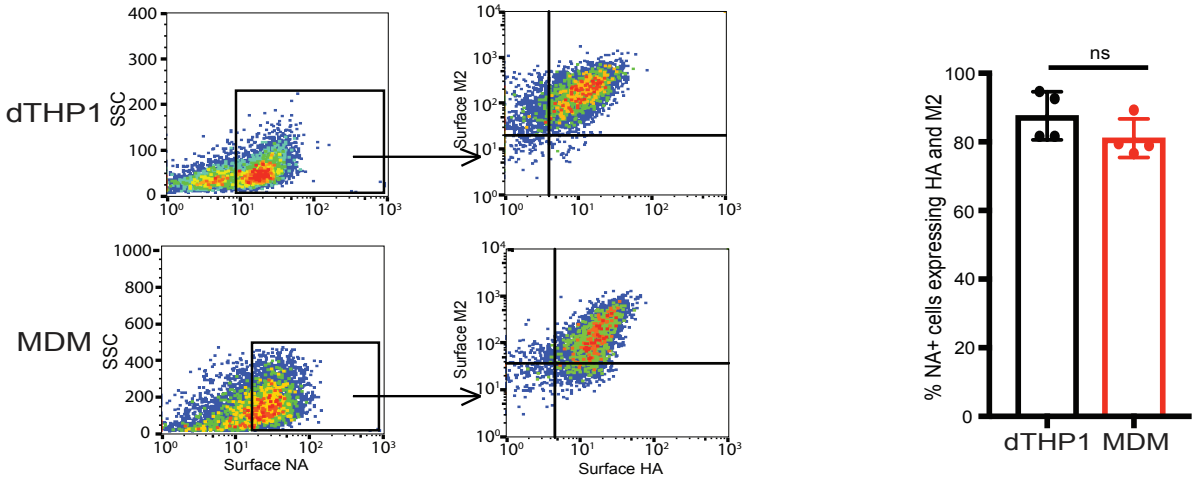

Figure 2.8: Majority of NA-expressing dTHP1 cells and MDM co-express both HA and M2. dTHP1 cells and MDM were infected with WSN at MOI 0.1 for 16 hours. Cells were fixed and stained for surface HA, M2, and NA. Representative plots are shown in the left panel. % cells expressing HA and M2 within the NA-positive cell population were determined and shown in the right panel. Data are from at least three independent experiments and shown as mean +/- SD. ns, non-significant.

Inhibition of actin polymerization increases HA-M2 PLA and bud formation in MDM

HA associates with lipid rafts on the plasma membrane, while M2 mainly localizes in non-lipid raft areas [18,22]. It is suggested that M2 is recruited to cholesterol-rich lipid rafts during IAV particle assembly [25,86]; however, host cell functions and factors that regulate this step are not known. It is possible that in MDM, HA-containing plasma membrane microdomains stay segregated from those containing M2, leading to defective association between the two glycoproteins. The cortical actin cytoskeleton, a network of filaments that underlies and interacts with the plasma membrane, is suggested to play a role in formation and maintenance of plasma membrane microdomains [143-145]. Therefore, we next asked whether the actin network regulates the association between HA and M2 in dTHP1 cells and MDM. Infected cells were treated with cytochalasin D (Cyto D), an inhibitor of actin polymerization, at 14 hpi for 2 hours, fixed, and

examined for HA-M2 association using PLA. Phalloidin staining confirmed that Cyto D disrupts the cellular actin network in both dTHP1 cells and MDM under these treatment conditions (Figure 2.10A). Infected dTHP1 cells showed high PLA signal for HA-M2 association under both vehicle-and Cyto D-treated conditions. As observed in Figure 2.7A, vehicle-treated MDM showed very few PLA spots between HA and M2. In contrast, Cyto D-treated MDM showed PLA signal between HA and M2 at levels similar to that observed for dTHP1 cells (Figures 2.9A and 2.9B). No PLA signal was observed between HA and TfR in untreated or Cyto D-treated dTHP1 cells and MDM. The increase in HA-M2 PLA signal upon Cyto D treatment of MDM was not due to an increase in surface expression of HA and M2 in drug-treated cells, as shown by the flow cytometry analysis (Figures 2.10B and 2.10C). These results suggest that actin polymerization suppresses HA-M2 association in MDM.

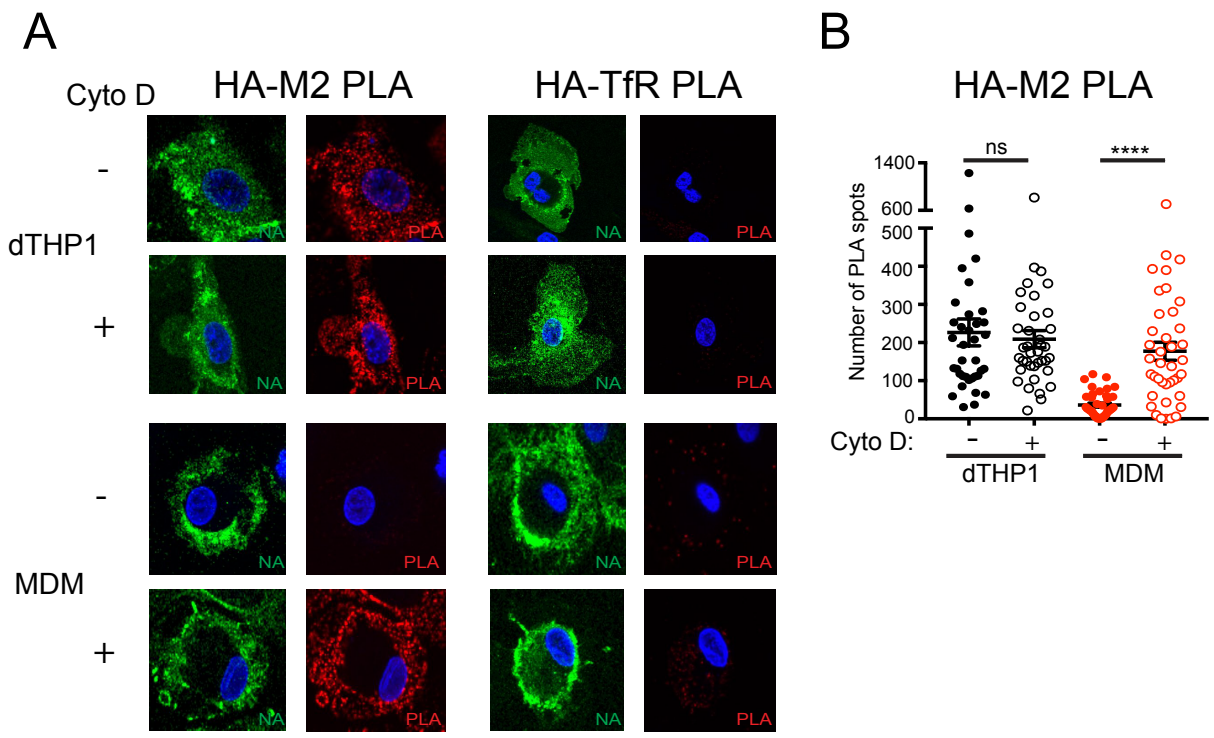

Figure 2.9: Cytochalasin D treatment restores HA-M2 PLA in MDM to levels comparable to that in dTHP1 cells. dTHP1 cells and MDM were infected with WSN at MOI 0.1. At 14 hpi, cells were treated with vehicle control (DMSO) or 20 μM cytochalasin D (Cyto D) for 2 hours before fixation. (A) Cells were analyzed as in Figure 2.7A. Representative maximum intensity projection images are shown. (B) Number of PLA spots were counted for each cell. These experiments were performed in parallel with the experiments shown in Figures 2.8A and 2.8B using MDM from the same donors. Data are from at least three independent experiments, and 8-10 cells were analyzed per experiment. Error bars represent standard error of mean. ****, $p < 0.0001$; ns, non-significant.

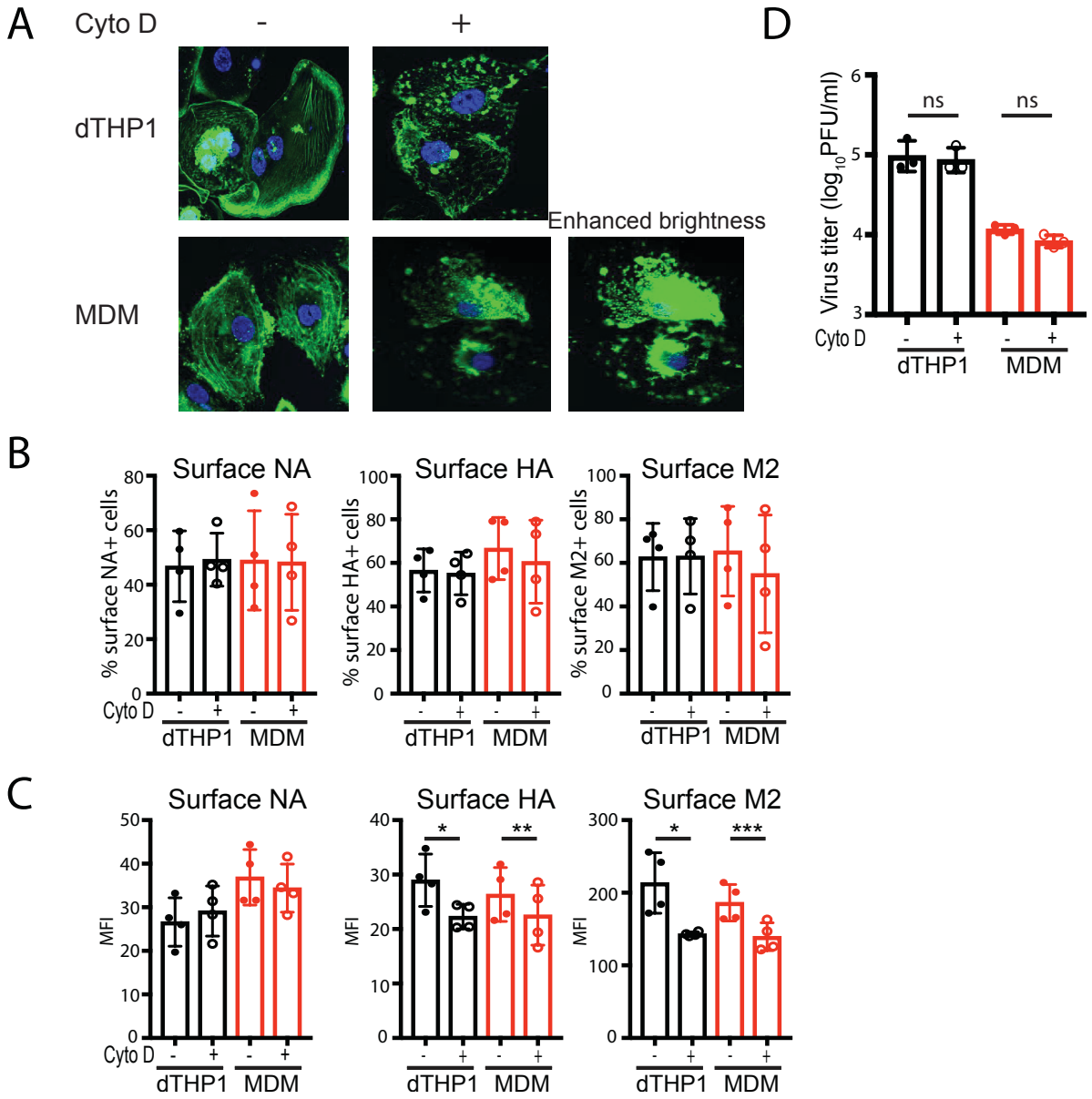

Figure 2.10: Effects of cytochalasin D treatment on the actin cytoskeleton, cell surface expression of viral transmembrane proteins, and released virus titers in dTHP1 cells and MDM. dTHP1 cells and MDM were infected with WSN at MOI 0.1 for 14 hours. Cells were treated with vehicle control (DMSO) or 20 μM Cyto D for 2 hours (A-C) or 4 hours (D). (A) Cells were fixed at 16 hpi, and the actin cytoskeleton was visualized using fluorescently tagged-phalloidin. Images are representative of three independent experiments with 10 cells visualized per experiment. Image with enhanced brightness is also shown for Cyto D-treated MDM. (B and C) Cells were fixed at 16 hpi. % cells expressing HA, NA, and M2 on the cell surface (B) and MFIs for the indicated proteins in positive cell populations (C) are shown. (D) Infectious virus titers released in culture supernatants were measured at 18 hpi. Data are from three independent experiments and shown as mean +/- SD. *, $p<0.05$; **,$p<0.01$; ***$p<0.005$.

We next asked whether treatment with Cyto D restores virus budding in MDM. To this end, we performed CFSEM of dTHP1 cells and MDM treated either with vehicle or Cyto D at 14 hpi for 4 hours and examined virus bud formation in cells expressing HA on the cell surface. We counted the number of virus particle-like buds (~100 nm in diameter) within the same sized area (100 μm^2 in size) of each cell. Consistent with the results shown in Figure 2.6, vehicle-treated, HA-positive MDM showed significantly lower number of buds on the cell surface than vehicle-treated, HA-positive dTHP1 cells. Notably, Cyto D treatment significantly increased the number of buds on the surface of MDM to levels comparable to those in vehicle-treated dTHP1 cells (Figures 2.11A and 2.11B). Cyto D-treated dTHP1 cells showed no significant increase in bud formation relative to vehicle-treated dTHP1 cells. Very few such budding structures corresponding to the size of IAV particles were observed on the surface of untreated or Cyto D-treated, mock-infected dTHP1 cells and MDM (Figure 2.11B). These data suggest that disruption of the actin cytoskeleton promotes IAV particle assembly in MDM. To determine whether the increase in efficiency of bud formation leads to an increase in virus release, we measured the PB2 vRNA release efficiency as shown in Figure 3A. Again, vRNA release efficiency was 4-5 fold reduced in vehicle-treated MDM cultures relative to vehicle-treated dTHP1 cell cultures. Contrary to expectation, Cyto D treatment did not enhance vRNA release efficiency (Figure 2.11C). We also did not observe any increase in infectious virus titers (Figure 2.10D) in supernatants of MDM cultures upon Cyto D treatment. These results indicate that disruption of the actin cytoskeleton promotes virus budding but not virus release. It is conceivable that there is an additional MDM-specific block in the late assembly/release stages of IAV life cycle, which cannot be reversed by Cyto D. Overall, these data show that virus particle assembly, more specifically HA-M2 association, is negatively regulated by the actin cytoskeleton in MDM.

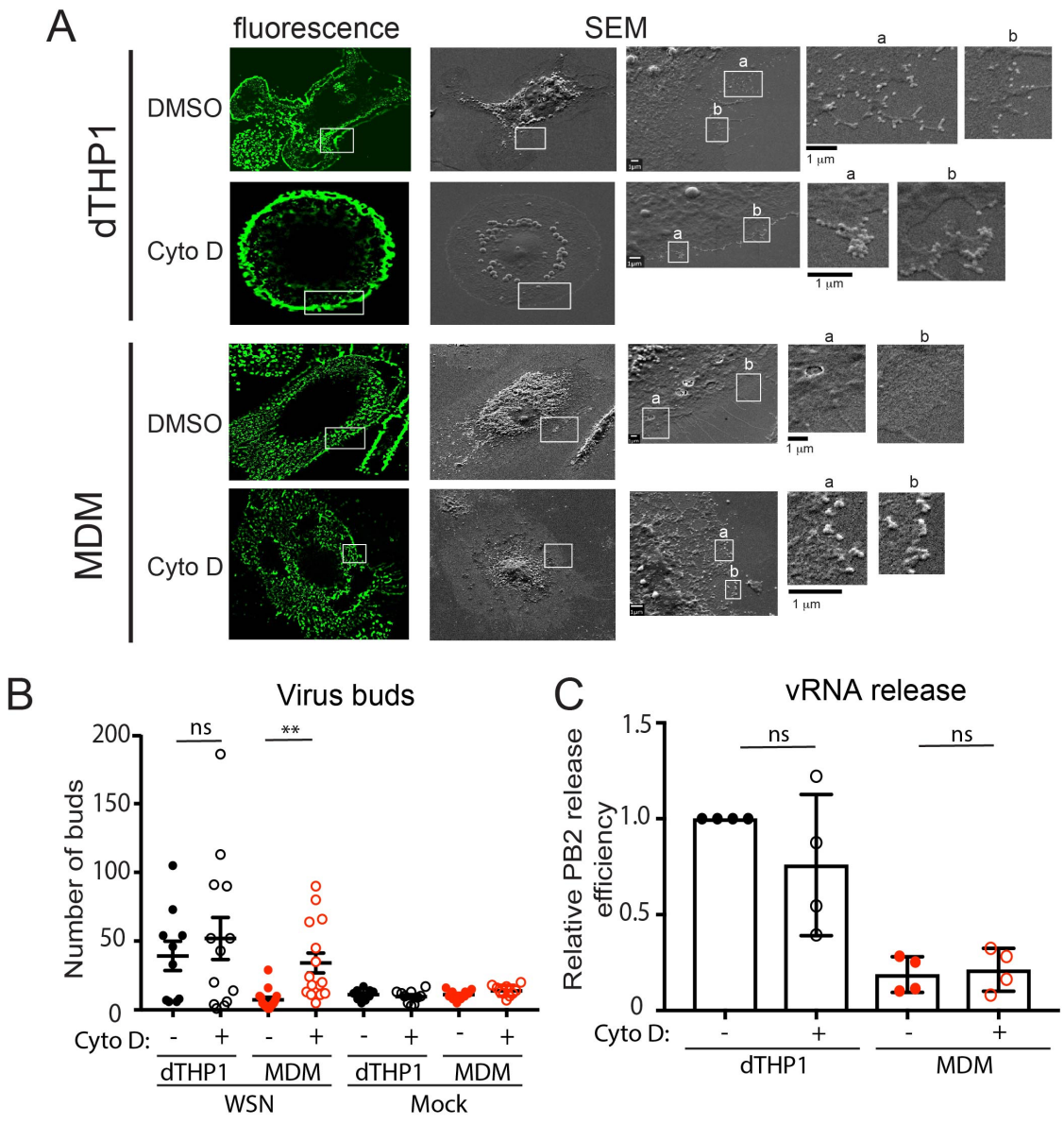

Figure 2.11: Cytochalasin D treatment increases bud formation in MDM to levels comparable to that in dTHP1 cells. dTHP1 cells and MDM were infected with WSN at MOI 0.1. At 14 hpi, cells were treated with vehicle control (DMSO) or 20 μM Cyto D for 4 hours before fixation and immunostaining with anti-HA. After identification of HA-positive cells by confocal fluorescence microscopy, cells were processed for SEM. The same cells were identified based on grid positions and analyzed by SEM. (A) Representative SEM images for WSN-infected HA-positive cells are shown. Fluorescence images corresponding to the SEM images are also included. Boxed areas for SEM images are magnified and shown on the right of original images. Alphabetic labels are used to distinguish between the individual boxed areas. (B) The number of ~100-nm buds identified in SEM images were counted within the same sized area (100 μm^2 in size) in each cell. Data are shown for 10-20 cells from three independent experiments. (C) vRNA release efficiency was measured in infected MDM and dTHP1 cell cultures treated with DMSO or Cyto D for 4 hours. For B, error bars represent standard error of mean. For C, error bars represent SD. **, $P<0.01$; ns, non-significant.

Promotion of actin polymerization reduces HA-M2 PLA in dTHP1 cells

Since inhibition of actin polymerization restores association of HA and M2 in MDM, we next asked whether promoting actin polymerization inhibits HA-M2 association in dTHP1 cells. To this end, infected dTHP1 cells were treated with jasplakinolide (Jasp), which nucleates and stabilizes actin polymerization, at 14 hpi for 2 hours and examined for HA-M2 association using PLA at 16 hpi as in Figure 2.9. Two hours of Jasp treatment reduced HA-M2 PLA in 50% of the examined dTHP1 cells, while the remaining infected cell population showed HA-M2 PLA signal comparable to that in untreated cells (data not shown). We reasoned that high HA-M2 PLA signal in 50% of Jasp-treated dTHP1 cells is due to pre-existing association between HA and M2 at the time of Jasp addition. Therefore, we next examined the effect of Jasp on HA-M2 association at an earlier time point in infection when pre-existing HA-M2 coclusters are unlikely to be abundant. We treated infected dTHP1 cells with Jasp or Cyto D at 10 hpi for 4 hours and examined for HA-M2 association using PLA at 14 hpi. Since Jasp and phalloidin compete for binding to the same site on F-actin [214], we were unable to use phalloidin staining to determine the effect of Jasp treatment on the actin cytoskeleton in dTHP1 cells. However, using an actin fractionation assay [211], we confirmed that treatment with Jasp for 4 hours increases the ratio of insoluble (i.e., polymerized) actin to soluble actin in dTHP1 cells, in comparison to vehicle-treated cells (Figure 2.12A). Under these conditions, most Jasp-treated dTHP1 cells showed reduced HA-M2 PLA signal, in comparison to vehicle- or Cyto D-treated cells (Figures 2.13A and 2.13B). We note that surface HA and M2 expression in Jasp-treated cells was somewhat reduced relative to that in vehicle-treated cells (Figures 2.12B and 2.12C). However, this reduction in surface expression of HA and M2 does not explain the decrease in HA-M2 PLA signal upon Jasp treatment; when HA or M2 expression on the cell surface and number of HA-M2 PLA spots were simultaneously assessed in the same cells, little correlation was observed

between them (Figure 2.14). Despite diminished HA-M2 association, vRNA release efficiency of Jasp-treated cells was not reduced in comparison to those of vehicle- and CytoD-treated cells (Figure 2.13C), suggesting that HA-M2 association, as measured by PLA, may not play as important a role in virus particle assembly/release in dTHP1 cells as it does in MDM (see discussion). Consistent with this possibility, at 14 hpi, no obvious difference was observed in virus bud formation on the cell surface of dTHP1 cells following 4 hours of treatment with Jasp versus vehicle or Cyto D (Figure 2.15).

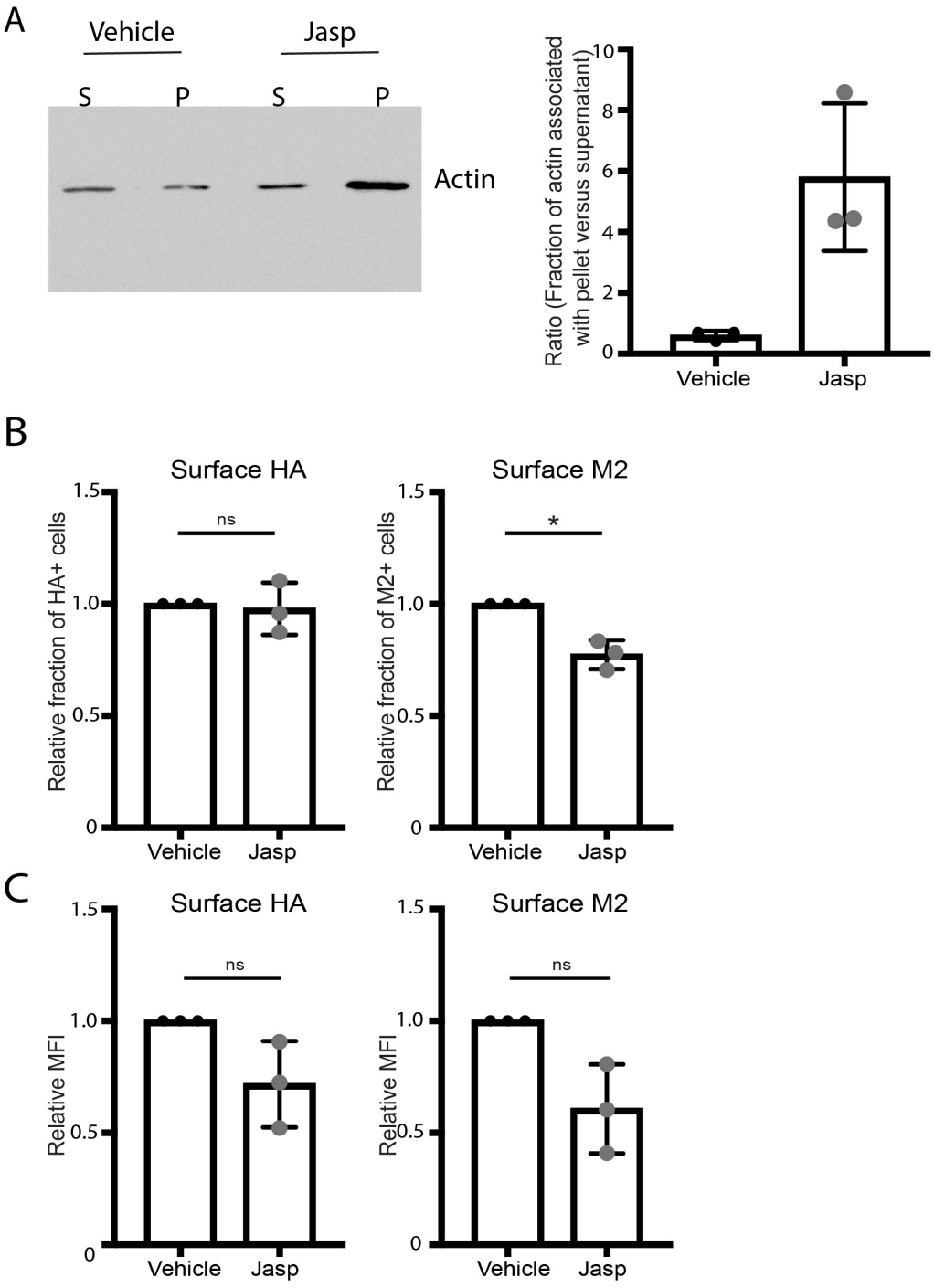

Figure 2.12: Effect of jasplakinolide treatment on the actin cytoskeleton and cell surface expression of HA and M2 in dTHP1 cells. (A) dTHP1 cells were treated with vehicle control (0.5% Ethanol) or 1 μM Jasp for 4 hours. Cells were extracted with actin stabilization buffer and centrifuged. Pellet (P) and supernatant (S) fractions were analyzed using immunoblotting. (B, C) dTHP1 cells were infected with WSN at MOI 0.1 for 10 hours. Cells were treated with vehicle control or 1 μM Jasp for 4 hours. (B) % cells expressing HA and M2 on the cell surface are shown. (C) MFIs for the indicated proteins in positive cell populations are shown. Data are from three independent experiments and shown as mean +/- SD. ns, non-significant; *, $p<0.05$.

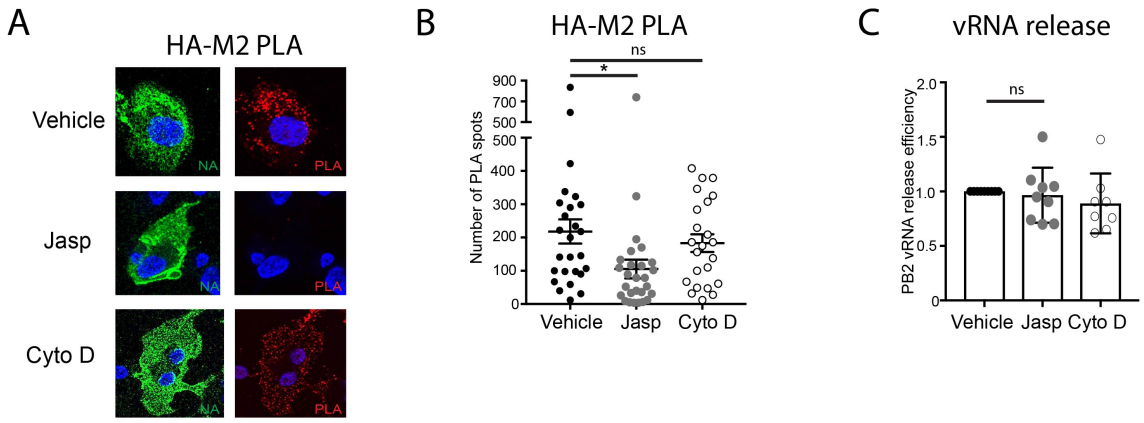

Figure 2.13: Jasplakinolide treatment reduces HA-M2 PLA in dTHP1 cells. dTHP1 cells were infected with WSN at MOI 0.1. (A, B) At 10 hpi, cells were treated with vehicle control (0.5% Ethanol), 1 μM jasplakinolide (Jasp), or 20 μM Cyto D for 4 hours before fixation. (A) Representative maximum intensity projection images are shown as in Figure 5A. (B) Number of PLA spots were counted for each cell, and data are shown for 7-10 cells per experiment. (C) vRNA release efficiency was measured in infected dTHP1 cell cultures treated with vehicle, Jasp, and Cyto D for 4 hours. Data are from at least three independent experiments. For panel B, error bars represent standard error of mean. For panel C, error bars represent SD. *, $p < 0.05$; ns, non-significant.

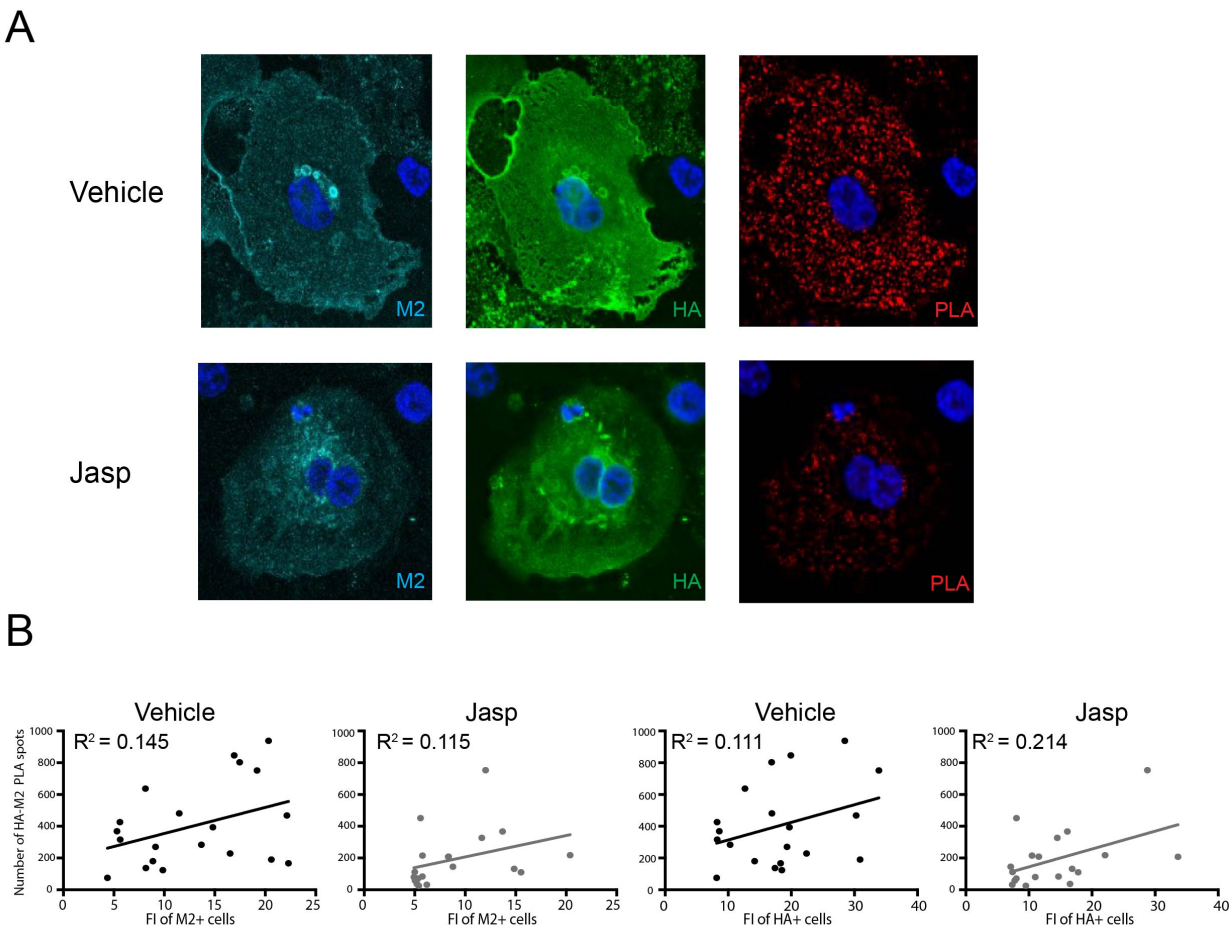

Figure 2.14: Weak correlation observed between the level of expression of HA or M2 and number of HA-M2 PLA spots in dTHP1 cells. dTHP1 cells were infected with WSN at MOI 0.1 for 10 hours. Cells were treated with vehicle control or 1 μM Jasp for 4 hours. (A) Cells were fixed and labeled with goat anti-HA and mouse anti-M2. Subsequently, cells were treated with PLA probes and then with fluorescently tagged secondary antibodies. Cells with similar levels of cell surface HA and M2 expression were compared for PLA signals. (B) Scatterplots between fluorescence intensity (FI) for cell surface HA or M2 signals and number of HA-M2 PLA plots are shown for vehicle- and Jasp-treated cells. The best-fit line was determined for each set of X-Y data points using linear regression analyses. Correlation between the MFI and PLA values was calculated as R^2 values for each plot. Note that the correlation between MFI and PLA values are generally low and that vehicle-treated cultures generally show higher PLA signals than Jasp-treated cultures when compared at similar MFI values. Data are pooled from two independent experiments.

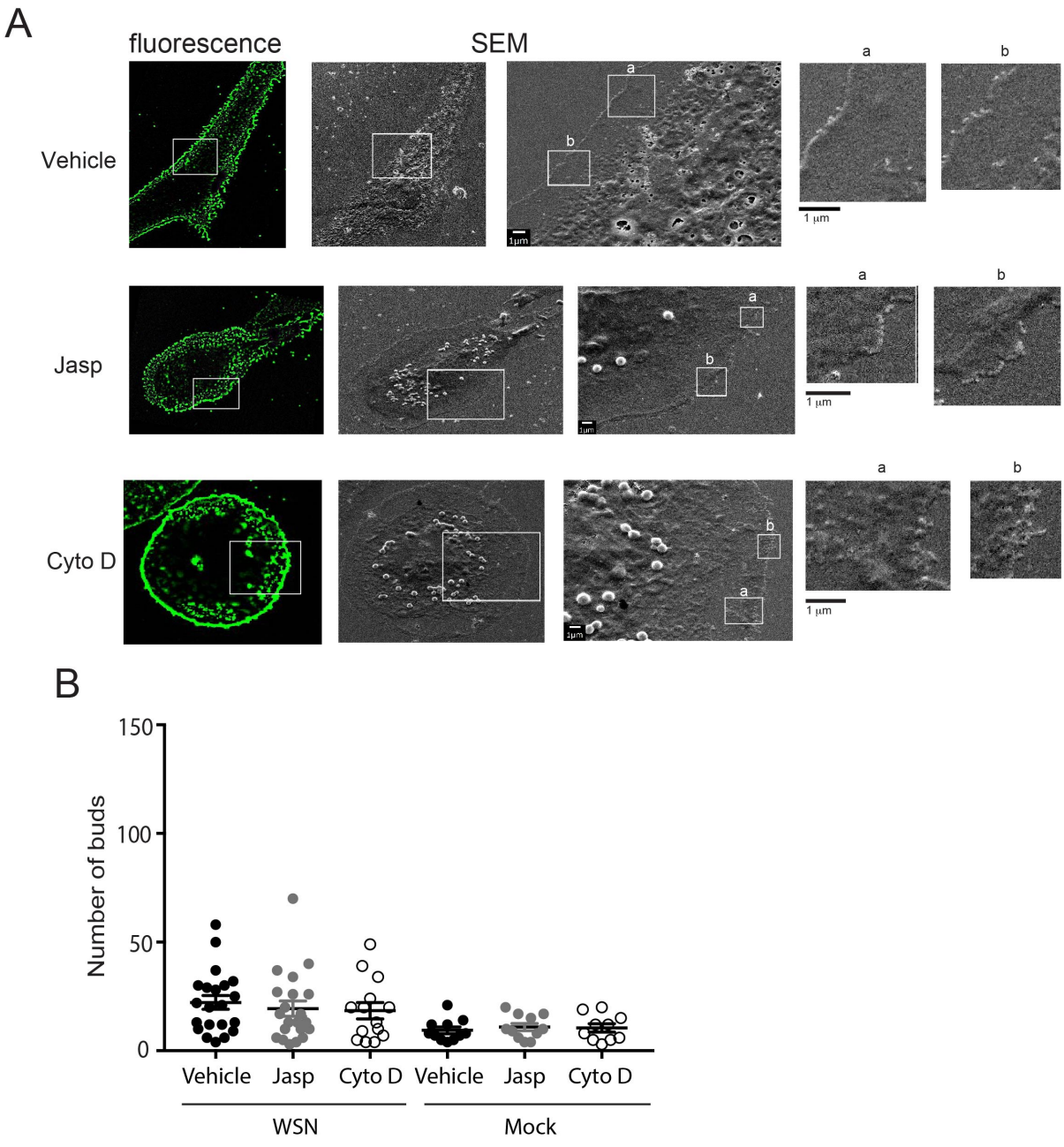

Figure 2.15: Jasplakinolide treatment has no effect on virus bud formation in dTHP1 cells. dTHP1 cells were infected with WSN at MOI 0.1. At 10 hpi, cells were treated with vehicle control (0.5% Ethanol), 1 μM Jasp, or 20 μM Cyto D for 4 hours before fixation and immunostaining with anti-HA. After identification of HA-positive cells by confocal fluorescence microscopy, cells were processed for SEM. The same cells were identified based on grid positions and analyzed by SEM. (A) Fluorescence and SEM images for representative WSN-infected HA-positive cells are shown. Boxed areas for SEM images are magnified and shown on the right of original images. Alphabetic labels are used to distinguish between individual boxed areas. (B) The number of ~100-nm buds identified in SEM images were counted within the same sized area (100 μm^2 in size) in each cell. Data are shown for 10-20 cells from two independent experiments. Error bars represent standard error of mean.

It is important to emphasize, however, that the defect in HA-M2 association is rescued upon inhibition of actin polymerization in MDM, while it is induced upon stabilization of actin in dTHP1 cells. Therefore, regardless of the effect on release of assembled particles, our data overall highlight a macrophage-specific role for actin polymerization in suppressing association between HA and M2 at the plasma membrane.

Discussion

In a previous study, a post-translational defect in productive IAV infection was observed in human MDM [205]. A similar defect was also reported for murine macrophages in one study [201] but not the other [205]. The exact nature of these defects that lead to inefficient IAV production has not been determined. Here, we have shown that despite efficient trafficking of the viral glycoproteins to the cell surface (Figure 2.5), infectious virus particle formation at the plasma membrane is inefficient in human MDM (Figures 2.3 and 2.6). The current study further identified HA-M2 association as an IAV assembly step suppressed in MDM (Figure 2.7). This restriction is specific to primary macrophages, as the THP1 monocytic cell line differentiated to macrophage-like cells (dTHP1 cells) support HA-M2 association and efficient IAV production. Notably, defective HA-M2 association and bud formation in MDM can be ameliorated by the disruption of actin polymerization, revealing a role for the actin cytoskeleton in suppressing IAV particle assembly in MDM (Figures 2.9 and 2.11). However, virus particle release remains inefficient even when HA-M2 association and bud formation are restored by actin disruption (Figure 2.11C), implying the presence of an additional defect in a post-assembly step in MDM. Consistent with the restrictive role of actin polymerization, HA-M2 association in dTHP1 cells was blocked upon a treatment that promotes actin polymerization (Figure 2.13).

Previous studies observed strain-specific differences for IAV replication in human macrophages. Some strains such as highly pathogenic H5N1 and pandemic 1918 strains can replicate in macrophages albeit at a lower efficiency than in epithelial cells [199,200,203,206]. Marvin *et al.* recently reported that the laboratory strain WSN is able to overcome blocks in IAV replication in human macrophages, while replication of the A/California/04/2009 strain is completely blocked [205]. In our study, we observed that all tested strains, including WSN and A/California/04/2009, released significantly lower titers in MDM than in dTHP1 cells (Figure 2.1C). Thus, it is likely that the cell-type-specific difference observed in this study is distinct from the previously reported strain-specific difference.

In addition to identifying a defective step for IAV replication in primary human macrophages, our study also lends mechanistic insights into the assembly and budding process of IAV in host cells. IAV is thought to assemble in cholesterol-enriched microdomains, or membrane rafts, of the plasma membrane in host cells [14,15,215,216]. HA and NA accumulate at these assembly sites [17,18,21-23], also known as the budozones, while the third transmembrane protein M2 is suggested to localize at the edge of the budozone [16,25,26]. Coclustering between HA and M2 has been observed at steady state in epithelial cells [26,86,176]. However, the sequence of events leading to recruitment of M2 to the budozone is unknown. Whether there is a mechanism regulating these events, other than simple diffusion over the plasma membrane, also remains to be determined. Our PLA data suggest that different molecular mechanisms mediate association between HA and NA and association between HA and M2 at the plasma membrane. Consistent with this possibility, a recent study showed that NA but not M2 accelerates HA trafficking to the apical surface of epithelial cells, presumably through co-trafficking [23]. Thus,

recruitment of M2 to assembly sites enriched in HA (and perhaps NA) is a discrete and host-cell-dependent step in the IAV assembly process.

The actin cytoskeleton has been implicated in assembly of IAV particles, in particular formation of filamentous particles [82,137,159]. However, the actin-dependent mechanism(s) regulating IAV assembly are not well understood. Previous studies have shown that disruption of actin dynamics by both inhibition of actin polymerization [82,137] (by latrunculin A or cytochalasin D) and promotion of actin polymerization [137] (by jasplakinolide) disrupts filamentous IAV assembly. In contrast, our study showed that drugs inhibiting actin polymerization and depolymerization have distinct and opposing effects on HA-M2 association: blocking actin polymerization in IAV non-permissive cells (MDM) restores HA-M2 association, whereas enhancement of polymerization in permissive cells (dTHP1 cells) reduces HA-M2 association. Therefore, it is likely that distinct actin-dependent mechanisms regulate the association between HA and M2 at the plasma membrane and formation of filamentous particles. As for the mechanism regulating HA-M2 association, one can speculate that subcortical actin promotes the segregation of HA- and M2-enriched plasma membrane microdomains. Consistent with this possibility, previous studies support a role for actin polymerization in maintaining HA-enriched microdomains compact and dense [180,217].

Of note, even though particle assembly is enhanced in MDM upon disruption of the actin cytoskeleton, virus release still remains defective in this cell type (Figure 2.11). This suggests that additional defect(s), for example, incomplete scission between viral envelope and plasma membrane or tethering of nascent particles to the cell surface, occurs in MDM. In addition to the nature of this late defect, whether the defect manifests due to the absence of a host factor enabling virus release or whether it is caused by the presence of a restriction factor blocking

release of assembled virus particles warrants further investigation. It is also possible that cytochalasin D treatment blocks the release of assembled virus particles in an MDM-specific manner. These results, together with the pleiotropic effects of actin perturbation discussed above, also highlight the importance of specifically examining individual steps (e.g., HA-M2 association) rather than just monitoring the end result, i.e., virus release efficiencies or released virus titers, when assessing the effect(s) of actin disruption on the virus assembly/release process.

The cytoplasmic domain of M2 comprises of an amphipathic helix, which plays a role in scission of the IAV particle after budding [16,26,59]. In epithelial (MDCK) or epithelial-like (293T) cell lines, viruses or VLP systems lacking M2 or expressing mutant M2 proteins are still able to initiate particle assembly and budding, presumably driven by HA and NA [21,31]. However, these buds adopt an abnormal morphology and/or fail to undergo scission or release [16,26,59], latter of which results in accumulation of particles at the cell surface. In contrast, MDM showed very few buds on their surface under conditions where HA-M2 association was impaired (Figures 2.6 and 2.11). These results suggest that in MDM, M2 plays an earlier role(s) in the assembly of virus particles, which is not apparent with 293T or MDCK cells that express M2-deficient virus or VLP systems. Such an earlier role may require other functions of M2. For example, in addition to scission of nascent particles, M2 functions in recruitment of M1 and vRNP to assembly sites [59,60,81,86-88,90], which is important for initiation of IAV particle assembly or elongation of filamentous particles [39,54,56,57,59,60,92,218,219]. A defect in incorporation of M1 and/or vRNP into budding virus particles due to the failure of M2 recruitment may also explain the reduction in infectivity per particle observed for MDM-derived virus relative to dTHP1-derived virus (Figure 2.3B). We also do not rule out the possibility that a

failure in association of M1 and/or vRNP with the assembly sites may contribute to the observed defect in M2-HA association specific to MDM.

While jasplakinolide reduces HA-M2 association in dTHP1 cells, no reduction in virus bud formation is observed under this condition (Figure 2.15), which is consistent with previous studies performed with M2-lacking viruses in epithelial cell lines [16,26,59]. However, we do not observe an arrest in virus release from dTHP1 cells, which was observed in the previous studies using M2-deficient viruses. In this regard, it is important to note that, unlike cells infected with M2-lacking mutant viruses, dTHP1 cells treated with jasplakinolide still show a residual level of M2 recruitment based on HA-M2 association detected by PLA. It is possible that this residual level of HA-M2 association is sufficient to promote the scission of virus buds in dTHP1 cells.

Overall, in this study, we have compared IAV replication in MDM with that in dTHP1 cells and found that MDM replicate vRNA, express viral proteins, and traffic HA, NA and M2 to the plasma membrane at levels similar to those in dTHP1 cells. However, MDM are defective in assembling virus particles, likely due to actin-dependent suppression of association between the viral transmembrane proteins HA and M2. Comparison of actin regulatory mechanisms operating in MDM and dTHP1 cells, which are of the same lineage, will likely facilitate identification of additional host cellular factors involved in the assembly stage of the IAV life cycle.

Acknowledgments

I thank the members of Ono laboratory for helpful discussions and critical review of the manuscript. I thank Christopher Sumner for help with optimization of the *in situ* Proximity Ligation Assay. I would also like to thank M. Bachman, C. Brooke, F. Momose, and A. S. Monto for reagents and Adam Lauring and his laboratory for advice on experimental protocols used in this study. The following reagent was obtained through BEI Resources, NIAID, NIH: polyclonal anti-influenza virus H1 (H0) hemagglutinin (HA), A/Puerto Rico/8/1934 (H1N1), (antiserum, goat), NR-3148. The microscopy data presented in this study was collected at the BRCF Microscopy core, University of Michigan.

This work was supported by funding from the National Institutes of Health (R01 AI071727) (to Akira Ono). I was supported by a Clayton Willison- and Emma Elizabeth Willison-Endowed Graduate Fellowship.

Chapter 3

The Actin Cytoskeleton Suppresses Influenza A Virus Assembly In Primary Human Macrophages In An M2-Dependent Manner

Abstract

Influenza A virus (IAV) assembly at the plasma membrane is orchestrated by at least five viral components: hemagglutinin (HA), neuraminidase (NA), matrix (M1), the ion channel M2, and viral ribonucleoprotein (vRNP) complexes. While these five viral components are expressed in primary human monocyte-derived macrophages (MDM) upon IAV infection, this cell type is inefficient at supporting IAV assembly. Notably, the defect in IAV assembly in MDM correlates with a defect in HA-M2 association at the plasma membrane of this cell type. Moreover, the defects in HA-M2 association and IAV particle assembly, which are specific to MDM and not observed in a monocytic cell line differentiated into macrophage-like cells, are reversed upon disruption of the actin cytoskeleton. Hence, the actin network plays a negative role in IAV assembly in MDM. In this chapter, I determine the viral and host mechanisms that are involved in the F-actin-mediated suppression of IAV assembly in MDM. Using drugs that specifically block F-actin elongation or branching, I show that both linear and branched actin filaments contribute to the suppressive role of the actin cytoskeleton in HA-M2 association in MDM. In addition, I elucidate the viral components involved in the MDM-specific suppression of virus assembly by the actin cytoskeleton. To address whether HA-M2 association precedes and is essential for virus particle formation upon F-actin disruption in MDM, I generated an M2-

deficient virus and analyzed formation of budding structures at the cell surface using correlative fluorescence scanning electron microscopy. While MDM infected with the M2-expressing wild-type virus gain the ability to support particle assembly upon F-actin disruption, cells infected with the M2-deficient virus remain defective at particle formation even after F-actin disruption. These data indicate that M2 plays a role in virus particle formation in MDM, perhaps in addition to the well-known role in particle release, and suggest that the actin cytoskeleton in MDM suppresses IAV particle assembly by restricting HA-M2 association.

Introduction

Events at the plasma membrane during IAV assembly

IAV buds from cholesterol-rich microdomains or lipid rafts, which are also known as budozones, of the plasma membrane. Assembly of new virus particles requires trafficking of at least four viral structural proteins, HA, NA, M1, and M2 as well as vRNPs to the plasma membrane [14,15]. In epithelial cells, IAV transmembrane proteins HA and NA intrinsically localize to cholesterol-rich microdomains of the apical plasma membrane [17-19,22,23] and drive their coalescence into larger domains [17,18,23], which could lead to stabilization of lipid rafts. The third transmembrane protein M2 also intrinsically traffics to the apical plasma membrane [169]; however, it does not associate with lipid rafts when expressed by itself [22]. In infected cells, M2 is shown to associate closely with HA [176] while still localizing to the boundary of lipid rafts [18]. The M1 protein is predominantly cytosolic when expressed alone [21,28,65,75]. However, in infected cells, the cytoplasmic tails of HA [27,28], NA [27,28], and M2 [86,87] recruit M1 to cholesterol-rich membranes. The vRNP complex, which also promotes IAV assembly, is recruited to the budozones by several viral proteins such as HA [70], M1 [34,74,220], and M2 [59,60,90,91].

Mechanisms driving association of M2 with the HA-enriched budozones

As mentioned above, M2 intrinsically traffics to the apical plasma membrane [169]. The transmembrane domain and the cytoplasmic tail of M2 are important for its targeting to the plasma membrane [221,222]. As for whether M2 traffics along with and/or associates with HA and NA in the ER-Golgi transport pathway, earlier studies showed that the M2 ion channel raises the pH of the Golgi and prevents the premature exposure of the HA fusion peptide in the low pH environment of the Golgi, suggesting that HA and M2 traffic together through the ER-Golgi pathway [223,224]. However, a recent study showed that while HA and NA mutually accelerate their apical targeting, M2 inhibits apical targeting of HA, suggesting that HA and M2 might compete for the same transport mechanism [23]. Once at the plasma membrane, M2 localizes to microdomains distinct from HA-enriched microdomains [18,22] but is later recruited to the assembling virus particle [25,86,176]. As for the timing of this recruitment, some *in silico* data suggest that M2 is preferentially recruited to curved membranes versus flat membranes [225,226]. Hence, it has been proposed that M2 is recruited to the edge of the budozone after induction of membrane curvature by other viral structural proteins. My data in **chapter 2** suggest that association between HA and M2 at the cell surface is a discrete step that occurs after trafficking of the two proteins to the plasma membrane. However, the timing (prior to or post initiation of particle assembly) of association of M2 with HA-enriched budozones has not been determined in cells. In addition, the viral and host components that drive this association at the plasma membrane are not known. While an early study proposed that localization of M2 at the budozone edge depends on acylation and cholesterol binding sites in the cytoplasmic tail of the protein [227], later studies show that HA and M2 cocluster at the plasma membrane and virus particles are formed even when M2 lacks acylation and/or cholesterol-binding sites [228-231].

Other viral proteins may also be involved in promoting HA-M2 association. For instance, M1 may play a role in promoting HA-M2 association since mutations in M2 that reduce its interactions with M1 lead to reduced coclustering between HA and M2 [86,176]. With respect to the host proteins involved in recruitment of M2 to the budozone, my findings in **chapter 2** show that the actin cytoskeleton suppresses this association in a cell-type-dependent manner. However, it is not clear whether F-actin suppresses HA-M2 association prior to initiation of particle assembly or whether it suppresses induction of membrane curvature, which in turn reduces the efficiency of M2 recruitment to the budozone.

Role(s) of M2 in IAV particle assembly and budding

Of the three transmembrane proteins involved in particle assembly, HA and/or NA expression at the plasma membrane has been shown to be sufficient for induction of curvature for spherical virus bud formation [21,31]. On the other hand, M2 is thought to be dispensable for curvature induction but rather plays important roles in pinching off of the spherical virus bud prior to virus release [16,26,46]. However, some lines of evidence suggest that M2 may play a role(s) during the early stages of spherical IAV particle assembly. First, mutations in M2 alter the morphology of assembling virus particles [57,59,60]. Second, M segment-encoded proteins (M1 and M2) stabilize curvature induced by HA and/or NA and allow for formation and release of virus-like particles [31]. Third, incorporation of M1 into assembling virus particles, which is important for providing structure to the virus particle, is at least partially dependent on M2 [86,87]. Despite these lines of evidence, there is little data in support of a direct role(s) of M2 during the early stages of spherical IAV particle formation.

Potential mechanisms behind restriction of IAV assembly by F-actin

As described in **chapter 2**, the actin cytoskeleton suppresses IAV assembly, which correlates with inefficient HA-M2 association, in MDM. The restrictive role of F-actin in MDM could

either be due to the distinct structure and/or function of the actin network or due to the differential function or expression of an actin-dependent host factor(s) in this cell type. Taking into account the previously described role of M2 and other viral structural proteins during IAV assembly, I propose three different possible mechanisms by which the actin cytoskeleton suppresses IAV assembly in macrophages:

i. Microdomain segregation: In this model, the actin cytoskeleton restricts the movement of HA- and M2-enriched microdomains and keeps the microdomains (and hence, HA and M2) segregated from each other. This is consistent with previous findings that M2 is present in microdomains distinct from HA-enriched microdomains early on in the assembly process [18,22] but is later recruited to these assembly sites [25,86,176]. The cortical actin network in primary macrophages may keep these plasma membrane microdomains apart via interactions with either lipids [232,233] or cytoplasmic tails of transmembrane proteins [211,234,235].

ii. Suppression of membrane curvature: According to this model, the actin cytoskeleton suppresses HA- and/or NA-induced membrane curvature by modulating the plasma membrane stiffness [236,237]. This possibility is consistent with several studies that have shown that M2 is not required for induction of membrane curvature during particle assembly [16,25,59,87] and that M2 may be recruited after induction of membrane curvature [225,226], which is likely mediated by HA, NA or M1. Therefore, F-actin may be modulating membrane curvature in a manner that is independent of recruitment of M2 to assembly sites.

iii. Blocking of cytoplasmic components: In this model, the actin network inhibits IAV assembly by restricting the trafficking, incorporation or function of additional

components essential for IAV assembly, that is, M1 and vRNPs. Both M1 [148] and NP [149] are reported to associate with F-actin, and this association might suppress their mobility and trafficking to assembly sites. In addition, the dense F-actin cortex could also serves as a physical barrier to diffusion of proteins or vesicles carrying these proteins [238,239].

These three potential mechanisms of action for the actin cytoskeleton in IAV assembly in MDM are depicted in Figure 3.1. In some cases, disruption of F-actin in epithelial cells modestly increases spherical virus production [82,137]. Therefore, it is possible that the mechanisms described above may also operate in IAV-permissive cells depending on the condition.

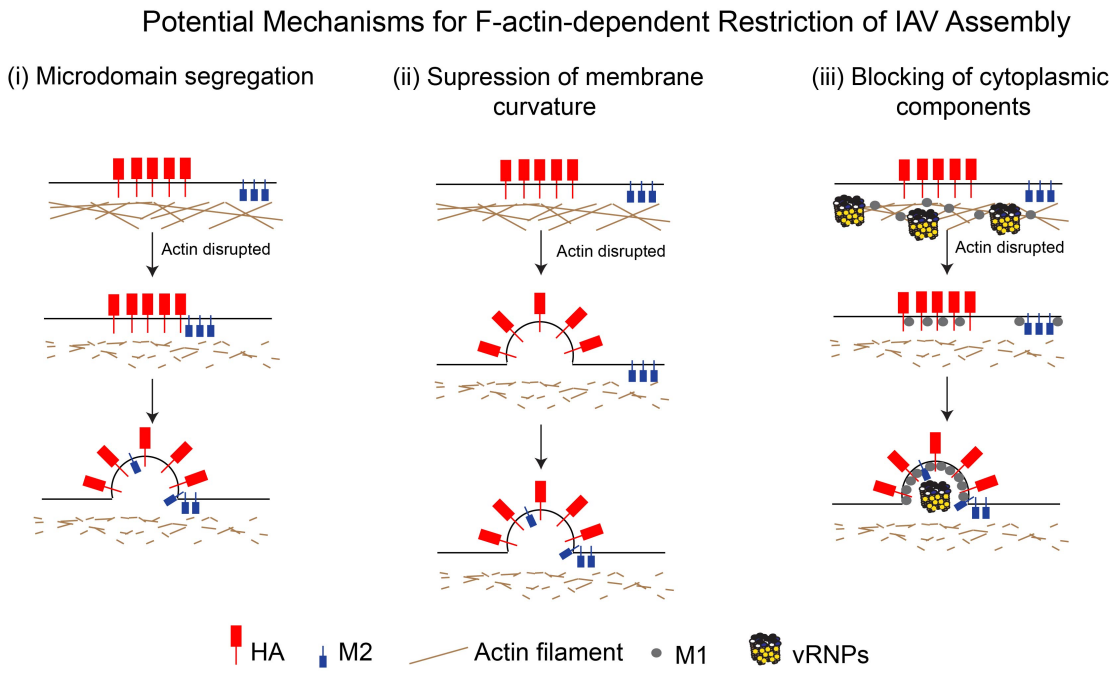

Figure 3.1: Proposed mechanisms by which F-actin restricts spherical IAV assembly in primary human macrophages. (i) Microdomain segregation: F-actin partitions HA- and M2-enriched plasma membrane microdomains. (ii) Suppression of membrane curvature: F-actin restricts HA-mediated curvature induction at the plasma membrane, which is required for M2 recruitment to the assembling particle. (iii) Blocking of cytoplasmic components: F-actin restricts trafficking and incorporation of other curvature-inducing structural components, that is, M1 and vRNP, to virus assembly sites.

In this chapter, I use drugs that specifically inhibit elongation or branching of actin filaments to show that both linear and branched F-actin contributes to suppression of HA-M2 association in MDM. In addition, using an M2-deficient virus, I show that actin disruption fails to restore IAV particle assembly in MDM in the absence of M2. In addition, M2 is also required for efficient particle assembly in dTHP1 cells, which are macrophage-like but are inherently permissive to IAV assembly. Hence, in addition to its role in scission of the virus bud late during IAV assembly, M2 plays a role(s) early during virus particle formation in macrophages. My data also suggest that HA-M2 association likely precedes IAV particle assembly in macrophages. Overall, the findings presented in this chapter suggest that both linear and branched actin filaments suppress IAV particle assembly in MDM by directly restricting HA-M2 association (model (i)) or by blocking trafficking of viral components that promote HA-M2 association (model (iii))..

Materials and methods

Cells and reagents: Monocytes were isolated by plate adhesion from peripheral blood mononuclear cells, which were obtained from buffy coats derived from unidentified healthy donors (New York Blood Center, NY). Cells were cultured in RPMI 1640(Gibco) supplemented with 10% fetal bovine serum (FBS, Hyclone) for 7 days before they were used for experiments. THP1 (ATCC® TIB202™) cells were cultured in RPMI 1640 supplemented with 10% FBS, 1 mM Sodium Pyruvate (Gibco) and 0.05 mM 2-mercaptoethanol. To generate differentiated THP1 cells (dTHP1), THP1 cells were cultured in the medium containing 0.1 μM phorbol 12-myristate 13-acetate (PMA; Sigma) and 0.1 μM Vitamin D3 (Sigma) for 2-3 days. Madin-Darby canine kidney (MDCK) cells were provided by Dr. Arnold S. Monto (University of Michigan)

and were cultured in DMEM (Gibco) supplemented with 10% FBS and 25 mM HEPES. Human embryonic kidney-derived 293T cell line (ATCC) was cultured and maintained in DMEM (Lonza) supplemented with 10% FBS.

The following antibodies were used for immunofluorescence microscopy: mouse anti-HA monoclonal antibody (clone C179 [207]; Takara), mouse anti-M2 monoclonal antibody (clone 14C2 [93]; Thermofisher), goat anti-HA antiserum (BEI NR-3148), rabbit anti-M1 (GTX125928; GeneTex) All secondary antibodies used for immunofluorescence and Alexa Fluor 488-labeled phalloidin were purchased from Thermofisher. All actin-disrupting drugs were purchased from Sigma and re-constituted in DMSO.

Generation of M2-MDCK stable cell line: cDNA corresponding to the M2 protein was cloned into the pCABSD plasmid, which expresses a blasticidin S resistance gene. MDCK cells were transfected with the pCABSD-M2 plasmid using lipofectamine (Invitrogen). Cells stably expressing M2 were selected in growth medium containing 1 μg/ml blasticidin and were enriched for high M2 expression by staining with an anti-M2 antibody (clone 14C2) and an Alexa 488-conjugated secondary antibody followed by fluorescence-activated cell sorting (FACSAria II, BD Biosciences).

Generation of ΔM2 WSN virus: Virus deficient in expression of M2 was generated as described previously [240]. Briefly, a WSN M segment with a disrupted splicing signal (WSN M SS) was generated by introducing mutations in the 3' splice site of the WSN M segment using QuikChange II site-directed mutagenesis protocol (Agilent). Wild-type (WT) WSN virus was generated using reverse genetics as described in **chapter 2**. ΔM2 WSN virus was generated in 293T cells using the pPolI plasmids encoding the 7 RNA segments of the WT WSN strain, pPolI WSN M SS, and the 5 pCAGGS plasmids that express the PA, PB1, PB2, NP, and M2 proteins.

Virus generated from 293T cells was propagated in M2-MDCK cells. Viral titers were determined by plaque assays performed using M2-MDCK cells.

Correlative fluorescence and scanning electron microscopy (CFSEM): CFSEM experiments were performed as described in **chapter 2**.

***In situ* Proximity Ligation Assay (PLA):** PLA was performed using Duolink® PLA fluorescence kit as described in **chapter 2**. Cells fixed with 4% PFA (non-permeabilized) were incubated with goat anti-HA and mouse anti-M2 primary antibodies. PLA signals and identification of infected cells were performed using PLA probes specific to goat and mouse IgG. AlexaFluor-488-labeled secondary antibody was used to recognize anti-HA and hence, to identify HA-positive cells. Cells were observed using a Leica Inverted SP5X Confocal Microscope System with a 63X objective. Z-stacks extending from the focal plane corresponding to the middle plane of the nucleus (identified by DAPI staining) to the bottom of cells were acquired for each cell, and the maximum intensity projection for each cell was constructed using ImageJ. The PLA signal in projection images was thresholded to eliminate weak and hazy background signal in the nucleus, and the number of PLA-positive spots was counted using the *Analyze particle* function in ImageJ.

Results

Both linear and branched actin filaments contribute to the suppressive role of the actin cytoskeleton in HA-M2 association in MDM

Growth and organization of the actin cytoskeleton is driven by actin-nucleating factors, which bind actin and stimulate the formation and growth of an actin filament [140,141]. The most well studied actin-nucleating factors are: Arp2/3 and formins. While the Arp2/3 complex nucleates branched actin structures, formins nucleate unbranched actin filaments and serve as elongation

factors for the growing actin filament. To determine whether branched and/or linear actin filaments are involved in the suppressive role of the actin cytoskeleton during IAV assembly in MDM, we used inhibitors that specifically disrupt Arp2/3 and formins. CK666 [241] and SMIFH2 [242] were used to inhibit the Arp2/3 complex and formins, respectively. MDM were infected with the laboratory strain A/WSN/1933 (H1N1) (WSN) at MOI 0.1. Infected cells were treated with actin altering drugs, at 14 hpi for 2 hours, fixed, and examined for HA-M2 association using PLA. In addition to CK666 and SMIFH2, we treated cells with actin disrupting drugs Cytochalasin D (Cyto D) and Latrunculin B (Lat B). The effects of these drugs on the actin network in MDM were determined by staining drug-treated cells with Phalloidin-Alexa-Fluor-488. As expected, both Cyto D and Lat B (which inhibits F-actin polymerization) disrupted the actin network in MDM. Consistent with previous studies [242,243], the effects of CK666 and SMIFH2 were not detected by Phalloidin staining, suggesting that these drugs alter specific aspects of the actin network without its complete disruption in MDM (Figure 3.2A). Upon examining HA-positive cells for HA-M2 PLA, we observed very few HA-M2 PLA spots on the surface of vehicle (DMSO)-treated MDM. As observed in **chapter 2**, Cyto D treatment significantly increased the number of HA-M2 PLA spots on the surface of MDM. As expected, disruption of F-actin by Lat B also significantly increased HA-M2 PLA signal on the surface of MDM. Notably, treatment with CK666 or SMIFH2 significantly increased HA-M2 PLA signal on the surface of MDM even though the actin cytoskeleton was not completely disrupted under these conditions (Figures 3.2B and 3.2C). Overall, my data suggest that both linear and branched actin filaments contribute to the suppressive role of the actin cytoskeleton in HA-M2 association in MDM.

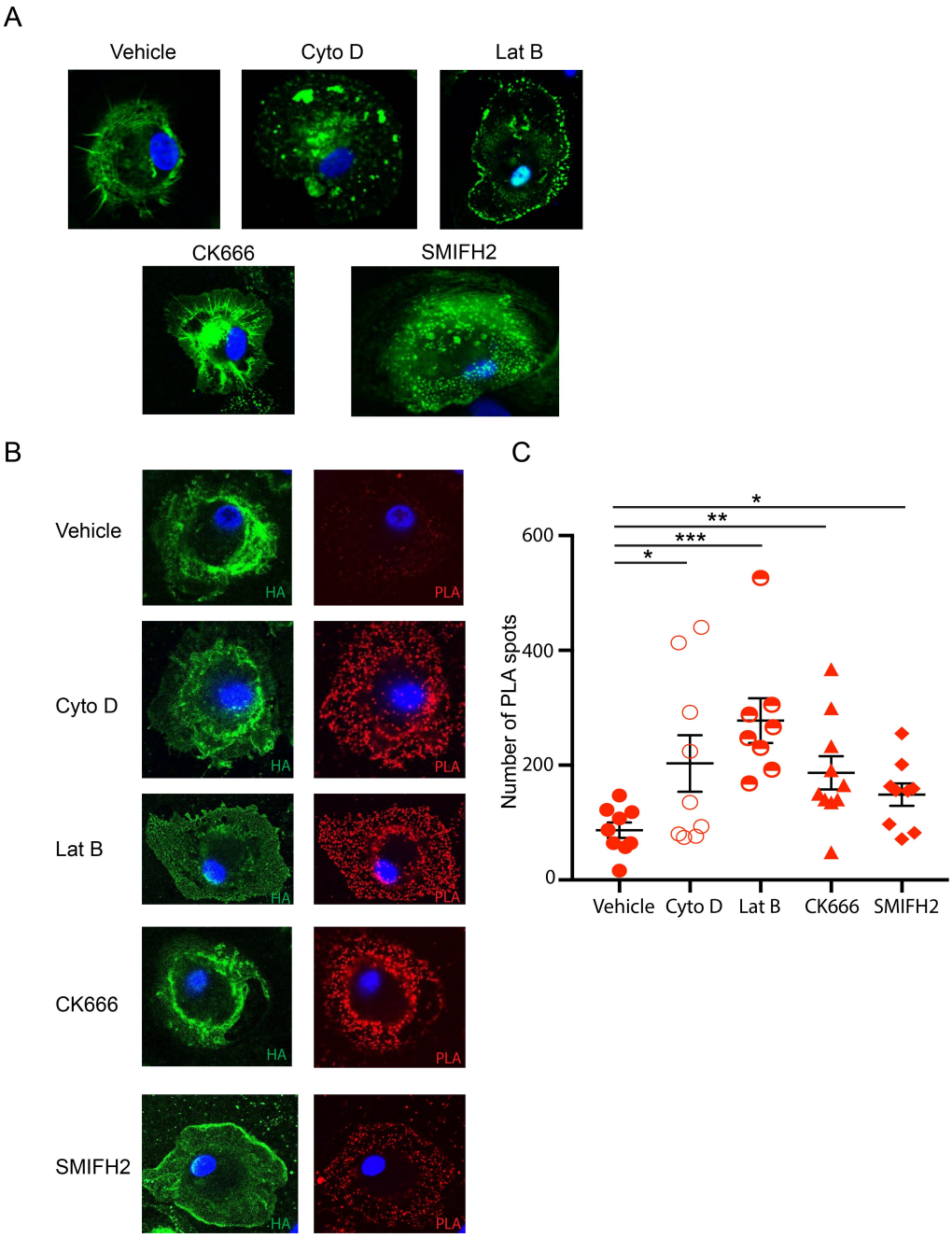

Figure 3.2: The effects of different actin-altering drugs on F-actin and HA-M2 association in MDM. (A) MDM were treated with Vehicle (DMSO), 20 µM cytochalasin D (Cyto D), 5 µM Latrunculin B (Lat B), 100 µM CK666, 25 µM SMIFH2 for 2 hours. Drug-treated cells were fixed, permeabilized and the actin cytoskeleton was visualized using fluorescently tagged-phalloidin. Images are representative of 10 cells. (B and C) MDM were infected with WSN at MOI 0.1 for 14 hours. Infected cells were treated with the indicated drugs for 2 hours and fixed. Cells were analyzed as in **chapter 2**. (B) Representative maximum intensity projection images are shown. (C) Number of PLA spots was counted for each cell. Data are shown for 8-10 cells per condition. Error bars represent standard error of mean. *, $p<0.05$; **, $p<0.01$; ***, $p<0.005$.

Expression levels of HA and M1 are comparable between ΔM2 virus- and WT virus-infected MDM

Since the actin cytoskeleton suppresses HA-M2 association and IAV assembly in MDM, we asked whether HA-M2 association precedes and is essential for particle assembly (mechanism (i) in Figure 3.1) or particle assembly is initiated prior to association of M2 with HA (mechanisms (ii) and (iii) in Figure 3.1). To distinguish between the M2-dependent (i) and M2-independent mechanisms ((ii) and (iii)) for the role of F-actin in IAV assembly in MDM, we generated a mutant WSN virus that fails to express M2 (WSN ΔM2) in infected cells. This virus incorporates the WSN M segment with a disrupted 3' splice site (WSN M SS), which allows for generation of the M1-encoding mRNA but not the M2-encoding mRNA from the M segment [240] (Figure 3.3A). Since the WSN ΔM2 virus is produced in MDCK cells stably expressing the WSN M2 protein, M2 is incorporated into virus particles and is able to complete its roles during the entry of IAV into cells; however, the virus is defective in expressing nascent M2 required during IAV assembly. To determine whether other viral structural proteins are expressed at comparable levels between WT virus- and ΔM2 virus-infected cells, I used flow cytometry to measure the total expression of M1 and cell surface expression of HA in cells infected with WT or ΔM2 virus. For comparison with MDM, I used the monocytic cell line THP1, which has been differentiated to adopt macrophage-like morphology (dTHP1) as described in **chapter 2**. dTHP1 cells, unlike MDM, support all steps of the IAV assembly process and have been used for comparison with MDM in **chapter 2**. dTHP1 cells and MDM were infected with WT or ΔM2 virus at MOI 0.1 for 18 hours, after which cell surface expression of HA was measured in non-permeabilized cells and total expression of M1 was measured in permeabilized cells. In addition, we measured the expression of M2 on the cell surface. As expected, dTHP1 cells and MDM infected with the ΔM2 virus failed to express M2 on the cell surface. Both HA and M1 were

expressed in ΔM2 virus-infected MDM at levels comparable to that in WT virus-infected cells. Cell surface expression of HA was about 2-fold reduced in dTHP1 cells infected with ΔM2 virus, relative to WT virus. Total M1 expression was comparable between dTHP1 cells infected with WT or ΔM2 virus. Overall, our data show that in MDM, cell surface expression of HA and total expression of M1 are comparable between cells infected with ΔM2 and WT viruses.

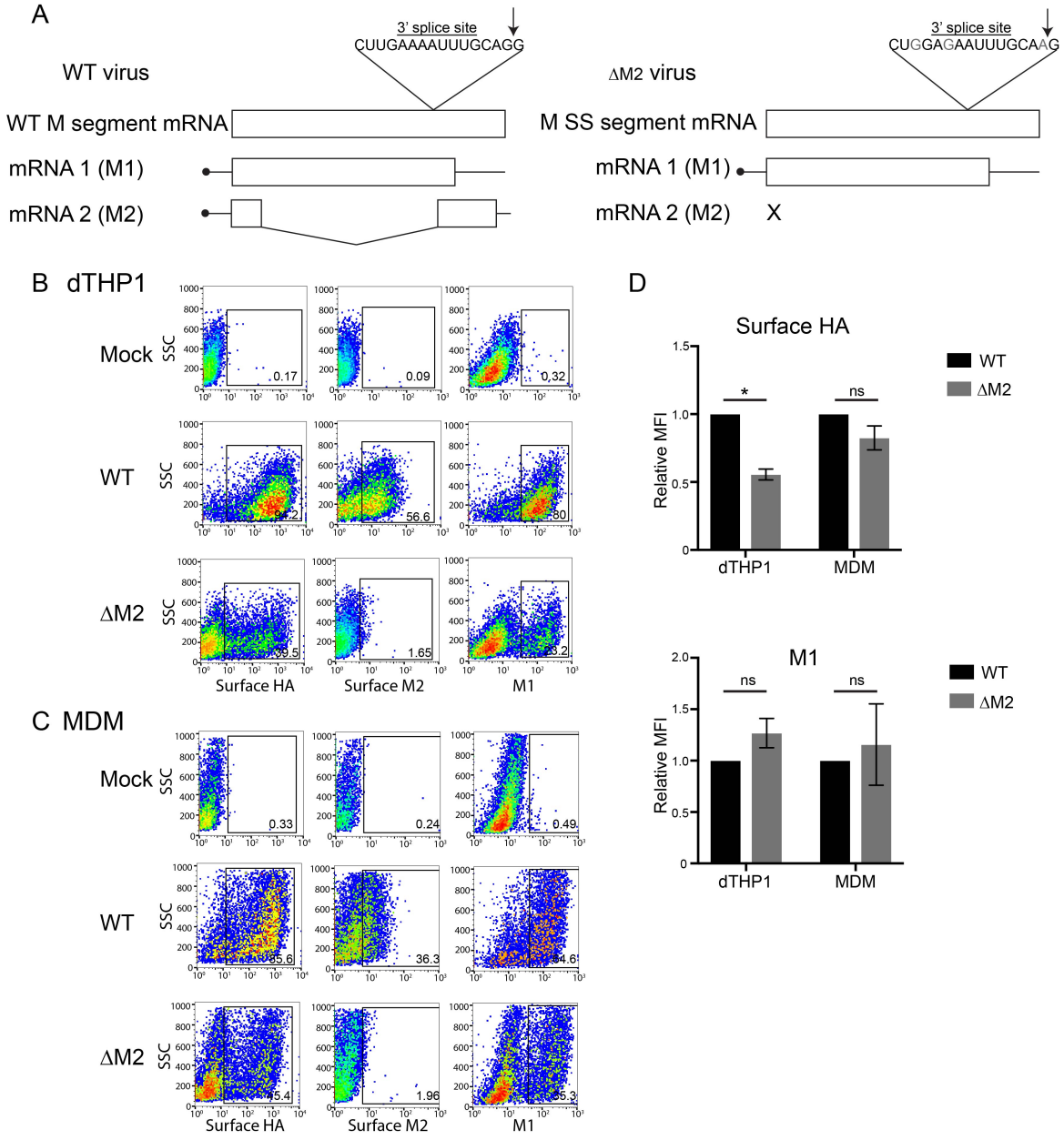

Figure 3.3: Generation and characterization of ΔM2 WSN virus. (A) The strategy used for generation of the WSN M segment that fails to encode for the M2 protein (WSN M SS) is depicted. (B-D) dTHP1 cells (B) and MDM (C) were infected with WT or ΔM2 virus at MOI 0.1 for 18 hours. (B and C) Infected cells were analyzed for cell surface expression of HA and M2 and intracellular expression of M1 by flow cytometry. Representative flow plots for mock-infected and virus-infected cells are shown. Percentages of cells positive for viral proteins (boxed) are shown. (D) Relative MFIs for signal of indicated proteins for positive cell populations (gated in panels B and C) are shown. Data are shown as mean +/- SD and are from at least three independent experiments. *, $p<0.05$; ns, non-significant.

Latrunculin B treatment restores IAV particle formation in MDM in an M2-dependent manner

I next asked whether restoration of IAV particle assembly upon F-actin disruption in MDM depends on expression of M2. To this end, I performed CFSEM with MDM infected with WT or ΔM2 virus and treated either with vehicle or Lat B at 14 hpi for 4 hours and examined virus bud formation in cells expressing HA on the cell surface. I counted the number of virus particle-like buds (~100 nm in diameter) within the same sized area (100 μm^2 in size) of each cell. Consistent with the results shown in **chapter 2**, WT virus-infected, vehicle-treated MDM showed very few buds on the cell surface. Similar to Cyto D treatment in **chapter 2**, Lat B treatment significantly increased the number of buds on the surface of WT virus-infected MDM (Figures 3.4A and 3.4B). As expected, very few bud-like structures were observed on the surface of vehicle-treated, ΔM2 virus-infected cells. Notably, no increase in number of buds was observed on the surface of ΔM2 virus-infected MDM upon treatment with Lat B, relative to treatment with vehicle (Figures 3.4A and 3.4B). These data show that disruption of the actin cytoskeleton promotes IAV particle assembly in MDM in an M2-dependent manner. Overall, these data suggest that HA-M2 association likely precedes and is essential for virus particle assembly in MDM.

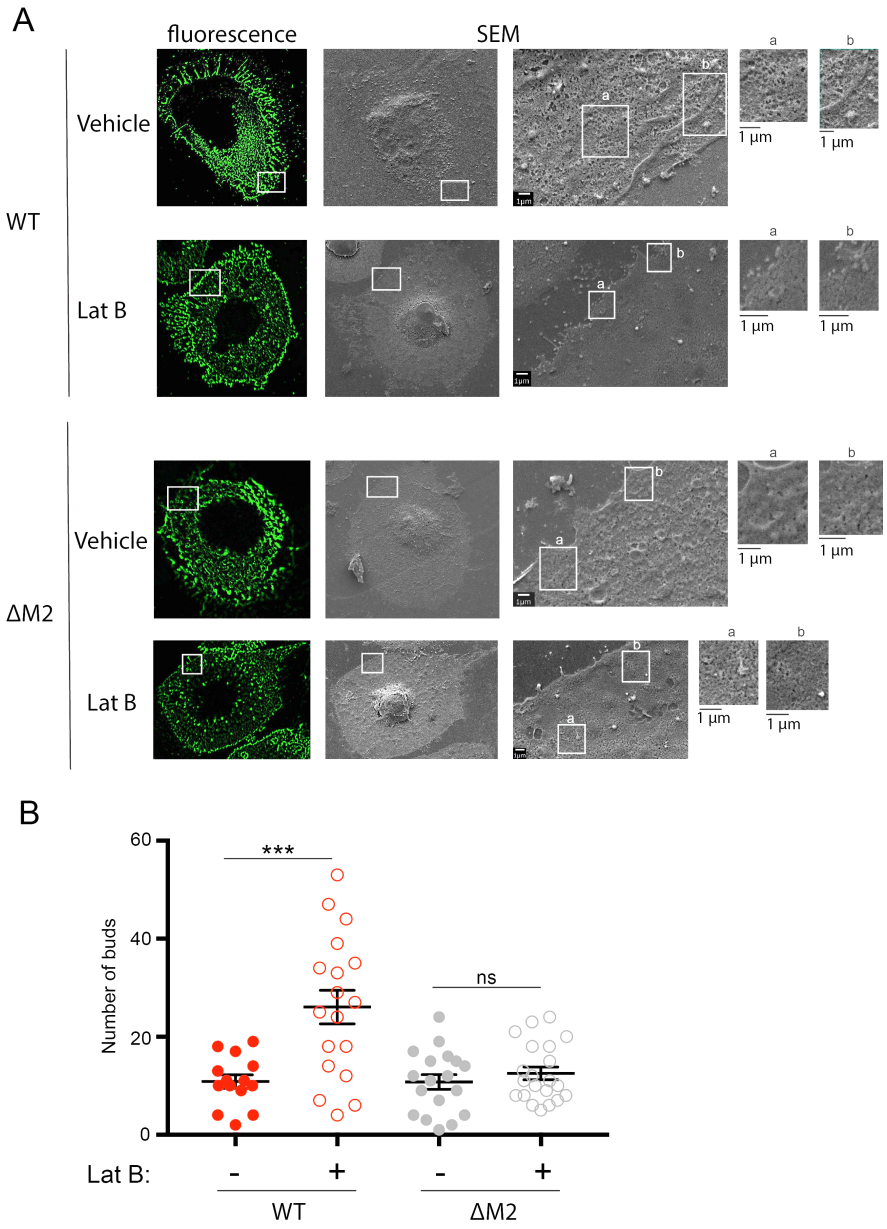

Figure 3.4: F-actin disruption restores virus bud formation in MDM in an M2-dependent manner. MDM were infected with WSN at MOI 0.1 for 14 hours. Infected cells were treated with vehicle (DMSO) or 5 µM Lat B for 4 hours, before fixation and immunostaining with anti-HA. After identification of HA-positive cells by confocal fluorescence microscopy, cells were processed for SEM. The same cells were identified based on grid positions and analyzed by SEM. (A) Representative SEM images for WSN-infected HA-positive cells are shown. Fluorescence images corresponding to the SEM images are also included. Boxed areas for SEM images are magnified and shown on the right of original images. Alphabetic labels are used to distinguish between the individual boxed areas. (B) The number of ~100-nm buds identified in SEM images were counted within the same sized area (100 µm2 in size) in each cell. Data are shown for 10-20 cells from two independent experiments. Error bars represent standard error of mean. ***, P<0.005; ns, non-significant.

dTHP1 cells support virus particle assembly in an M2-dependent manner

Since previous studies have shown that spherical IAV particle assembly is initiated in IAV-permissive epithelial cell lines even in the absence of M2 [16,25], we next asked whether dTHP1 cells, which are also permissive to IAV assembly, require M2 for particle formation on the cell surface. dTHP1 cells were infected with WT or ΔM2 virus and virus bud formation was analyzed on the surface of HA-positive cells by SEM. As expected, cells infected with the WT virus showed high number of bud-like structures on the cell surface. Notably, the number of buds observed on the surface of ΔM2 virus-infected dTHP1 cells was significantly reduced in comparison to that on WT virus-infected cells (Figures 3.5A and B). Since HA expression on the surface of ΔM2 virus-infected dTHP1 cells is reduced in comparison to WT virus-infected dTHP1 cells (Figure 3.3C), the reduction in bud formation in ΔM2 virus-infected cells may be due to the reduction in HA expression on these cells. However, in these experiments, cells expressing comparable levels of HA on the surface were analyzed for bud formation using SEM. This is more clearly observed upon measuring the fluorescence intensity of surface HA staining in dTHP1 cells that were analyzed by SEM. The fluorescence intensity of surface HA staining was comparable between the WT virus- and ΔM2 virus-infected dTHP1 cells (Figure 3.5C). Hence, the difference in surface HA expression does not explain the difference in bud formation between WT virus- versus ΔM2 virus-infected dTHP1 cells. These data indicate that both dTHP1 cells and MDM rely on M2 for efficient particle formation. Overall, these data suggest that in addition to its role in bud scission late during IAV assembly, M2 plays important roles early during IAV particle formation in MDM and dTHP1 cells.

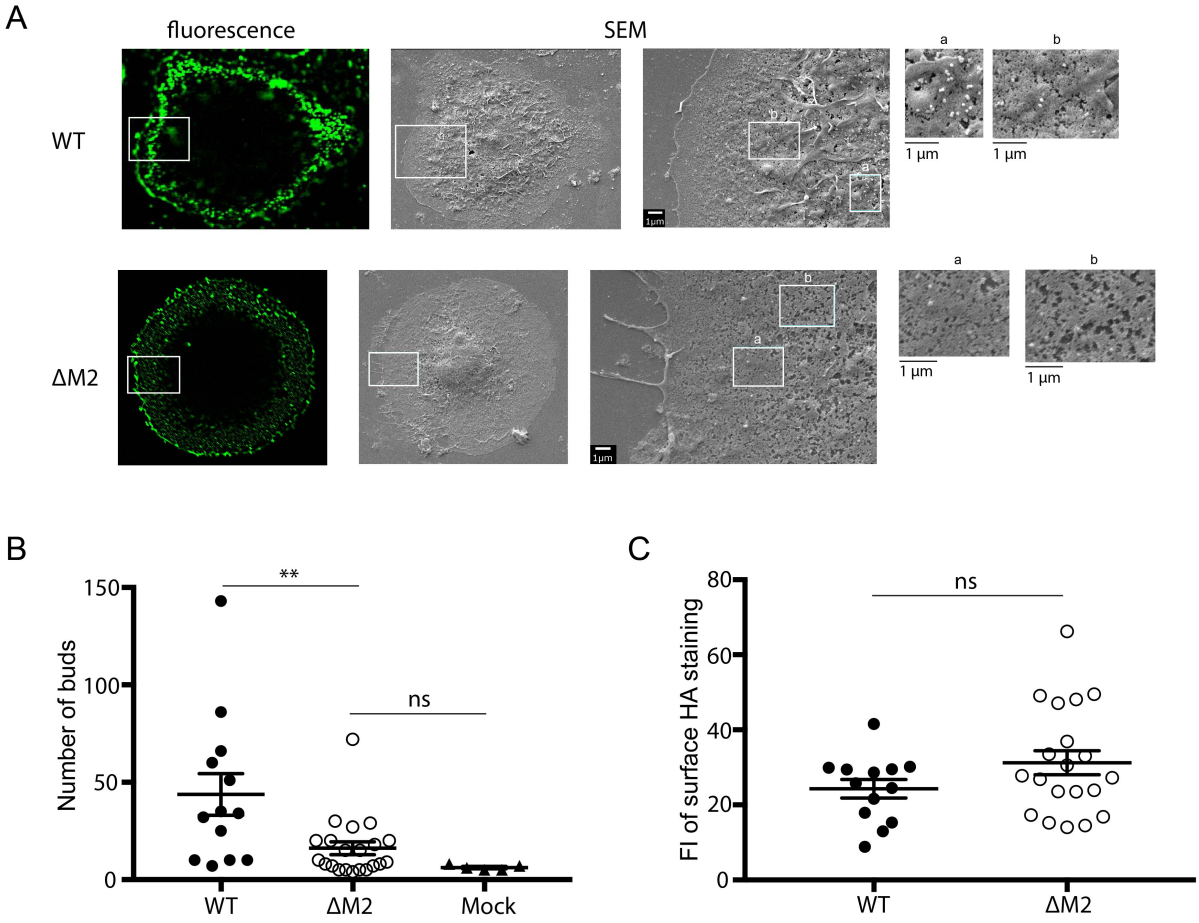

Figure 3.5: dTHP1 cells support IAV particle assembly in an M2-dependent manner. dTHP1 cells were infected with WT or ΔM2 virus for 18 hours. Infected cells were fixed and immunostained with anti-HA antibody. After identification of HA-positive cells by confocal fluorescence microscopy, cells were processed for SEM. The same cells were identified based on grid positions and analyzed by SEM. (A) Representative SEM images for WSN-infected HA-positive cells are shown. Fluorescence images corresponding to the SEM images are also included. Boxed areas for SEM images are magnified and shown on the right of original images. Alphabetic labels are used to distinguish between the individual boxed areas. (B) The number of ~100-nm buds identified in SEM images were counted within the same sized area (100 μm^2 in size) in each cell. (C) Fluorescence intensity (FI) of surface HA expression was determined for each cell analyzed for virus bud formation using SEM. Data are shown for 10-20 cells from two independent experiments. Error bars represent standard error of mean. **, $P<0.01$; ns, non-significant.

Discussion

In **chapter 2**, I showed that both HA-M2 association and IAV assembly are suppressed by the actin cytoskeleton in MDM. In this chapter, I delve into the mechanisms by which the actin cytoskeleton suppresses IAV assembly in MDM. I show that disruption of F-actin elongation or branching restores HA-M2 association in MDM, suggesting that both linear and branched actin filaments are important for the suppressive role of F-actin in HA-M2 association in MDM (Figure 3.2). In terms of the viral proteins involved in the F-actin-dependent suppression of IAV assembly in MDM, I propose three possible mechanisms in Figure 3.1. While the 'microdomain segregation' model suggests an essential role for recruitment of M2 to HA-enriched budozones for initiation of particle assembly upon F-actin disruption, the remaining two models suggest that other viral structural proteins initiate particle assembly upon F-actin disruption, after which M2 is recruited to the virus bud. Using a virus that fails to express M2 but expresses HA and M1 in infected cells (Figure 3.3), I show that F-actin suppresses IAV assembly in MDM in an M2-dependent manner (Figure 3.4). Hence, my data support the M2-dependent 'microdomain segregation' model for F-actin-dependent restriction of IAV assembly in MDM. In addition, I show that similar to the case with MDM, initiation of IAV assembly in dTHP1 cells also depends on M2 (Figure 3.5). Overall, my data indicate that in macrophages, M2 plays important roles early in the process of IAV particle formation.

The cortical actin cytoskeleton, which underlies the plasma membrane to organize and maintain the structure of the plasma membrane, is likely the component of the cellular actin network that regulates HA-M2 association at the plasma membrane. The cortical actin cytoskeleton consists of both linear and branched actin filaments [244], which influence the shape and structure of the plasma membrane to regulate processes such as microdomain segregation,

formation of membrane protrusions, cell migration, and endocytosis [245]. My data suggest that the cortical actin cytoskeleton restricts association between HA and M2 at the plasma membrane of MDM, which results in a defect in IAV particle assembly in this cell type. Since HA and M2 are present in distinct microdomains of the plasma membrane early during IAV assembly [18,22], the cortical F-actin may prevent mixing between HA- and M2-enriched microdomains. In an apparent contrast with my findings, Thaa et al. previously used Fluorescence Resonance Energy Transfer (FRET) microscopy and observed that cytochalasin D treatment reduces co-clustering between fluorescent protein fusions of HA and M2, indicating that the actin cytoskeleton plays a positive role in the association between the two proteins in the absence of any other viral proteins [181]. The discrepancies in the role of F-actin in HA-M2 association between my study and the previous study might be due to differences in the cell types used in these studies (Chinese Hamster Ovary cells in [181] versus primary human blood derived macrophages in my study). In addition, technical differences could account for the discrepancies; for example, the presence of other viral components in infection-based experiments (my study) or attachment of fluorescent proteins to the cytoplasmic domains of HA and M2 in the FRET study [181] may affect the interaction with cortical actin. Future studies focusing on the live cell tracking of HA and M2 on the surface of infected cells using super-resolution microscopy will help address whether the 'microdomain segregation' model explains the role of actin cytoskeleton in IAV assembly in MDM.

The cortical actin cytoskeleton regulates plasma membrane structure via both lipid-actin and protein-actin interactions [245]. Hence, differential expression or function of a factor, which bridges interactions between the cortical F-actin and the plasma membrane, between different cell types may explain how F-actin suppresses HA-M2 association in one cell type (MDM) but

not another (dTHP1 cells). Alternatively, it is possible that the cortical F-actin suppresses HA-M2 association in both cell types; however, dTHP1 cells (and likely epithelial cells) express an additional factor(s) that helps overcome this suppressive role of F-actin. As for the mechanisms by which the cortical actin network segregates plasma membrane-associated proteins, the most well accepted model in the field is the 'picket-fence' model [211,246-248]. According to this model, the actin network (fence) interacts with membrane linker proteins (pickets) to compartmentalize the plasma membrane. Proteins diffuse freely within these individual compartments and, only occasionally, "hop" into an adjacent compartment, where they can again undergo free diffusion. It is possible that HA and M2 localize to distinct compartments of the plasma membrane in both dTHP1 cells and MDM; however, they are unable to overcome the barriers imposed by the 'picket' proteins in MDM but not in dTHP1 cells.

In addition to lending insight into the mechanism by which the cortical actin cytoskeleton suppresses IAV assembly in MDM, my data also suggest that association of M2 with HA is essential for initiation of IAV particle assembly. This is in contrast with previous studies in epithelial cell lines, which assemble spherical particles at the plasma membrane even without M2 expression; however, the virus particles fail to undergo scission and remain attached to the plasma membrane [16,26]. This discrepancy between my study and previous studies could be due to a cell-type-dependency for the role of M2 in early stages of particle assembly. Future studies focusing on the role of M2 at specific stages of IAV assembly in different cell types, including primary epithelial cells, will provide a better understanding of the IAV assembly process. In addition, it remains to be understood whether the timing of recruitment of M2 to the HA-enriched budozone varies between assembling spherical versus filamentous IAV particles. As for the role of M2 during IAV assembly, M2 recruitment to HA-enriched microdomains may

either directly induce membrane curvature required for particle formation or M2 plays a more indirect role in particle formation by recruiting other curvature inducing components such as M1 and/or vRNPs to HA-enriched budozones.

Overall, in this chapter, I show that both linear and branched actin filaments contribute to the suppressive role of the actin cytoskeleton in HA-M2 association in MDM. In addition, I provide evidence that the actin cytoskeleton suppresses IAV particle assembly in MDM by restricting HA-M2 association at the plasma membrane. Importantly, data in this chapter suggest that M2, in addition to its role in pinching off of assembled virus particles, plays an essential role early during IAV particle formation in macrophages. Overall, my data provide a better understanding of the viral and host mechanisms that operate during IAV assembly.

Acknowledgments

I thank the members of Ono laboratory for helpful discussions. I thank Amanda Haag for constructing the pCABSD-M2 plasmid and generating the M2-MDCK cell line. The microscopy data presented in this study was collected at the BRCF Microscopy core, University of Michigan. This work was supported by funding from the National Institutes of Health (R01 AI071727; R21 AI143276) (to Akira Ono).

Chapter 4

Discussion

The focus of my thesis was to identify the mechanisms by which viral and host cell proteins regulate IAV assembly in host cells. The strategy I employed for this purpose is comparison between cells that support IAV assembly (permissive) and those that are defective at IAV assembly (non-permissive). In **chapter 2**, I characterize the primary human monocyte-derived macrophage as a cell type that is non-permissive to IAV particle assembly. In addition, I identify HA-M2 association as a discrete step in IAV assembly, which is defective in primary human monocyte-derived macrophages (MDM). With respect to the host cell mechanism regulating this step, I identify the actin cytoskeleton as the host cellular system that suppresses HA-M2 association and IAV assembly in MDM. In **chapter 3**, I show that the actin cytoskeleton regulates IAV assembly in MDM in an M2-dependent manner. In addition, my data suggest that both elongation and branching of F-actin are important for restriction of HA-M2 association in MDM. In this chapter, I will summarize the findings from the previous two chapters and discuss the implications and future directions of my work.

Summary of data

(i) MDM are inefficient at supporting IAV replication due to a defect at a specific step in IAV assembly

While several groups have identified species-specific defects in IAV replication [189,190,192,194,195], limited information is available with respect to cell-type-specific defects in

IAV replication. Abortive IAV infection in murine alveolar macrophages was first reported in 1981 [249]. More recent studies show that while both human epithelial cells and macrophages can be infected by IAV *ex vivo* [250], macrophages are less permissive or non-permissive to replication of seasonal virus strains [199-205]. The respiratory tract is suggested to harbor two distinct macrophage populations: lung-resident alveolar macrophages and monocyte-derived macrophages [251,252]. In case of humans, both alveolar macrophages and monocyte-derived macrophages are similarly inefficient at supporting IAV propagation [200,204]. Notably, species-specific differences exist for IAV propagation in macrophages. While murine macrophages are non-permissive to seasonal IAV strains [199,201,206], IAV replication is not completely blocked in human macrophages although it is still less efficient than in epithelial cells [200,202,203,205,206]. With respect to the nature of the block, human macrophages were shown to support early stages of IAV lifecycle but have a block in the late stage [205].

My results in **chapter 2** confirm the findings from previous studies that MDM are inefficient at supporting productive infection of seasonal H1N1 and H3N2 IAV strains. In addition, I identify particle assembly as a step in the IAV life cycle that is defective in MDM. Notably, I also identify association between HA and M2 at the plasma membrane as a discrete step that is defective in MDM. Overall, these findings have filled a major gap in the field. Future studies looking into whether HA-M2 association is blocked in terms of infection with other IAV strains will shed light on whether this MDM-specific defect is conserved between different IAV strains. In addition, it remains to be determined whether alveolar macrophages also block IAV replication by mechanisms similar to that in MDM.

(ii) The defect in IAV assembly in MDM is restored upon disruption of the actin cytoskeleton

In addition to identifying HA-M2 association as a step that is defective in MDM in **chapter 2**, I also provide evidence that this defect manifests in an F-actin-dependent manner. Upon disruption of the actin cytoskeleton in MDM, HA-M2 association is restored at the plasma membrane, which correlates with a restoration in virus bud formation. Of note, virus release is not restored upon F-actin disruption even when particle assembly is restored, suggesting the presence of an additional defect(s) in particle assembly/release in MDM. The restrictive role of F-actin in MDM could either be due to the distinct structure and/or function of the actin network or due to the differential function or expression of an actin-dependent host factor(s) in this cell type. In **chapter 3**, I provide evidence that the complete disruption of the actin cytoskeleton is not necessary for restoration of HA-M2 association. Relatively more subtle alterations in the actin cytoskeleton such as halting of elongation or branching without complete disruption of the cytoskeleton also restore HA-M2 association in MDM, suggesting that a finer mechanism(s) underlies the suppressive role of the actin cytoskeleton in IAV assembly.

(iii) The actin cytoskeleton regulates IAV assembly in MDM in an M2-dependent manner

While the findings in **chapter 2** indicate that the actin cytoskeleton regulates both HA-M2 association and IAV assembly in MDM, it was not clear whether HA-M2 association precedes particle assembly or HA-M2 association takes place after particle assembly is initiated by other viral structural components (Figure 3.1, **chapter 3**). To better understand the mechanism(s) by which the actin cytoskeleton suppresses IAV assembly, in **chapter 3**, I use an M2-deficient virus to show that M2 expression is necessary for restoration of IAV assembly following F-actin disruption in MDM. These findings indicate that association between HA and M2 likely precedes

and is essential for IAV assembly upon F-actin disruption in MDM. Based on these results, in **chapter 3**, I propose that the actin cytoskeleton exerts its effect on IAV assembly in MDM by segregating HA- and M2-enriched microdomains at the plasma membrane. An alternative mechanism for the restrictive role of the actin cytoskeleton in HA-M2 association is also discussed in the following section.

Implications and Future Directions

Visualizing individual steps of IAV assembly

Previously, most groups studying the role of viral and host factors in IAV assembly have used virus release as a read-out for IAV assembly and budding [26,39,59,60,82,86,91,92,137]. In some cases, transmission electron microscopy (TEM) or scanning electron microscopy (SEM) were used to analyze either the lack of assembled particles [25,26] or assembled virus particles that fail to be released from the cells [16,26,131,136]. However, the efficiency of particle formation on the cell surface has only been quantified in a few cases [42,131,136]. In addition, viral protein expression or clustering on the cell surface has not been correlated with the efficiency of particle formation before. In my studies, I use correlative fluorescence SEM (CFSEM) to simultaneously analyze HA clusters and virus buds on the surface of the same cell. Using this technique, virus particle formation can be specifically analyzed in cells that form HA clusters on the plasma membrane and the efficiency of virus particle formation can be determined with more confidence. Of note, my data in **chapter 2** (Figure 2.6) show that HA clusters do not always correspond to virus buds. Hence, visualization and quantification of HA clusters is not a direct read-out for assembling virus particles and better tools are required to better visualize virus assembly sites. For this purpose, I employed an *in situ* proximity ligation assay (PLA), which

allows for detection of two proteins localized within 40-nm distance of each other, to quantify co-clustering between viral proteins at the plasma membrane. While this assay has been previously used to show sites of association between HA and M2 at the plasma membrane [42], it was not known whether these sites of HA-M2 association represent sites of virus assembly. My studies, which utilize both PLA and CFSEM, show that under conditions where either HA-M2 association is not observed (on MDM infected with WT virus or on dTHP1 cells) or M2 is absent (on MDM and dTHP1 cells infected with virus lacking M2), virus particle assembly is highly inefficient. Therefore, sites of HA-M2 association likely represent sites of virus assembly. Overall, the tools developed in my thesis allow for better visualization of the individual steps of IAV assembly. In the future, these tools will potentially help advance our understanding of the different viral and host factors involved in different steps of IAV assembly.

Potential mechanisms by which the actin cytoskeleton restricts association between HA and M2 in MDM

My data in **chapter 3** suggest that restoration in association between HA and M2 upon F-actin disruption is essential for IAV assembly in MDM under these conditions. Hence, the actin cytoskeleton may be suppressing HA-M2 association by two possible mechanisms: (i) mobility and organization of HA- and M2-containing plasma membrane microdomains; and/or (ii) blocking the trafficking of cytoplasmic viral components to the plasma membrane. These two non-mutually exclusive mechanisms are further described below.

i. *Mobility and organization of HA- and M2-containing plasma membrane microdomains:* The plasma membrane is heterogeneous in composition and fluidic in nature. It is composed of discrete but often dynamic domains with unique physical and biological properties. These specialized regions are referred to as microdomains. Of these, the most extensively studied are lipid rafts or membrane rafts, which are enriched in cholesterol

and sphingolipids [253,254]. IAV is thought to assemble in cholesterol-enriched microdomains, or membrane rafts, of the plasma membrane in host cells [14,15,215,216]. While HA and NA accumulate in membrane rafts [17,18,21-23], also known as the budozones, M2 is suggested to localize at the edge of the budozone [16,25,26]. While lipid compositions were initially thought to be the main determinant for formation and stability of the microdomains, it has been suggested more recently that membrane-associated proteins also play important roles in formation and maintenance of plasma membrane microdomains [254]. The cortical actin cytoskeleton, which underlies the plasma membrane, plays an important role in stabilizing microdomains [255]. In addition, increases in local F-actin concentration in response to activation signals drive the large-scale clustering of microdomains [145,256-258]. Since M2 is present in microdomains distinct from HA-enriched microdomains early on in the assembly process [18,22] but is later recruited to these assembly sites [25,86,176], the cortical actin network in primary macrophages may keep these plasma membrane microdomains apart via interactions with either lipids [232,233] or cytoplasmic tails of transmembrane proteins [211,234,235]. Future studies focusing on the live cell tracking of HA and M2 on the surface of infected cells using super-resolution microscopy will help address whether the cortical actin cytoskeleton segregates HA- and M2-enriched plasma membrane microdomains

ii. *Blocking the trafficking of cytoplasmic viral components to the plasma membrane:* While M2 functions in recruitment of M1 and vRNP to assembly sites [59,60,81,86-88,90], it is not clear whether interaction of M2 with M1 and/or vRNPs drives its recruitment to HA-enriched budozones. Previously, it has been shown that mutations in the M2 cytoplasmic tail, which reduce the interaction of M2 with M1 and/or vRNP, reduce the extent of

coclustering between HA and M2 at the plasma membrane [86,176]. This suggests that the recruitment of M2 to HA-enriched budozones may at least be partially dependent on its association with M1 and/or vRNPs. Therefore, the actin network may inhibit HA-M2 association by restricting the trafficking, incorporation or function of additional components essential for IAV assembly, that is, M1 and vRNPs. Both M1 [148] and NP [149] are reported to associate with F-actin, and this association might suppress their mobility and trafficking to virus assembly sites. In addition, the dense F-actin cortex could also serve as a physical barrier to diffusion of proteins or vesicles carrying these proteins [238,239].

Additional defect(s) in IAV assembly/release in macrophages

While F-actin disruption restores HA-M2 association and IAV particle assembly in MDM, virus release is still defective in this cell type. This suggests the presence of an additional defect(s) in virus assembly, budding or release in MDM. For example, recruitment of M1 and/or vRNPs may still be defective and thus, particle assembly or scission of assembled particles may not be completed in MDM. Future studies aimed towards studying the localization of these cytoplasmic viral components are necessary to determine whether their trafficking/recruitment is defective in MDM. My preliminary data, using anti-M1 and anti-vRNP antibodies, show that while both M1 and vRNPs are readily detected in the cytoplasm, their detection at the plasma membrane is poor (Figures 4.1A and B). This is likely due to the inaccessibility of antibody epitopes due to the tight packaging of these components into the assembling virus particle. This is more clearly observable in the case of M1 when viral uncoating is artificially induced at the plasma membrane using an acidic buffer (Figure 4.1C). In comparison to treatment with a neutral buffer, treatment with an acidic buffer allows for visualization of M1 at the HA-enriched budozones. However, since, an acidic environment reduces the membrane binding efficiency of M1 [76,259,260], only a

sub-population of membrane-bound M1 may be visualized using this approach. Therefore, better approaches utilizing viruses encoding fluorescently-tagged proteins are needed to visualize M1 and vRNPs at the plasma membrane of infected cells. Comparisons between dTHP1 and MDM using fluorescently-tagged viral proteins is likely to lend insight into whether trafficking of M1 and vRNPs is efficient in MDM, in comparison to that in dTHP1 cells.

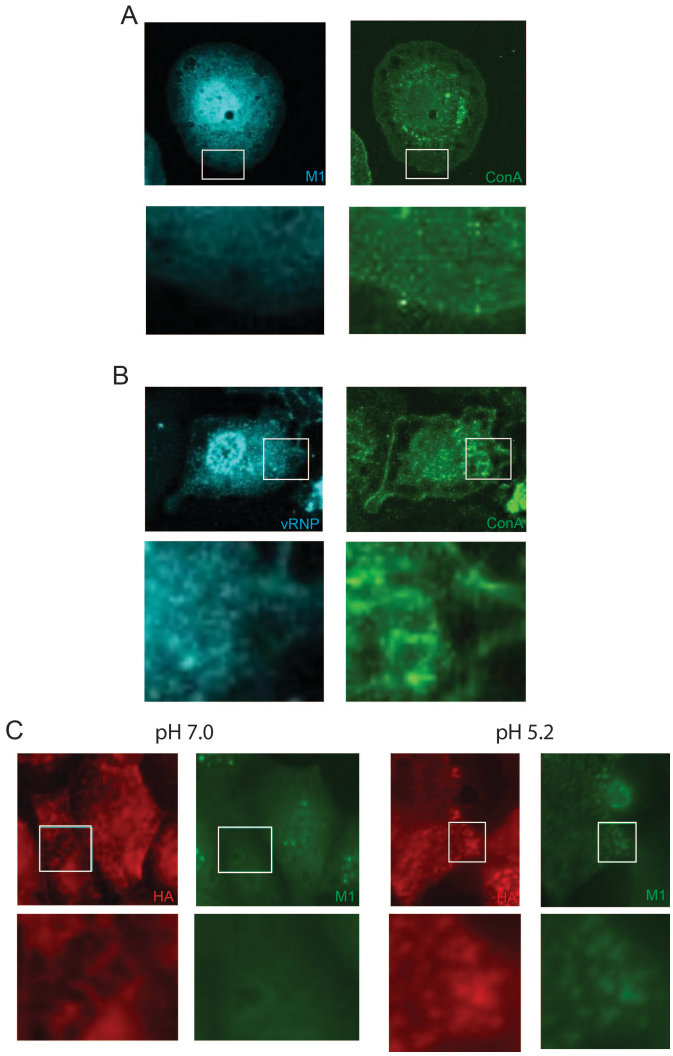

Figure 4.1: Detecting HA and vRNPs at the plasma membrane of IAV-infected cells. (A, B) dTHP1 cells and MDM were infected with WSN at MOI 0.01. At 24 hours post infection, cells were stained with a cell surface marker, ConA. Cells were then permeabilized and immunostained with anti-M1 (A) or anti-vRNP (B) antibodies. (C) MDCK cells were infected with WSN at MOI 0.01 for 12 hours. Cells were incubated in PBS at pH 7.0 or 5.2 for 10 minutes at room temperature, following which they were fixed and immunostained with anti-HA antibody. Cells were then permeabilized and immunostained with anti-M1 antibody. Boxed areas from the images in the top panel are shown in the lower panel. Data are representative of at least two experiments.

Alternative to defects in particle assembly and/or pinching off, fully assembled nascent particles may remain tethered to the cell surface in MDM. While IAV is not sensitive to membrane retention via tetherin [261,262], other host cellular proteins such as viperin [136] may be involved. NA, which cleaves sialic acid residues prior to virus release, associates efficiently with HA at the plasma membrane in MDM. However, it remains to be determined whether the sialidase function of NA, which is required for release of nascent virus particles, is efficient in this cell type.

Virus spread despite defective virus release in IAV-infected cells

My data in **chapter 2** (Figure 2.2) show that the fraction of infected cells increase over time with comparable efficiency in both dTHP1 and MDM cultures despite a drastic reduction in virus particle release from MDM, relative to dTHP1 cells. However, the mechanism(s) by which MDM support virus spread despite reduced virus release is not understood. The other virus population that can allow for virus spread when infectious cell-free virions are scarce is comprised of cell-associated virus particles. Cell-associated virus particles use cell-to-cell transmission for spread. It is possible that IAV-infected MDM rely more on cell-to-cell spread than cell-free spread, in comparison to dTHP1 cells or epithelial cells. MDM promote HIV-1 transmission via cell-cell contact with T cells to allow viruses to spread efficiently and in some cases to evade antiviral drugs or immunity [263-265]. For IAV, cell-to-cell spread, mediated by cell-bound virus, may allow the virus to evade respiratory tract conditions that can restrict infection of a distant cell. Notably, cell-to-cell virus spread of IAV can occur in the presence of oseltamivir [266], an anti-NA drug that abolishes virus release. While long-distance intercellular bridges were implicated in spread of cell-associated virus [267,268], it is not clear whether all infected cell types employ this mechanism for virus spread. In the context of HIV-1 infection,

intercellular bridges have been implicated in cell-to-cell virus spread in macrophages [269]. The extent to which cell-to-cell spread contributes to IAV transmission is also dependent on the morphology of IAV particles. My preliminary data show that both spherical and filamentous variants of the same IAV strain spread with comparable kinetics in epithelial cells even when significantly lower levels of cell-free filamentous virus particles are present, relative to spherical particles, suggesting that the filamentous IAV particles use the cell-to-cell mode of virus spread to a higher extent than spherical viruses (Figure 4.2B). To understand the extent to which cell-to-cell spread contributes to spherical IAV propagation in MDM, virus spread kinetics need to be measured under conditions that block cell-free virus spread (such as in the presence of oseltamivir).

Alternative to cell-associated virus, cell-free semi-infectious virus particles, which are not detected by viral plaque assays, may contribute to spread in MDM. The presence of a relatively high number of semi-infectious particles in MDM culture supernatants is suggested by my data showing higher proportion of non-fully infectious particles in MDM culture supernatants, relative to dTHP1 culture supernatants (Figure 2.3, **chapter 2**).

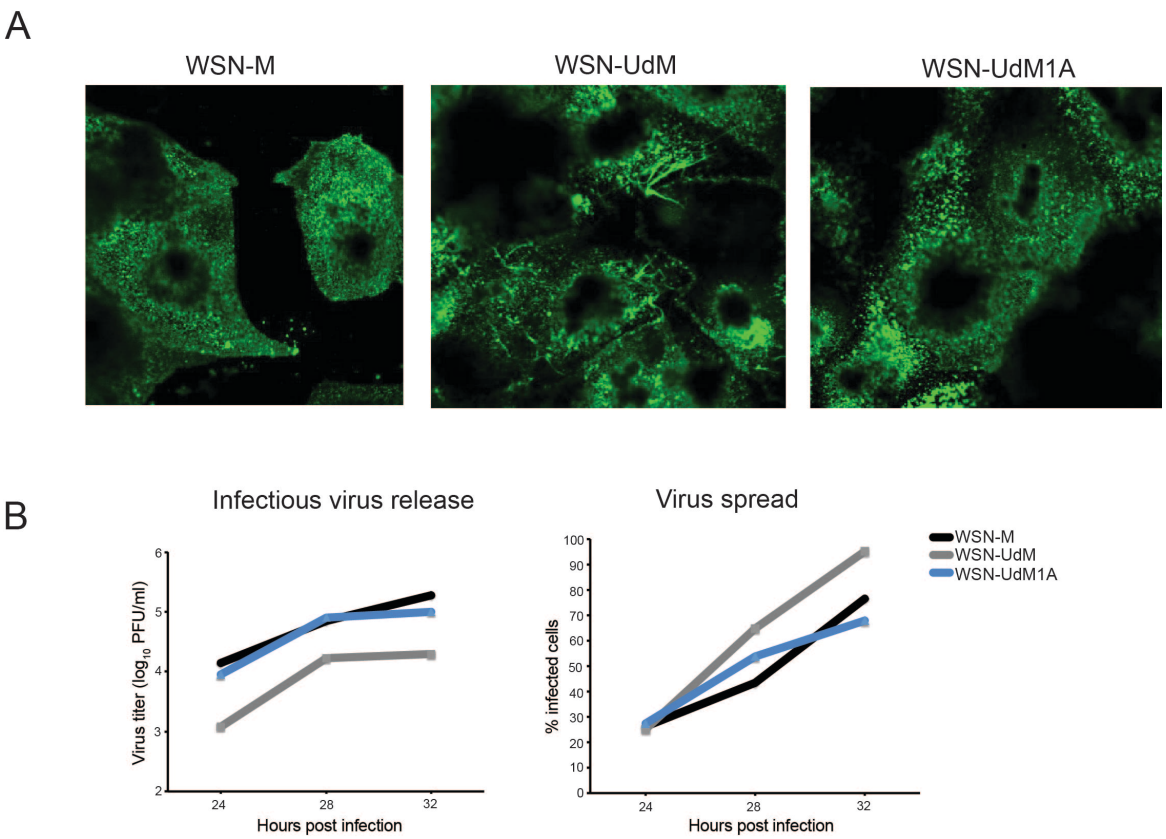

Figure 4.2: Virus spread and infectious virion release of spherical and filamentous IAV strains. MDCK (A) or A549 (B) cells were infected with WSN; reassortant WSN encoding the M segment of Udorn (UdM), a filamentous IAV strain; or reassortant WSN encoding a mutant version of the Udorn M segment (UdM1A). (A) MDCK cells inoculated with indicated viral strains were immunostained with anti-HA antibody at 24 hours post infection and analyzed by confocal microscopy. While WSN forms spherical virus particles, which are represented by HA-positive puncta on the cell surface, WSN-Udorn assembles both filamentous and spherical particles. An A41V mutation in UdM (UdM1A) abolishes the ability of UdM to assemble filamentous virus particles. (B) Titers in culture supernatants were measured using plaque assays (left panel) and virus spread in the cultures was measured by flow cytometry using anti-HA antibody. Data are representative of four independent experiments.

Physiological relevance of defective IAV replication in macrophages

Macrophages play a central role in controlling IAV infection. Alveolar macrophages, which reside in the lung, are important for clearance of virus and reducing IAV-related morbidity and mortality in mice [270-273]. In addition, monocyte-derived macrophages (MDM) also infiltrate into the respiratory tract in response to viral or bacterial infection, ageing, and smoking-induced damage [274,275]. A recently published study shows that human MDM, and not alveolar

macrophages, express receptors for IAV binding and subsequent endocytosis [276], suggesting a role for MDM in interacting with IAV. While MDM may serve as a 'dead end' for IAV infection, the ability of MDM to support the early stages but not the late stages of the IAV life cycle may have additional implications for the innate immune response against IAV.

IAV is sensed by different pathogen recognition receptors (PRRs), which leads to secretion of type I IFNs, proinflammatory cytokines, and chemokines, and acquisition of activation status [277]. PRRs such as C-type lectin receptors (CLR) and Toll-like receptors (TLR) 2 and 4 detect IAV on the cell surface of innate immune cells such as monocytes, macrophages, neutrophils, dendritic cells (DCs). Other TLRs such as TLR3 and TLR7/8, which are expressed in the endosome of innate immune cells, sense viral RNA or DNA. While CLRs and TLRs are mainly expressed in immune cells, cytoplasmic PRRs such as NOD-like receptors (NLRs) and RIG-I-like receptors (RLRs) are expressed in both innate immune and epithelial cells. In IAV-infected cells as well as in immune cells that have phagocytosed IAV-infected cells, the NLRs NLRP3, NLRC3, and NLRX1 sense viral RNA or other viral proteins generated upon active viral replication in the cell [278]. The most well studied PRR for IAV is the RLR RIG-I, which senses the 5'-triphosphate-RNA containing the dsRNA panhandle generated upon active viral replication within the cell [279-281]. More recent studies have also shown that RIG-I preferentially binds shorter genomic segments, which include mini viral RNAs and defective interfering (DI) RNAs, and not full-length genomes [282-284].

While the interferon response is likely induced upon IAV infection in both MDM and epithelial cells (and dTHP1 cells), the defect(s) in IAV assembly and release in MDM may further enhance interferon induction in this cell type. The defect(s) in particle assembly and release in MDM may lead to intracellular accumulation of viral genomes, which could then be

sensed by cytoplasmic PRRs. In addition, it is tempting to speculate whether higher levels of short viral genomic RNAs, which are more efficient at binding RIG-I, are produced in MDM, relative to dTHP1 cells or epithelial cells. My preliminary data show that vRNPs, which are a proxy for viral RNA, are more dispersed in the cytoplasm of MDM, in comparison to a more clustered localization at the perinuclear region in dTHP1 cells (similar to epithelial cells [42,285]) (Figure 4.3). These data suggest that viral RNAs may rely on a different pathway for cytoplasmic transport in MDM, in comparison to dTHP1 cells. In cells infected with Sendai virus, which is also a single-stranded negative sense RNA virus that is sensed by RIG-I, shorter defective viral genomes show a more disperse cytoplasmic distribution whereas, full-length genomes accumulate in the perinuclear region of the cell [286]. Therefore, the mode of cytoplasmic transport may vary between full-length and incomplete viral genomes. If IAV defective genomes, like in the case of Sendai virus, use transport pathways distinct from that of full-length genomes for trafficking to the plasma membrane, my data suggest the possibility that higher levels of shorter defective viral RNAs may be present in MDM, in comparison to dTHP1 cells. More detailed studies will provide more insight into the differences in viral RNA populations present in infected MDM versus dTHP1 cells (and epithelial cells).

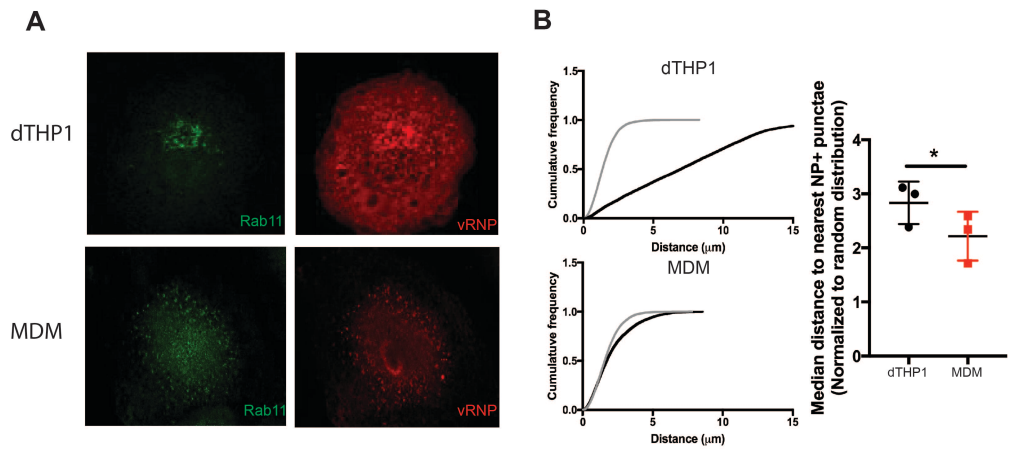

Figure 4.3: vRNP distribution is altered in MDM, in comparison to dTHP1 cells. dTHP1 cells and MDM were infected with WSN at MOI 0.01 for 24 hours. Infected cells were fixed, permeabilized, immunostained for Rab11 and vRNP, and analyzed by confocal microscopy. (B) Distances from typical positions in a WSN-infected cell to the nearest vRNP signal were measured (black) using an ImageJ plugin, Spatial Statistics 2D/3D, and shown as cumulative frequency. Gray lines represent estimated random pattern for the same number of vRNP signals. While vRNPs show a more random distribution in MDM, they are more clustered in dTHP1 cells. Distances at cumulative frequency= 0.5 were calculated for the each cell and averages per experiment are shown in the right panel. Data are averages of three independent experiments with 8-10 cells analyzed per experiment. *, $p<0.05$

Cell-type-dependent role of M2 in IAV particle formation

Previous studies using epithelial cells show that while M2 is required for pinching off of virus bud and its subsequent release, it is not required for induction of membrane curvature during spherical particle assembly [16,25,59,87]. It has also been proposed that M2 is recruited after induction of membrane curvature [225,226], which is likely mediated by HA, NA or M1. At sites of virus assembly, M2 is enriched at the neck of the virus bud [16,25,26] and is thought to induce positive membrane curvature, which may be sufficient for membrane scission [16,46]. Contrary to the case with spherical IAV assembly, M2 is required for assembly as well as membrane scission of filamentous particles in epithelial cells [25]. In contrast with epithelial cells, M2 is essential for induction of membrane curvature during spherical IAV assembly in both dTHP1 cells and MDM (**chapter 3**). In addition, I show that HA-M2 association likely precedes initiation of spherical IAV particle assembly in MDM, suggesting that M2 plays an important role(s) early during IAV

assembly in macrophages. This discrepancy between macrophages (dTHP1 and MDM) and epithelial cells may be due to the differences in the stoichiometry of other viral structural proteins at the plasma membrane of different cell types. Since there is some redundancy in the roles of M1 and M2 during IAV assembly [92,287], it is possible that in the absence of M2, other viral structural proteins such as M1 can compensate for its functions in epithelial cells. In contrast, in dTHP1 cells and MDM, other viral structural proteins may either not be present at the plasma membrane at a high enough concentration or may not cocluster to a high enough density. Under such circumstances, recruitment of M2 to HA-enriched virus budozones is required to initiate particle assembly. Alternatively, M2 may induce membrane curvature indirectly through its association with and subsequent recruitment of M1 and/vRNPs [59,60,81,86-88,90] to viral budozones. While HA and NA are also involved in the recruitment of M1 [27,28,176] and vRNPs [69], it is not clear which of the two modes of recruitment, M2- or HA/NA-dependent, is more dominant. It is possible that in epithelial cells, both modes of recruitment are equally efficient. On the other hand, HA/NA-dependent recruitment of M1 and/or vRNPs may be inefficient in dTHP1 cells and MDM and hence, M2-dependent recruitment may be more dominant in these cell types. In the future, analysis of M2 truncation mutants for their ability to support virus particle assembly in dTHP1 cells and MDM will provide more insight into the functions of M2 that are important for induction of membrane curvature during IAV assembly in macrophages.

Actin-dependent host factor(s) regulate IAV assembly

In MDM, the actin cytoskeleton plays a negative role in assembly of spherical (and likely filamentous) IAV particles, likely by restricting HA-M2 association at assembly sites. The restrictive role of F-actin in MDM could either be due to the distinct structure and/or function of the actin network or be due to the differential function or expression of an actin-dependent host

factor(s) in this cell type. Since the actin cytoskeleton is highly conserved among mammalian cells, it is unlikely that the structure or function of the actin network in MDM is drastically different from that in dTHP1 cells. If subtle differences exist in the actin network between these two cell types, they are likely to be due to differential expression or function of an actin-binding protein. As for the nature of this host factor, it could either serve as a restriction factor that suppresses particle assembly in MDM or as a dependency factor that allows the virus to overcome the suppressive effect of the actin cytoskeleton in IAV-permissive cells (epithelial and dTHP1 cells). To distinguish between these two possibilities, our future studies will focus on generating MDM-dTHP1 heterokaryons and analyzing their ability to support IAV assembly. This approach is described in Figure 4.4. Since the host factor of interest regulates IAV assembly by modulating HA-M2 association at the plasma membrane, it is likely to be either a transmembrane protein or a cytoplasmic factor that localizes close to the plasma membrane. A cytoplasmic host protein can associate with the actin network and/or the membrane lipids or membrane-associated viral proteins. Some examples of cytosolic proteins that associate with both the actin network and membrane lipids or membrane-associated viral proteins are the ERM (Ezrin, Radixin and Moesin) proteins [288-290] and talin [291,292]. On the other hand, a transmembrane host protein can associate with the actin network via its cytoplasmic domain and/or with lipids or membrane-associated viral proteins via its ecto- or transmembrane domains. Some examples of transmembrane proteins that associate with actin and aid in organization of other plasma membrane-associated proteins are CD44 [211], Cystic Fibrosis Transmembrane Conductance Regulator (CFTR) [234,293], and Csk-binding protein (CBP) [235]. Irrespective of whether the host factor is cytoplasmic or transmembrane in nature, it may function in regulating IAV assembly by organizing HA- and M2-containing microdomains. Alternatively, if the defect

in HA-M2 association in MDM is due to a block in trafficking/recruitment of M1 and/or vRNPs, the host factor regulating this step is more likely to be a cytoplasmic protein. In the future, heterokaryon studies and more high-throughput approaches such as proteomics or RNAseq will potentially help identify the host factor regulating IAV assembly in MDM.

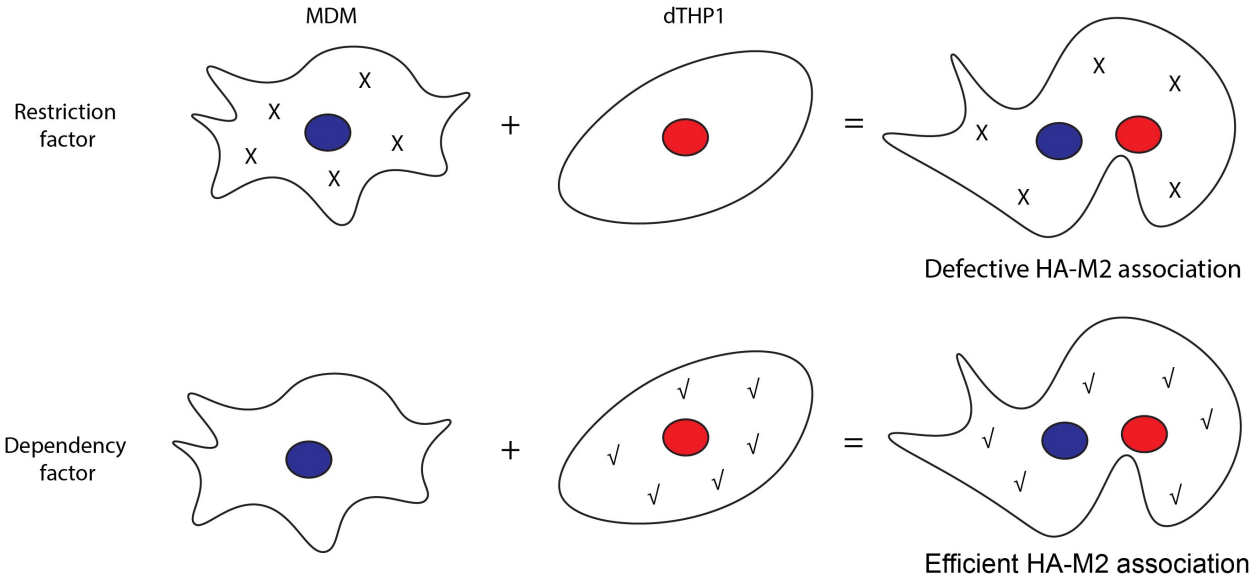

Figure 4.4: Using heterokaryons to determine the nature of the host factor suppressing HA-M2 association in MDM. dTHP1-MDM heterokaryons can be used to the determine whether the defect in HA-M2 association in MDM is due to the presence of restriction factor that blocks HA-M2 association or the absence of a dependency factor that supports HA-M2 association in dTHP1 cells.

The actin cytoskeleton as a potential drug target

The actin cytoskeleton plays positive and/or negative roles during infection of many enveloped viruses such as HIV-1 [294-297], IAV [137,155,159,161,163,298,299], Measles virus [300-303], and Ebola virus [304,305]. Since F-actin disruption promotes IAV assembly in MDM, which are non-permissive to virus assembly, stabilization of the actin cytoskeleton in cell types permissive to IAV assembly (dTHP1 and epithelial cells) may potentially restrict association between HA and M2 and hence, block IAV assembly in these cells. However, the actin cytoskeleton is a highly

conserved network that is required for many key cellular functions and hence, its disruption or stabilization results in cell death. An important implication of my data in **chapters 2 and 3** is that subtle cell-type-dependent differences in the structure and/or function of the actin cytoskeleton or actin-dependent proteins can have a substantial impact on IAV replication. The distinct structure and/or function of the actin cytoskeleton in MDM accounts for the ability of this cell type to suppress IAV assembly without compromising essential cellular functions. Hence, identification of the host factor(s) that regulates these differences in the structure and/or function of the actin cytoskeleton between different cell types will potentially help develop strategies to target more specific aspects of F-actin dynamics and hence, block IAV assembly, without affecting the essential functions of the cell.

References

1. Wahlgren, J. Influenza A viruses: an ecology review. *Infect Ecol Epidemiol* **2011**, *1*, doi:10.3402/iee.v1i0.6004.
2. Iuliano, A.D.; Roguski, K.M.; Chang, H.H.; Muscatello, D.J.; Palekar, R.; Tempia, S.; Cohen, C.; Gran, J.M.; Schanzer, D.; Cowling, B.J., et al. Estimates of global seasonal influenza-associated respiratory mortality: a modelling study. *Lancet* **2018**, *391*, 1285-1300, doi:10.1016/S0140-6736(17)33293-2.
3. Zimmer, S.M.; Burke, D.S. Historical perspective--Emergence of influenza A (H1N1) viruses. *N Engl J Med* **2009**, *361*, 279-285, doi:10.1056/NEJMra0904322.
4. Simonsen, L.; Spreeuwenberg, P.; Lustig, R.; Taylor, R.J.; Fleming, D.M.; Kroneman, M.; Van Kerkhove, M.D.; Mounts, A.W.; Paget, W.J.; Teams, G.C. Global mortality estimates for the 2009 Influenza Pandemic from the GLaMOR project: a modeling study. *PLoS Med* **2013**, *10*, e1001558, doi:10.1371/journal.pmed.1001558.
5. Calder, L.J.; Wasilewski, S.; Berriman, J.A.; Rosenthal, P.B. Structural organization of a filamentous influenza A virus. *Proc Natl Acad Sci U S A* **2010**, *107*, 10685-10690, doi:10.1073/pnas.1002123107.
6. Compans, R.W.; Content, J.; Duesberg, P.H. Structure of the ribonucleoprotein of influenza virus. *J Virol* **1972**, *10*, 795-800.
7. Chen, W.; Calvo, P.A.; Malide, D.; Gibbs, J.; Schubert, U.; Bacik, I.; Basta, S.; O'Neill, R.; Schickli, J.; Palese, P., et al. A novel influenza A virus mitochondrial protein that induces cell death. *Nat Med* **2001**, *7*, 1306-1312, doi:10.1038/nm1201-1306.
8. Wise, H.M.; Foeglein, A.; Sun, J.; Dalton, R.M.; Patel, S.; Howard, W.; Anderson, E.C.; Barclay, W.S.; Digard, P. A complicated message: Identification of a novel PB1-related protein translated from influenza A virus segment 2 mRNA. *J Virol* **2009**, *83*, 8021-8031, doi:10.1128/JVI.00826-09.
9. Jagger, B.W.; Wise, H.M.; Kash, J.C.; Walters, K.A.; Wills, N.M.; Xiao, Y.L.; Dunfee, R.L.; Schwartzman, L.M.; Ozinsky, A.; Bell, G.L., et al. An overlapping protein-coding region in influenza A virus segment 3 modulates the host response. *Science* **2012**, *337*, 199-204, doi:10.1126/science.1222213.
10. Muramoto, Y.; Noda, T.; Kawakami, E.; Akkina, R.; Kawaoka, Y. Identification of novel influenza A virus proteins translated from PA mRNA. *J Virol* **2013**, *87*, 2455-2462, doi:10.1128/JVI.02656-12.
11. Greber, U.F. Virus and Host Mechanics Support Membrane Penetration and Cell Entry. *J Virol* **2016**, *90*, 3802-3805, doi:10.1128/JVI.02568-15.
12. Dou, D.; Revol, R.; Östbye, H.; Wang, H.; Daniels, R. Influenza A Virus Cell Entry, Replication, Virion Assembly and Movement. *Front Immunol* **2018**, *9*, 1581, doi:10.3389/fimmu.2018.01581.
13. Smrt, S.T.; Lorieau, J.L. Membrane Fusion and Infection of the Influenza Hemagglutinin. *Adv Exp Med Biol* **2017**, *966*, 37-54, doi:10.1007/5584_2016_174.

14. Rossman, J.S.; Lamb, R.A. Influenza virus assembly and budding. *Virology* **2011**, *411*, 229-236, doi:10.1016/j.virol.2010.12.003.
15. Nayak, D.P.; Balogun, R.A.; Yamada, H.; Zhou, Z.H.; Barman, S. Influenza virus morphogenesis and budding. *Virus Res* **2009**, *143*, 147-161, doi:10.1016/j.virusres.2009.05.010.
16. Rossman, J.S.; Jing, X.; Leser, G.P.; Lamb, R.A. Influenza virus M2 protein mediates ESCRT-independent membrane scission. *Cell* **2010**, *142*, 902-913, doi:10.1016/j.cell.2010.08.029.
17. Takeda, M.; Leser, G.P.; Russell, C.J.; Lamb, R.A. Influenza virus hemagglutinin concentrates in lipid raft microdomains for efficient viral fusion. *Proc Natl Acad Sci U S A* **2003**, *100*, 14610-14617, doi:10.1073/pnas.2235620100.
18. Leser, G.P.; Lamb, R.A. Influenza virus assembly and budding in raft-derived microdomains: a quantitative analysis of the surface distribution of HA, NA and M2 proteins. *Virology* **2005**, *342*, 215-227, doi:10.1016/j.virol.2005.09.049.
19. Hess, S.T.; Kumar, M.; Verma, A.; Farrington, J.; Kenworthy, A.; Zimmerberg, J. Quantitative electron microscopy and fluorescence spectroscopy of the membrane distribution of influenza hemagglutinin. *J Cell Biol* **2005**, *169*, 965-976, doi:10.1083/jcb.200412058.
20. Kerviel, A.; Thomas, A.; Chaloin, L.; Favard, C.; Muriaux, D. Virus assembly and plasma membrane domains: which came first? *Virus Res* **2013**, *171*, 332-340, doi:10.1016/j.virusres.2012.08.014.
21. Chen, B.J.; Leser, G.P.; Morita, E.; Lamb, R.A. Influenza virus hemagglutinin and neuraminidase, but not the matrix protein, are required for assembly and budding of plasmid-derived virus-like particles. *J Virol* **2007**, *81*, 7111-7123, doi:10.1128/JVI.00361-07.
22. Zhang, J.; Pekosz, A.; Lamb, R.A. Influenza virus assembly and lipid raft microdomains: a role for the cytoplasmic tails of the spike glycoproteins. *J Virol* **2000**, *74*, 4634-4644.
23. Ohkura, T.; Momose, F.; Ichikawa, R.; Takeuchi, K.; Morikawa, Y. Influenza A virus hemagglutinin and neuraminidase mutually accelerate their apical targeting through clustering of lipid rafts. *J Virol* **2014**, *88*, 10039-10055, doi:10.1128/JVI.00586-14.
24. Scolari, S.; Engel, S.; Krebs, N.; Plazzo, A.P.; De Almeida, R.F.; Prieto, M.; Veit, M.; Herrmann, A. Lateral distribution of the transmembrane domain of influenza virus hemagglutinin revealed by time-resolved fluorescence imaging. *J Biol Chem* **2009**, *284*, 15708-15716, doi:10.1074/jbc.M900437200.
25. Rossman, J.S.; Jing, X.; Leser, G.P.; Balannik, V.; Pinto, L.H.; Lamb, R.A. Influenza virus m2 ion channel protein is necessary for filamentous virion formation. *J Virol* **2010**, *84*, 5078-5088, doi:10.1128/JVI.00119-10.
26. Roberts, K.L.; Leser, G.P.; Ma, C.; Lamb, R.A. The amphipathic helix of influenza A virus M2 protein is required for filamentous bud formation and scission of filamentous and spherical particles. *J Virol* **2013**, *87*, 9973-9982, doi:10.1128/JVI.01363-13.
27. Barman, S.; Ali, A.; Hui, E.K.; Adhikary, L.; Nayak, D.P. Transport of viral proteins to the apical membranes and interaction of matrix protein with glycoproteins in the assembly of influenza viruses. *Virus Res* **2001**, *77*, 61-69.
28. Ali, A.; Avalos, R.T.; Ponimaskin, E.; Nayak, D.P. Influenza virus assembly: effect of influenza virus glycoproteins on the membrane association of M1 protein. *J Virol* **2000**, *74*, 8709-8719.

29. Jin, H.; Leser, G.P.; Zhang, J.; Lamb, R.A. Influenza virus hemagglutinin and neuraminidase cytoplasmic tails control particle shape. *EMBO J* **1997**, *16*, 1236-1247, doi:10.1093/emboj/16.6.1236.
30. Zhang, J.; Lamb, R.A. Characterization of the membrane association of the influenza virus matrix protein in living cells. *Virology* **1996**, *225*, 255-266, doi:10.1006/viro.1996.0599.
31. Chlanda, P.; Schraidt, O.; Kummer, S.; Riches, J.; Oberwinkler, H.; Prinz, S.; Kräusslich, H.G.; Briggs, J.A. Structural Analysis of the Roles of Influenza A Virus Membrane-Associated Proteins in Assembly and Morphology. *J Virol* **2015**, *89*, 8957-8966, doi:10.1128/JVI.00592-15.
32. Elster, C.; Larsen, K.; Gagnon, J.; Ruigrok, R.W.; Baudin, F. Influenza virus M1 protein binds to RNA through its nuclear localization signal. *J Gen Virol* **1997**, *78 (Pt 7)*, 1589-1596, doi:10.1099/0022-1317-78-7-1589.
33. Bui, M.; Wills, E.G.; Helenius, A.; Whittaker, G.R. Role of the influenza virus M1 protein in nuclear export of viral ribonucleoproteins. *J Virol* **2000**, *74*, 1781-1786.
34. Baudin, F.; Petit, I.; Weissenhorn, W.; Ruigrok, R.W. In vitro dissection of the membrane and RNP binding activities of influenza virus M1 protein. *Virology* **2001**, *281*, 102-108, doi:10.1006/viro.2000.0804.
35. Sakaguchi, A.; Hirayama, E.; Hiraki, A.; Ishida, Y.; Kim, J. Nuclear export of influenza viral ribonucleoprotein is temperature-dependently inhibited by dissociation of viral matrix protein. *Virology* **2003**, *306*, 244-253.
36. Elton, D.; Simpson-Holley, M.; Archer, K.; Medcalf, L.; Hallam, R.; McCauley, J.; Digard, P. Interaction of the influenza virus nucleoprotein with the cellular CRM1-mediated nuclear export pathway. *J Virol* **2001**, *75*, 408-419, doi:10.1128/JVI.75.1.408-419.2001.
37. O'Neill, R.E.; Talon, J.; Palese, P. The influenza virus NEP (NS2 protein) mediates the nuclear export of viral ribonucleoproteins. *EMBO J* **1998**, *17*, 288-296, doi:10.1093/emboj/17.1.288.
38. Jo, S.; Kawaguchi, A.; Takizawa, N.; Morikawa, Y.; Momose, F.; Nagata, K. Involvement of vesicular trafficking system in membrane targeting of the progeny influenza virus genome. *Microbes Infect* **2010**, *12*, 1079-1084, doi:10.1016/j.micinf.2010.06.011.
39. Amorim, M.J.; Bruce, E.A.; Read, E.K.; Foeglein, A.; Mahen, R.; Stuart, A.D.; Digard, P. A Rab11- and microtubule-dependent mechanism for cytoplasmic transport of influenza A virus viral RNA. *J Virol* **2011**, *85*, 4143-4156, doi:10.1128/JVI.02606-10.
40. Eisfeld, A.J.; Kawakami, E.; Watanabe, T.; Neumann, G.; Kawaoka, Y. RAB11A is essential for transport of the influenza virus genome to the plasma membrane. *J Virol* **2011**, *85*, 6117-6126, doi:10.1128/JVI.00378-11.
41. de Castro Martin, I.F.; Fournier, G.; Sachse, M.; Pizarro-Cerda, J.; Risco, C.; Naffakh, N. Influenza virus genome reaches the plasma membrane via a modified endoplasmic reticulum and Rab11-dependent vesicles. *Nat Commun* **2017**, *8*, 1396, doi:10.1038/s41467-017-01557-6.
42. Kawaguchi, A.; Hirohama, M.; Harada, Y.; Osari, S.; Nagata, K. Influenza Virus Induces Cholesterol-Enriched Endocytic Recycling Compartments for Budozone Formation via Cell Cycle-Independent Centrosome Maturation. *PLoS Pathog* **2015**, *11*, e1005284, doi:10.1371/journal.ppat.1005284.

43. Amorim, M.J.; Kao, R.Y.; Digard, P. Nucleozin targets cytoplasmic trafficking of viral ribonucleoprotein-Rab11 complexes in influenza A virus infection. *J Virol* **2013**, *87*, 4694-4703, doi:10.1128/JVI.03123-12.
44. Bialas, K.M.; Bussey, K.A.; Stone, R.L.; Takimoto, T. Specific nucleoprotein residues affect influenza virus morphology. *J Virol* **2014**, *88*, 2227-2234, doi:10.1128/JVI.03354-13.
45. Chlanda, P.; Mekhedov, E.; Waters, H.; Sodt, A.; Schwartz, C.; Nair, V.; Blank, P.S.; Zimmerberg, J. Palmitoylation Contributes to Membrane Curvature in Influenza A Virus Assembly and Hemagglutinin-Mediated Membrane Fusion. *J Virol* **2017**, *91*, doi:10.1128/JVI.00947-17.
46. Martyna, A.; Bahsoun, B.; Badham, M.D.; Srinivasan, S.; Howard, M.J.; Rossman, J.S. Membrane remodeling by the M2 amphipathic helix drives influenza virus membrane scission. *Sci Rep* **2017**, *7*, 44695, doi:10.1038/srep44695.
47. Palese, P.; Tobita, K.; Ueda, M.; Compans, R.W. Characterization of temperature sensitive influenza virus mutants defective in neuraminidase. *Virology* **1974**, *61*, 397-410.
48. Palese, P.; Compans, R.W. Inhibition of influenza virus replication in tissue culture by 2-deoxy-2,3-dehydro-N-trifluoroacetylneuraminic acid (FANA): mechanism of action. *J Gen Virol* **1976**, *33*, 159-163, doi:10.1099/0022-1317-33-1-159.
49. KILBOURNE, E.D.; MURPHY, J.S. Genetic studies of influenza viruses. I. Viral morphology and growth capacity as exchangeable genetic traits. Rapid in ovo adaptation of early passage Asian strain isolates by combination with PR8. *J Exp Med* **1960**, *111*, 387-406.
50. CHOPPIN, P.W.; MURPHY, J.S.; TAMM, I. Studies of two kinds of virus particles which comprise influenza A2 virus strains. III. Morphological characteristics: independence to morphological and functional traits. *J Exp Med* **1960**, *112*, 945-952.
51. CHU, C.M.; DAWSON, I.M.; ELFORD, W.J. Filamentous forms associated with newly isolated influenza virus. *Lancet* **1949**, *1*, 602.
52. Seladi-Schulman, J.; Steel, J.; Lowen, A.C. Spherical influenza viruses have a fitness advantage in embryonated eggs, while filament-producing strains are selected in vivo. *J Virol* **2013**, *87*, 13343-13353, doi:10.1128/JVI.02004-13.
53. MOSLEY, V.M.; WYCKOFF, R.W. Electron micrography of the virus of influenza. *Nature* **1946**, *157*, 263.
54. Burleigh, L.M.; Calder, L.J.; Skehel, J.J.; Steinhauer, D.A. Influenza a viruses with mutations in the m1 helix six domain display a wide variety of morphological phenotypes. *J Virol* **2005**, *79*, 1262-1270, doi:10.1128/JVI.79.2.1262-1270.2005.
55. Bourmakina, S.V.; García-Sastre, A. Reverse genetics studies on the filamentous morphology of influenza A virus. *J Gen Virol* **2003**, *84*, 517-527.
56. Elleman, C.J.; Barclay, W.S. The M1 matrix protein controls the filamentous phenotype of influenza A virus. *Virology* **2004**, *321*, 144-153, doi:10.1016/j.virol.2003.12.009.
57. Roberts, P.C.; Lamb, R.A.; Compans, R.W. The M1 and M2 proteins of influenza A virus are important determinants in filamentous particle formation. *Virology* **1998**, *240*, 127-137, doi:10.1006/viro.1997.8916.
58. Campbell, P.J.; Danzy, S.; Kyriakis, C.S.; Deymier, M.J.; Lowen, A.C.; Steel, J. The M segment of the 2009 pandemic influenza virus confers increased neuraminidase activity, filamentous morphology, and efficient contact transmissibility to A/Puerto Rico/8/1934-based reassortant viruses. *J Virol* **2014**, *88*, 3802-3814, doi:10.1128/JVI.03607-13.

59. Iwatsuki-Horimoto, K.; Horimoto, T.; Noda, T.; Kiso, M.; Maeda, J.; Watanabe, S.; Muramoto, Y.; Fujii, K.; Kawaoka, Y. The cytoplasmic tail of the influenza A virus M2 protein plays a role in viral assembly. *J Virol* **2006**, *80*, 5233-5240, doi:10.1128/JVI.00049-06.
60. Grantham, M.L.; Stewart, S.M.; Lalime, E.N.; Pekosz, A. Tyrosines in the influenza A virus M2 protein cytoplasmic tail are critical for production of infectious virus particles. *J Virol* **2010**, *84*, 8765-8776, doi:10.1128/JVI.00853-10.
61. Chen, B.J.; Takeda, M.; Lamb, R.A. Influenza virus hemagglutinin (H3 subtype) requires palmitoylation of its cytoplasmic tail for assembly: M1 proteins of two subtypes differ in their ability to support assembly. *J Virol* **2005**, *79*, 13673-13684, doi:10.1128/JVI.79.21.13673-13684.2005.
62. Scheiffele, P.; Roth, M.G.; Simons, K. Interaction of influenza virus haemagglutinin with sphingolipid-cholesterol membrane domains via its transmembrane domain. *EMBO J* **1997**, *16*, 5501-5508, doi:10.1093/emboj/16.18.5501.
63. Scolari, S.; Imkeller, K.; Jolmes, F.; Veit, M.; Herrmann, A.; Schwarzer, R. Modulation of cell surface transport and lipid raft localization by the cytoplasmic tail of the influenza virus hemagglutinin. *Cell Microbiol* **2016**, *18*, 125-136, doi:10.1111/cmi.12491.
64. Lin, S.; Naim, H.Y.; Rodriguez, A.C.; Roth, M.G. Mutations in the middle of the transmembrane domain reverse the polarity of transport of the influenza virus hemagglutinin in MDCK epithelial cells. *J Cell Biol* **1998**, *142*, 51-57.
65. Latham, T.; Galarza, J.M. Formation of wild-type and chimeric influenza virus-like particles following simultaneous expression of only four structural proteins. *J Virol* **2001**, *75*, 6154-6165, doi:10.1128/JVI.75.13.6154-6165.2001.
66. Gómez-Puertas, P.; Albo, C.; Pérez-Pastrana, E.; Vivo, A.; Portela, A. Influenza virus matrix protein is the major driving force in virus budding. *J Virol* **2000**, *74*, 11538-11547.
67. Barman, S.; Adhikary, L.; Kawaoka, Y.; Nayak, D.P. Influenza A virus hemagglutinin containing basolateral localization signal does not alter the apical budding of a recombinant influenza A virus in polarized MDCK cells. *Virology* **2003**, *305*, 138-152.
68. Mora, R.; Rodriguez-Boulan, E.; Palese, P.; García-Sastre, A. Apical budding of a recombinant influenza A virus expressing a hemagglutinin protein with a basolateral localization signal. *J Virol* **2002**, *76*, 3544-3553.
69. Zhang, J.; Leser, G.P.; Pekosz, A.; Lamb, R.A. The cytoplasmic tails of the influenza virus spike glycoproteins are required for normal genome packaging. *Virology* **2000**, *269*, 325-334, doi:10.1006/viro.2000.0228.
70. Takizawa, N.; Momose, F.; Morikawa, Y.; Nomoto, A. Influenza A Virus Hemagglutinin is Required for the Assembly of Viral Components Including Bundled vRNPs at the Lipid Raft. *Viruses* **2016**, *8*, doi:10.3390/v8090249.
71. Kundu, A.; Avalos, R.T.; Sanderson, C.M.; Nayak, D.P. Transmembrane domain of influenza virus neuraminidase, a type II protein, possesses an apical sorting signal in polarized MDCK cells. *J Virol* **1996**, *70*, 6508-6515.
72. Barman, S.; Nayak, D.P. Analysis of the transmembrane domain of influenza virus neuraminidase, a type II transmembrane glycoprotein, for apical sorting and raft association. *J Virol* **2000**, *74*, 6538-6545.
73. Barman, S.; Adhikary, L.; Chakrabarti, A.K.; Bernas, C.; Kawaoka, Y.; Nayak, D.P. Role of transmembrane domain and cytoplasmic tail amino acid sequences of influenza a virus neuraminidase in raft association and virus budding. *J Virol* **2004**, *78*, 5258-5269.

74. Noton, S.L.; Medcalf, E.; Fisher, D.; Mullin, A.E.; Elton, D.; Digard, P. Identification of the domains of the influenza A virus M1 matrix protein required for NP binding, oligomerization and incorporation into virions. *J Gen Virol* **2007**, *88*, 2280-2290, doi:10.1099/vir.0.82809-0.
75. Arzt, S.; Petit, I.; Burmeister, W.P.; Ruigrok, R.W.; Baudin, F. Structure of a knockout mutant of influenza virus M1 protein that has altered activities in membrane binding, oligomerisation and binding to NEP (NS2). *Virus Res* **2004**, *99*, 115-119.
76. Zhang, K.; Wang, Z.; Liu, X.; Yin, C.; Basit, Z.; Xia, B.; Liu, W. Dissection of influenza A virus M1 protein: pH-dependent oligomerization of N-terminal domain and dimerization of C-terminal domain. *PLoS One* **2012**, *7*, e37786, doi:10.1371/journal.pone.0037786.
77. Ye, Z.; Liu, T.; Offringa, D.P.; McInnis, J.; Levandowski, R.A. Association of influenza virus matrix protein with ribonucleoproteins. *J Virol* **1999**, *73*, 7467-7473.
78. Liu, T.; Ye, Z. Introduction of a temperature-sensitive phenotype into influenza A/WSN/33 virus by altering the basic amino acid domain of influenza virus matrix protein. *J Virol* **2004**, *78*, 9585-9591, doi:10.1128/JVI.78.18.9585-9591.2004.
79. Ruigrok, R.W.; Barge, A.; Durrer, P.; Brunner, J.; Ma, K.; Whittaker, G.R. Membrane interaction of influenza virus M1 protein. *Virology* **2000**, *267*, 289-298, doi:10.1006/viro.1999.0134.
80. Arzt, S.; Baudin, F.; Barge, A.; Timmins, P.; Burmeister, W.P.; Ruigrok, R.W. Combined results from solution studies on intact influenza virus M1 protein and from a new crystal form of its N-terminal domain show that M1 is an elongated monomer. *Virology* **2001**, *279*, 439-446, doi:10.1006/viro.2000.0727.
81. Wang, D.; Harmon, A.; Jin, J.; Francis, D.H.; Christopher-Hennings, J.; Nelson, E.; Montelaro, R.C.; Li, F. The lack of an inherent membrane targeting signal is responsible for the failure of the matrix (M1) protein of influenza A virus to bud into virus-like particles. *J Virol* **2010**, *84*, 4673-4681, doi:10.1128/JVI.02306-09.
82. Roberts, P.C.; Compans, R.W. Host cell dependence of viral morphology. *Proc Natl Acad Sci U S A* **1998**, *95*, 5746-5751.
83. Bialas, K.M.; Desmet, E.A.; Takimoto, T. Specific residues in the 2009 H1N1 swine-origin influenza matrix protein influence virion morphology and efficiency of viral spread in vitro. *PLoS One* **2012**, *7*, e50595, doi:10.1371/journal.pone.0050595.
84. Wharton, S.A.; Belshe, R.B.; Skehel, J.J.; Hay, A.J. Role of virion M2 protein in influenza virus uncoating: specific reduction in the rate of membrane fusion between virus and liposomes by amantadine. *J Gen Virol* **1994**, *75 (Pt 4)*, 945-948.
85. Helenius, A. Unpacking the incoming influenza virus. *Cell* **1992**, *69*, 577-578.
86. Chen, B.J.; Leser, G.P.; Jackson, D.; Lamb, R.A. The influenza virus M2 protein cytoplasmic tail interacts with the M1 protein and influences virus assembly at the site of virus budding. *J Virol* **2008**, *82*, 10059-10070, doi:10.1128/JVI.01184-08.
87. McCown, M.F.; Pekosz, A. The influenza A virus M2 cytoplasmic tail is required for infectious virus production and efficient genome packaging. *J Virol* **2005**, *79*, 3595-3605, doi:10.1128/JVI.79.6.3595-3605.2005.
88. McCown, M.F.; Pekosz, A. Distinct domains of the influenza a virus M2 protein cytoplasmic tail mediate binding to the M1 protein and facilitate infectious virus production. *J Virol* **2006**, *80*, 8178-8189, doi:10.1128/JVI.00627-06.

89. Martyna, A.; Rossman, J. Alterations of membrane curvature during influenza virus budding. *Biochem Soc Trans* **2014**, *42*, 1425-1428, doi:10.1042/BST20140136.
90. Su, W.C.; Yu, W.Y.; Huang, S.H.; Lai, M.M.C. Ubiquitination of the Cytoplasmic Domain of Influenza A Virus M2 Protein is Crucial for Production of Infectious Virus Particles. *J Virol* **2017**, doi:10.1128/JVI.01972-17.
91. Wohlgemuth, N.; Lane, A.P.; Pekosz, A. Influenza A Virus M2 Protein Apical Targeting Is Required for Efficient Virus Replication. *J Virol* **2018**, *92*, doi:10.1128/JVI.01425-18.
92. Liu, H.; Grantham, M.L.; Pekosz, A. Mutations in the Influenza A Virus M1 Protein Enhance Virus Budding To Complement Lethal Mutations in the M2 Cytoplasmic Tail. *J Virol* **2018**, *92*, doi:10.1128/JVI.00858-17.
93. Zebedee, S.L.; Lamb, R.A. Influenza A virus M2 protein: monoclonal antibody restriction of virus growth and detection of M2 in virions. *J Virol* **1988**, *62*, 2762-2772.
94. Hao, L.; Sakurai, A.; Watanabe, T.; Sorensen, E.; Nidom, C.A.; Newton, M.A.; Ahlquist, P.; Kawaoka, Y. Drosophila RNAi screen identifies host genes important for influenza virus replication. *Nature* **2008**, *454*, 890-893, doi:10.1038/nature07151.
95. Shapira, S.D.; Gat-Viks, I.; Shum, B.O.; Dricot, A.; de Grace, M.M.; Wu, L.; Gupta, P.B.; Hao, T.; Silver, S.J.; Root, D.E., et al. A physical and regulatory map of host-influenza interactions reveals pathways in H1N1 infection. *Cell* **2009**, *139*, 1255-1267, doi:10.1016/j.cell.2009.12.018.
96. Karlas, A.; Machuy, N.; Shin, Y.; Pleissner, K.P.; Artarini, A.; Heuer, D.; Becker, D.; Khalil, H.; Ogilvie, L.A.; Hess, S., et al. Genome-wide RNAi screen identifies human host factors crucial for influenza virus replication. *Nature* **2010**, *463*, 818-822, doi:10.1038/nature08760.
97. König, R.; Stertz, S.; Zhou, Y.; Inoue, A.; Hoffmann, H.H.; Bhattacharyya, S.; Alamares, J.G.; Tscherne, D.M.; Ortigoza, M.B.; Liang, Y., et al. Human host factors required for influenza virus replication. *Nature* **2010**, *463*, 813-817, doi:10.1038/nature08699.
98. Su, W.C.; Chen, Y.C.; Tseng, C.H.; Hsu, P.W.; Tung, K.F.; Jeng, K.S.; Lai, M.M. Pooled RNAi screen identifies ubiquitin ligase Itch as crucial for influenza A virus release from the endosome during virus entry. *Proc Natl Acad Sci U S A* **2013**, *110*, 17516-17521, doi:10.1073/pnas.1312374110.
99. Watanabe, T.; Kawakami, E.; Shoemaker, J.E.; Lopes, T.J.; Matsuoka, Y.; Tomita, Y.; Kozuka-Hata, H.; Gorai, T.; Kuwahara, T.; Takeda, E., et al. Influenza virus-host interactome screen as a platform for antiviral drug development. *Cell Host Microbe* **2014**, *16*, 795-805, doi:10.1016/j.chom.2014.11.002.
100. Tripathi, S.; Pohl, M.O.; Zhou, Y.; Rodriguez-Frandsen, A.; Wang, G.; Stein, D.A.; Moulton, H.M.; DeJesus, P.; Che, J.; Mulder, L.C., et al. Meta- and Orthogonal Integration of Influenza "OMICs" Data Defines a Role for UBR4 in Virus Budding. *Cell Host Microbe* **2015**, *18*, 723-735, doi:10.1016/j.chom.2015.11.002.
101. Meliopoulos, V.A.; Andersen, L.E.; Birrer, K.F.; Simpson, K.J.; Lowenthal, J.W.; Bean, A.G.; Stambas, J.; Stewart, C.R.; Tompkins, S.M.; van Beusechem, V.W., et al. Host gene targets for novel influenza therapies elucidated by high-throughput RNA interference screens. *FASEB J* **2012**, *26*, 1372-1386, doi:10.1096/fj.11-193466.
102. Heaton, N.S.; Moshkina, N.; Fenouil, R.; Gardner, T.J.; Aguirre, S.; Shah, P.S.; Zhao, N.; Manganaro, L.; Hultquist, J.F.; Noel, J., et al. Targeting Viral Proteostasis Limits Influenza Virus, HIV, and Dengue Virus Infection. *Immunity* **2016**, *44*, 46-58, doi:10.1016/j.immuni.2015.12.017.

103. Heaton, B.E.; Kennedy, E.M.; Dumm, R.E.; Harding, A.T.; Sacco, M.T.; Sachs, D.; Heaton, N.S. A CRISPR Activation Screen Identifies a Pan-avian Influenza Virus Inhibitory Host Factor. *Cell Rep* **2017**, *20*, 1503-1512, doi:10.1016/j.celrep.2017.07.060.
104. Shaw, M.L.; Stone, K.L.; Colangelo, C.M.; Gulcicek, E.E.; Palese, P. Cellular proteins in influenza virus particles. *PLoS Pathog* **2008**, *4*, e1000085, doi:10.1371/journal.ppat.1000085.
105. Hutchinson, E.C.; Charles, P.D.; Hester, S.S.; Thomas, B.; Trudgian, D.; Martínez-Alonso, M.; Fodor, E. Conserved and host-specific features of influenza virion architecture. *Nat Commun* **2014**, *5*, 4816, doi:10.1038/ncomms5816.
106. Avilov, S.V.; Moisy, D.; Naffakh, N.; Cusack, S. Influenza A virus progeny vRNP trafficking in live infected cells studied with the virus-encoded fluorescently tagged PB2 protein. *Vaccine* **2012**, *30*, 7411-7417, doi:10.1016/j.vaccine.2012.09.077.
107. Chou, Y.Y.; Heaton, N.S.; Gao, Q.; Palese, P.; Singer, R.H.; Singer, R.; Lionnet, T. Colocalization of different influenza viral RNA segments in the cytoplasm before viral budding as shown by single-molecule sensitivity FISH analysis. *PLoS Pathog* **2013**, *9*, e1003358, doi:10.1371/journal.ppat.1003358.
108. Lakdawala, S.S.; Wu, Y.; Wawrzusin, P.; Kabat, J.; Broadbent, A.J.; Lamirande, E.W.; Fodor, E.; Altan-Bonnet, N.; Shroff, H.; Subbarao, K. Influenza a virus assembly intermediates fuse in the cytoplasm. *PLoS Pathog* **2014**, *10*, e1003971, doi:10.1371/journal.ppat.1003971.
109. Momose, F.; Sekimoto, T.; Ohkura, T.; Jo, S.; Kawaguchi, A.; Nagata, K.; Morikawa, Y. Apical transport of influenza A virus ribonucleoprotein requires Rab11-positive recycling endosome. *PLoS One* **2011**, *6*, e21123, doi:10.1371/journal.pone.0021123.
110. Nturibi, E.; Bhagwat, A.R.; Coburn, S.; Myerburg, M.M.; Lakdawala, S.S. Intracellular Colocalization of Influenza Viral RNA and Rab11A Is Dependent upon Microtubule Filaments. *J Virol* **2017**, *91*, doi:10.1128/JVI.01179-17.
111. Avilov, S.; Magnus, J.; Cusack, S.; Naffakh, N. Time-Resolved Visualisation of Nearly-Native Influenza A Virus Progeny Ribonucleoproteins and Their Individual Components in Live Infected Cells. *PLoS One* **2016**, *11*, e0149986, doi:10.1371/journal.pone.0149986.
112. Vale-Costa, S.; Alenquer, M.; Sousa, A.L.; Kellen, B.; Ramalho, J.; Tranfield, E.M.; Amorim, M.J. Influenza A virus ribonucleoproteins modulate host recycling by competing with Rab11 effectors. *J Cell Sci* **2016**, *129*, 1697-1710, doi:10.1242/jcs.188409.
113. Avilov, S.V.; Moisy, D.; Munier, S.; Schraidt, O.; Naffakh, N.; Cusack, S. Replication-competent influenza A virus that encodes a split-green fluorescent protein-tagged PB2 polymerase subunit allows live-cell imaging of the virus life cycle. *J Virol* **2012**, *86*, 1433-1448, doi:10.1128/JVI.05820-11.
114. Momose, F.; Kikuchi, Y.; Komase, K.; Morikawa, Y. Visualization of microtubule-mediated transport of influenza viral progeny ribonucleoprotein. *Microbes Infect* **2007**, *9*, 1422-1433, doi:10.1016/j.micinf.2007.07.007.
115. Welz, T.; Wellbourne-Wood, J.; Kerkhoff, E. Orchestration of cell surface proteins by Rab11. *Trends Cell Biol* **2014**, *24*, 407-415, doi:10.1016/j.tcb.2014.02.004.
116. Bruce, E.A.; Digard, P.; Stuart, A.D. The Rab11 pathway is required for influenza A virus budding and filament formation. *J Virol* **2010**, *84*, 5848-5859, doi:10.1128/JVI.00307-10.

117. Eisfeld, A.J.; Neumann, G.; Kawaoka, Y. Human immunodeficiency virus rev-binding protein is essential for influenza a virus replication and promotes genome trafficking in late-stage infection. *J Virol* **2011**, *85*, 9588-9598, doi:10.1128/JVI.05064-11.
118. Neville, M.; Stutz, F.; Lee, L.; Davis, L.I.; Rosbash, M. The importin-beta family member Crm1p bridges the interaction between Rev and the nuclear pore complex during nuclear export. *Curr Biol* **1997**, *7*, 767-775.
119. DesGroseillers, L.; Lemieux, N. Localization of a human double-stranded RNA-binding protein gene (STAU) to band 20q13.1 by fluorescence in situ hybridization. *Genomics* **1996**, *36*, 527-529, doi:10.1006/geno.1996.0499.
120. Kim, Y.K.; Furic, L.; Desgroseillers, L.; Maquat, L.E. Mammalian Staufen1 recruits Upf1 to specific mRNA 3'UTRs so as to elicit mRNA decay. *Cell* **2005**, *120*, 195-208, doi:10.1016/j.cell.2004.11.050.
121. de Lucas, S.; Peredo, J.; Marión, R.M.; Sánchez, C.; Ortín, J. Human Staufen1 protein interacts with influenza virus ribonucleoproteins and is required for efficient virus multiplication. *J Virol* **2010**, *84*, 7603-7612, doi:10.1128/JVI.00504-10.
122. Kawaguchi, A.; Matsumoto, K.; Nagata, K. YB-1 functions as a porter to lead influenza virus ribonucleoprotein complexes to microtubules. *J Virol* **2012**, *86*, 11086-11095, doi:10.1128/JVI.00453-12.
123. Huarte, M.; Sanz-Ezquerro, J.J.; Roncal, F.; Ortín, J.; Nieto, A. PA subunit from influenza virus polymerase complex interacts with a cellular protein with homology to a family of transcriptional activators. *J Virol* **2001**, *75*, 8597-8604.
124. Pérez-González, A.; Rodriguez, A.; Huarte, M.; Salanueva, I.J.; Nieto, A. hCLE/CGI-99, a human protein that interacts with the influenza virus polymerase, is a mRNA transcription modulator. *J Mol Biol* **2006**, *362*, 887-900, doi:10.1016/j.jmb.2006.07.085.
125. Rodriguez, A.; Pérez-González, A.; Nieto, A. Cellular human CLE/C14orf166 protein interacts with influenza virus polymerase and is required for viral replication. *J Virol* **2011**, *85*, 12062-12066, doi:10.1128/JVI.00684-11.
126. Rodriguez-Frandsen, A.; de Lucas, S.; Pérez-González, A.; Pérez-Cidoncha, M.; Roldan-Gomendio, A.; Pazo, A.; Marcos-Villar, L.; Landeras-Bueno, S.; Ortín, J.; Nieto, A. hCLE/C14orf166, a cellular protein required for viral replication, is incorporated into influenza virus particles. *Sci Rep* **2016**, *6*, 20744, doi:10.1038/srep20744.
127. Sun, E.; He, J.; Zhuang, X. Dissecting the role of COPI complexes in influenza virus infection. *J Virol* **2013**, *87*, 2673-2685, doi:10.1128/JVI.02277-12.
128. Wang, S.; Li, H.; Chen, Y.; Wei, H.; Gao, G.F.; Liu, H.; Huang, S.; Chen, J.L. Transport of influenza virus neuraminidase (NA) to host cell surface is regulated by ARHGAP21 and Cdc42 proteins. *J Biol Chem* **2012**, *287*, 9804-9816, doi:10.1074/jbc.M111.312959.
129. Zhu, P.; Liang, L.; Shao, X.; Luo, W.; Jiang, S.; Zhao, Q.; Sun, N.; Zhao, Y.; Li, J.; Wang, J., et al. Host Cellular Protein TRAPPC6AΔ Interacts with Influenza A Virus M2 Protein and Regulates Viral Propagation by Modulating M2 Trafficking. *J Virol* **2017**, *91*, doi:10.1128/JVI.01757-16.
130. Fan, Y.; Mok, C.K.; Chan, M.C.; Zhang, Y.; Nal, B.; Kien, F.; Bruzzone, R.; Sanyal, S. Cell Cycle-independent Role of Cyclin D3 in Host Restriction of Influenza Virus Infection. *J Biol Chem* **2017**, *292*, 5070-5088, doi:10.1074/jbc.M117.776112.
131. He, J.; Sun, E.; Bujny, M.V.; Kim, D.; Davidson, M.W.; Zhuang, X. Dual function of CD81 in influenza virus uncoating and budding. *PLoS Pathog* **2013**, *9*, e1003701, doi:10.1371/journal.ppat.1003701.

132. Demirov, D.; Gabriel, G.; Schneider, C.; Hohenberg, H.; Ludwig, S. Interaction of influenza A virus matrix protein with RACK1 is required for virus release. *Cell Microbiol* **2012**, *14*, 774-789, doi:10.1111/j.1462-5822.2012.01759.x.
133. Gorai, T.; Goto, H.; Noda, T.; Watanabe, T.; Kozuka-Hata, H.; Oyama, M.; Takano, R.; Neumann, G.; Watanabe, S.; Kawaoka, Y. F1Fo-ATPase, F-type proton-translocating ATPase, at the plasma membrane is critical for efficient influenza virus budding. *Proc Natl Acad Sci U S A* **2012**, *109*, 4615-4620, doi:10.1073/pnas.1114728109.
134. Ma, H.; Kien, F.; Manière, M.; Zhang, Y.; Lagarde, N.; Tse, K.S.; Poon, L.L.; Nal, B. Human annexin A6 interacts with influenza a virus protein M2 and negatively modulates infection. *J Virol* **2012**, *86*, 1789-1801, doi:10.1128/JVI.06003-11.
135. Helbig, K.J.; Beard, M.R. The role of viperin in the innate antiviral response. *J Mol Biol* **2014**, *426*, 1210-1219, doi:10.1016/j.jmb.2013.10.019.
136. Wang, X.; Hinson, E.R.; Cresswell, P. The interferon-inducible protein viperin inhibits influenza virus release by perturbing lipid rafts. *Cell Host Microbe* **2007**, *2*, 96-105, doi:10.1016/j.chom.2007.06.009.
137. Simpson-Holley, M.; Ellis, D.; Fisher, D.; Elton, D.; McCauley, J.; Digard, P. A functional link between the actin cytoskeleton and lipid rafts during budding of filamentous influenza virions. *Virology* **2002**, *301*, 212-225.
138. Davidson, A.J.; Wood, W. Unravelling the Actin Cytoskeleton: A New Competitive Edge? *Trends Cell Biol* **2016**, *26*, 569-576, doi:10.1016/j.tcb.2016.04.001.
139. Bezanilla, M.; Gladfelter, A.S.; Kovar, D.R.; Lee, W.L. Cytoskeletal dynamics: a view from the membrane. *J Cell Biol* **2015**, *209*, 329-337, doi:10.1083/jcb.201502062.
140. Chesarone, M.A.; Goode, B.L. Actin nucleation and elongation factors: mechanisms and interplay. *Curr Opin Cell Biol* **2009**, *21*, 28-37, doi:10.1016/j.ceb.2008.12.001.
141. Firat-Karalar, E.N.; Welch, M.D. New mechanisms and functions of actin nucleation. *Curr Opin Cell Biol* **2011**, *23*, 4-13, doi:10.1016/j.ceb.2010.10.007.
142. Bravo-Cordero, J.J.; Magalhaes, M.A.; Eddy, R.J.; Hodgson, L.; Condeelis, J. Functions of cofilin in cell locomotion and invasion. *Nat Rev Mol Cell Biol* **2013**, *14*, 405-415, doi:10.1038/nrm3609.
143. Liu, A.P.; Fletcher, D.A. Actin polymerization serves as a membrane domain switch in model lipid bilayers. *Biophys J* **2006**, *91*, 4064-4070, doi:10.1529/biophysj.106.090852.
144. Gaus, K.; Chklovskaia, E.; Fazekas de St Groth, B.; Jessup, W.; Harder, T. Condensation of the plasma membrane at the site of T lymphocyte activation. *J Cell Biol* **2005**, *171*, 121-131, doi:10.1083/jcb.200505047.
145. Chichili, G.R.; Rodgers, W. Clustering of membrane raft proteins by the actin cytoskeleton. *J Biol Chem* **2007**, *282*, 36682-36691, doi:10.1074/jbc.M702959200.
146. Hartman, M.A.; Spudich, J.A. The myosin superfamily at a glance. *J Cell Sci* **2012**, *125*, 1627-1632, doi:10.1242/jcs.094300.
147. Sit, S.T.; Manser, E. Rho GTPases and their role in organizing the actin cytoskeleton. *J Cell Sci* **2011**, *124*, 679-683, doi:10.1242/jcs.064964.
148. Avalos, R.T.; Yu, Z.; Nayak, D.P. Association of influenza virus NP and M1 proteins with cellular cytoskeletal elements in influenza virus-infected cells. *J Virol* **1997**, *71*, 2947-2958.
149. Digard, P.; Elton, D.; Bishop, K.; Medcalf, E.; Weeds, A.; Pope, B. Modulation of nuclear localization of the influenza virus nucleoprotein through interaction with actin filaments. *J Virol* **1999**, *73*, 2222-2231.

150. Mayer, D.; Molawi, K.; Martínez-Sobrido, L.; Ghanem, A.; Thomas, S.; Baginsky, S.; Grossmann, J.; García-Sastre, A.; Schwemmle, M. Identification of cellular interaction partners of the influenza virus ribonucleoprotein complex and polymerase complex using proteomic-based approaches. *J Proteome Res* **2007**, *6*, 672-682, doi:10.1021/pr060432u.
151. Bradel-Tretheway, B.G.; Mattiacio, J.L.; Krasnoselsky, A.; Stevenson, C.; Purdy, D.; Dewhurst, S.; Katze, M.G. Comprehensive proteomic analysis of influenza virus polymerase complex reveals a novel association with mitochondrial proteins and RNA polymerase accessory factors. *J Virol* **2011**, *85*, 8569-8581, doi:10.1128/JVI.00496-11.
152. Yu, G.; Liang, W.; Liu, J.; Meng, D.; Wei, L.; Chai, T.; Cai, Y. Proteomic Analysis of Differential Expression of Cellular Proteins in Response to Avian H9N2 Virus Infection of A549 Cells. *Front Microbiol* **2016**, *7*, 1962, doi:10.3389/fmicb.2016.01962.
153. Mindaye, S.T.; Ilyushina, N.A.; Fantoni, G.; Alterman, M.A.; Donnelly, R.P.; Eichelberger, M.C. Impact of Influenza A Virus Infection on the Proteomes of Human Bronchoepithelial Cells from Different Donors. *J Proteome Res* **2017**, *16*, 3287-3297, doi:10.1021/acs.jproteome.7b00286.
154. Coombs, K.M.; Berard, A.; Xu, W.; Krokhin, O.; Meng, X.; Cortens, J.P.; Kobasa, D.; Wilkins, J.; Brown, E.G. Quantitative proteomic analyses of influenza virus-infected cultured human lung cells. *J Virol* **2010**, *84*, 10888-10906, doi:10.1128/JVI.00431-10.
155. Liu, G.; Xiang, Y.; Guo, C.; Pei, Y.; Wang, Y.; Kitazato, K. Cofilin-1 is involved in regulation of actin reorganization during influenza A virus assembly and budding. *Biochem Biophys Res Commun* **2014**, *453*, 821-825, doi:10.1016/j.bbrc.2014.10.036.
156. Chen, D.Y.; Husain, M. Caspase-mediated degradation of host cortactin that promotes influenza A virus infection in epithelial cells. *Virology* **2016**, *497*, 146-156, doi:10.1016/j.virol.2016.07.017.
157. Jiang, W.; Wang, Q.; Chen, S.; Gao, S.; Song, L.; Liu, P.; Huang, W. Influenza A virus NS1 induces G0/G1 cell cycle arrest by inhibiting the expression and activity of RhoA protein. *J Virol* **2013**, *87*, 3039-3052, doi:10.1128/JVI.03176-12.
158. Jiang, W.; Sheng, C.; Gu, X.; Liu, D.; Yao, C.; Gao, S.; Chen, S.; Huang, Y.; Huang, W.; Fang, M. Suppression of Rac1 Signaling by Influenza A Virus NS1 Facilitates Viral Replication. *Sci Rep* **2016**, *6*, 35041, doi:10.1038/srep35041.
159. Kumakura, M.; Kawaguchi, A.; Nagata, K. Actin-myosin network is required for proper assembly of influenza virus particles. *Virology* **2015**, *476*, 141-150, doi:10.1016/j.virol.2014.12.016.
160. Griffin, J.A.; Compans, R.W. Effect of cytochalasin B on the maturation of enveloped viruses. *J Exp Med* **1979**, *150*, 379-391.
161. Arcangeletti, M.C.; De Conto, F.; Ferraglia, F.; Pinardi, F.; Gatti, R.; Orlandini, G.; Covan, S.; Motta, F.; Rodighiero, I.; Dettori, G., et al. Host-cell-dependent role of actin cytoskeleton during the replication of a human strain of influenza A virus. *Arch Virol* **2008**, *153*, 1209-1221, doi:10.1007/s00705-008-0103-0.
162. De Conto, F.; Di Lonardo, E.; Arcangeletti, M.C.; Chezzi, C.; Medici, M.C.; Calderaro, A. Highly dynamic microtubules improve the effectiveness of early stages of human influenza A/NWS/33 virus infection in LLC-MK2 cells. *PLoS One* **2012**, *7*, e41207, doi:10.1371/journal.pone.0041207.
163. Bedi, S.; Noda, T.; Kawaoka, Y.; Ono, A. A Defect in Influenza A Virus Particle Assembly Specific to Primary Human Macrophages. *MBio* **2018**, *9*, doi:10.1128/mBio.01916-18.

164. Rindler, M.J.; Ivanov, I.E.; Plesken, H.; Sabatini, D.D. Polarized delivery of viral glycoproteins to the apical and basolateral plasma membranes of Madin-Darby canine kidney cells infected with temperature-sensitive viruses. *J Cell Biol* **1985**, *100*, 136-151.
165. Rodriguez Boulan, E.; Sabatini, D.D. Asymmetric budding of viruses in epithelial monlayers: a model system for study of epithelial polarity. *Proc Natl Acad Sci U S A* **1978**, *75*, 5071-5075.
166. Rodriguez Boulan, E.; Pendergast, M. Polarized distribution of viral envelope proteins in the plasma membrane of infected epithelial cells. *Cell* **1980**, *20*, 45-54.
167. Rodriguez-Boulan, E.; Paskiet, K.T.; Sabatini, D.D. Assembly of enveloped viruses in Madin-Darby canine kidney cells: polarized budding from single attached cells and from clusters of cells in suspension. *J Cell Biol* **1983**, *96*, 866-874.
168. Rodriguez-Boulan, E.; Paskiet, K.T.; Salas, P.J.; Bard, E. Intracellular transport of influenza virus hemagglutinin to the apical surface of Madin-Darby canine kidney cells. *J Cell Biol* **1984**, *98*, 308-319.
169. Hughey, P.G.; Compans, R.W.; Zebedee, S.L.; Lamb, R.A. Expression of the influenza A virus M2 protein is restricted to apical surfaces of polarized epithelial cells. *J Virol* **1992**, *66*, 5542-5552.
170. Bonilha, V.L.; Marmorstein, A.D.; Cohen-Gould, L.; Rodriguez-Boulan, E. Apical sorting of influenza hemagglutinin by transcytosis in retinal pigment epithelium. *J Cell Sci* **1997**, *110 (Pt 15)*, 1717-1727.
171. Guerriero, C.J.; Lai, Y.; Weisz, O.A. Differential sorting and Golgi export requirements for raft-associated and raft-independent apical proteins along the biosynthetic pathway. *J Biol Chem* **2008**, *283*, 18040-18047, doi:10.1074/jbc.M802048200.
172. Cresawn, K.O.; Potter, B.A.; Oztan, A.; Guerriero, C.J.; Ihrke, G.; Goldenring, J.R.; Apodaca, G.; Weisz, O.A. Differential involvement of endocytic compartments in the biosynthetic traffic of apical proteins. *EMBO J* **2007**, *26*, 3737-3748, doi:10.1038/sj.emboj.7601813.
173. Carrasco, M.; Amorim, M.J.; Digard, P. Lipid raft-dependent targeting of the influenza A virus nucleoprotein to the apical plasma membrane. *Traffic* **2004**, *5*, 979-992, doi:10.1111/j.1600-0854.2004.00237.x.
174. Salas, P.J.; Misek, D.E.; Vega-Salas, D.E.; Gundersen, D.; Cereijido, M.; Rodriguez-Boulan, E. Microtubules and actin filaments are not critically involved in the biogenesis of epithelial cell surface polarity. *J Cell Biol* **1986**, *102*, 1853-1867.
175. Husain, M.; Cheung, C.Y. Histone deacetylase 6 inhibits influenza A virus release by downregulating the trafficking of viral components to the plasma membrane via its substrate, acetylated microtubules. *J Virol* **2014**, *88*, 11229-11239, doi:10.1128/JVI.00727-14.
176. Leser, G.P.; Lamb, R.A. Lateral Organization of Influenza Virus Proteins in the Budozone Region of the Plasma Membrane. *J Virol* **2017**, *91*, doi:10.1128/JVI.02104-16.
177. Henkel, J.R.; Weisz, O.A. Influenza virus M2 protein slows traffic along the secretory pathway. pH perturbation of acidified compartments affects early Golgi transport steps. *J Biol Chem* **1998**, *273*, 6518-6524.
178. Henkel, J.R.; Apodaca, G.; Altschuler, Y.; Hardy, S.; Weisz, O.A. Selective perturbation of apical membrane traffic by expression of influenza M2, an acid-activated ion channel, in polarized madin-darby canine kidney cells. *Mol Biol Cell* **1998**, *9*, 2477-2490.

179. Henkel, J.R.; Gibson, G.A.; Poland, P.A.; Ellis, M.A.; Hughey, R.P.; Weisz, O.A. Influenza M2 proton channel activity selectively inhibits trans-Golgi network release of apical membrane and secreted proteins in polarized Madin-Darby canine kidney cells. *J Cell Biol* **2000**, *148*, 495-504.
180. Gudheti, M.V.; Curthoys, N.M.; Gould, T.J.; Kim, D.; Gunewardene, M.S.; Gabor, K.A.; Gosse, J.A.; Kim, C.H.; Zimmerberg, J.; Hess, S.T. Actin mediates the nanoscale membrane organization of the clustered membrane protein influenza hemagglutinin. *Biophys J* **2013**, *104*, 2182-2192, doi:10.1016/j.bpj.2013.03.054.
181. Thaa, B.; Herrmann, A.; Veit, M. Intrinsic cytoskeleton-dependent clustering of influenza virus M2 protein with hemagglutinin assessed by FLIM-FRET. *J Virol* **2010**, *84*, 12445-12449, doi:10.1128/JVI.01322-10.
182. Spearman, P. HIV-1 Gag as an Antiviral Target: Development of Assembly and Maturation Inhibitors. *Curr Top Med Chem* **2016**, *16*, 1154-1166.
183. Zeisel, M.B.; Crouchet, E.; Baumert, T.F.; Schuster, C. Host-Targeting Agents to Prevent and Cure Hepatitis C Virus Infection. *Viruses* **2015**, *7*, 5659-5685, doi:10.3390/v7112898.
184. Rodgers, B.C.; Mims, C.A. Influenza virus replication in human alveolar macrophages. *J Med Virol* **1982**, *9*, 177-184.
185. Hartmann, B.M.; Li, W.; Jia, J.; Patil, S.; Marjanovic, N.; Martínez-Romero, C.; Albrecht, R.A.; Hayot, F.; García-Sastre, A.; Wetmur, J.G., et al. Mouse dendritic cell (DC) influenza virus infectivity is much lower than that for human DCs and is hemagglutinin subtype dependent. *J Virol* **2013**, *87*, 1916-1918, doi:10.1128/JVI.02980-12.
186. Graham, A.C.; Hilmer, K.M.; Zickovich, J.M.; Obar, J.J. Inflammatory response of mast cells during influenza A virus infection is mediated by active infection and RIG-I signaling. *J Immunol* **2013**, *190*, 4676-4684, doi:10.4049/jimmunol.1202096.
187. Lohmeyer, J.; Talens, L.T.; Klenk, H.D. Biosynthesis of the influenza virus envelope in abortive infection. *J Gen Virol* **1979**, *42*, 73-88, doi:10.1099/0022-1317-42-1-73.
188. Gujuluva, C.N.; Kundu, A.; Murti, K.G.; Nayak, D.P. Abortive replication of influenza virus A/WSN/33 in HeLa229 cells: defective viral entry and budding processes. *Virology* **1994**, *204*, 491-505, doi:10.1006/viro.1994.1563.
189. Moncorgé, O.; Mura, M.; Barclay, W.S. Evidence for avian and human host cell factors that affect the activity of influenza virus polymerase. *J Virol* **2010**, *84*, 9978-9986, doi:10.1128/JVI.01134-10.
190. Mehle, A.; Doudna, J.A. An inhibitory activity in human cells restricts the function of an avian-like influenza virus polymerase. *Cell Host Microbe* **2008**, *4*, 111-122, doi:10.1016/j.chom.2008.06.007.
191. Feng, Y.; Broder, C.C.; Kennedy, P.E.; Berger, E.A. HIV-1 entry cofactor: functional cDNA cloning of a seven-transmembrane, G protein-coupled receptor. *Science* **1996**, *272*, 872-877.
192. Bortz, E.; Westera, L.; Maamary, J.; Steel, J.; Albrecht, R.A.; Manicassamy, B.; Chase, G.; Martínez-Sobrido, L.; Schwemmle, M.; García-Sastre, A. Host- and strain-specific regulation of influenza virus polymerase activity by interacting cellular proteins. *MBio* **2011**, *2*, doi:10.1128/mBio.00151-11.

193. Hudjetz, B.; Gabriel, G. Human-like PB2 627K influenza virus polymerase activity is regulated by importin-α1 and -α7. *PLoS Pathog* **2012**, *8*, e1002488, doi:10.1371/journal.ppat.1002488.
194. Long, J.S.; Giotis, E.S.; Moncorgé, O.; Frise, R.; Mistry, B.; James, J.; Morisson, M.; Iqbal, M.; Vignal, A.; Skinner, M.A., et al. Species difference in ANP32A underlies influenza A virus polymerase host restriction. *Nature* **2016**, *529*, 101-104, doi:10.1038/nature16474.
195. Kuo, S.M.; Chen, C.J.; Chang, S.C.; Liu, T.J.; Chen, Y.H.; Huang, S.Y.; Shih, S.R. Inhibition of Avian Influenza A Virus Replication in Human Cells by Host Restriction Factor TUFM Is Correlated with Autophagy. *MBio* **2017**, *8*, doi:10.1128/mBio.00481-17.
196. Laguette, N.; Sobhian, B.; Casartelli, N.; Ringeard, M.; Chable-Bessia, C.; Ségéral, E.; Yatim, A.; Emiliani, S.; Schwartz, O.; Benkirane, M. SAMHD1 is the dendritic- and myeloid-cell-specific HIV-1 restriction factor counteracted by Vpx. *Nature* **2011**, *474*, 654-657, doi:10.1038/nature10117.
197. Neil, S.J.; Zang, T.; Bieniasz, P.D. Tetherin inhibits retrovirus release and is antagonized by HIV-1 Vpu. *Nature* **2008**, *451*, 425-430, doi:10.1038/nature06553.
198. Sheehy, A.M.; Gaddis, N.C.; Choi, J.D.; Malim, M.H. Isolation of a human gene that inhibits HIV-1 infection and is suppressed by the viral Vif protein. *Nature* **2002**, *418*, 646-650, doi:10.1038/nature00939.
199. Cline, T.D.; Karlsson, E.A.; Seufzer, B.J.; Schultz-Cherry, S. The hemagglutinin protein of highly pathogenic H5N1 influenza viruses overcomes an early block in the replication cycle to promote productive replication in macrophages. *J Virol* **2013**, *87*, 1411-1419, doi:10.1128/JVI.02682-12.
200. Yu, W.C.; Chan, R.W.; Wang, J.; Travanty, E.A.; Nicholls, J.M.; Peiris, J.S.; Mason, R.J.; Chan, M.C. Viral replication and innate host responses in primary human alveolar epithelial cells and alveolar macrophages infected with influenza H5N1 and H1N1 viruses. *J Virol* **2011**, *85*, 6844-6855, doi:10.1128/JVI.02200-10.
201. Londrigan, S.L.; Short, K.R.; Ma, J.; Gillespie, L.; Rockman, S.P.; Brooks, A.G.; Reading, P.C. Infection of Mouse Macrophages by Seasonal Influenza Viruses Can Be Restricted at the Level of Virus Entry and at a Late Stage in the Virus Life Cycle. *J Virol* **2015**, *89*, 12319-12329, doi:10.1128/JVI.01455-15.
202. Mok, C.K.; Lee, D.C.; Cheung, C.Y.; Peiris, M.; Lau, A.S. Differential onset of apoptosis in influenza A virus H5N1- and H1N1-infected human blood macrophages. *J Gen Virol* **2007**, *88*, 1275-1280, doi:10.1099/vir.0.82423-0.
203. Sakabe, S.; Iwatsuki-Horimoto, K.; Takano, R.; Nidom, C.A.; Le, M.; Nagamura-Inoue, T.; Horimoto, T.; Yamashita, N.; Kawaoka, Y. Cytokine production by primary human macrophages infected with highly pathogenic H5N1 or pandemic H1N1 2009 influenza viruses. *J Gen Virol* **2011**, *92*, 1428-1434, doi:10.1099/vir.0.030346-0.
204. van Riel, D.; Leijten, L.M.; van der Eerden, M.; Hoogsteden, H.C.; Boven, L.A.; Lambrecht, B.N.; Osterhaus, A.D.; Kuiken, T. Highly pathogenic avian influenza virus H5N1 infects alveolar macrophages without virus production or excessive TNF-alpha induction. *PLoS Pathog* **2011**, *7*, e1002099, doi:10.1371/journal.ppat.1002099.
205. Marvin, S.A.; Russier, M.; Huerta, C.T.; Russell, C.J.; Schultz-Cherry, S. Influenza overcomes cellular blocks to productively replicate impacting macrophage function. *J Virol* **2016**, doi:10.1128/JVI.01417-16.

206. Perrone, L.A.; Plowden, J.K.; García-Sastre, A.; Katz, J.M.; Tumpey, T.M. H5N1 and 1918 pandemic influenza virus infection results in early and excessive infiltration of macrophages and neutrophils in the lungs of mice. *PLoS Pathog* **2008**, *4*, e1000115, doi:10.1371/journal.ppat.1000115.
207. Okuno, Y.; Isegawa, Y.; Sasao, F.; Ueda, S. A common neutralizing epitope conserved between the hemagglutinins of influenza A virus H1 and H2 strains. *J Virol* **1993**, *67*, 2552-2558.
208. Neumann, G.; Watanabe, T.; Ito, H.; Watanabe, S.; Goto, H.; Gao, P.; Hughes, M.; Perez, D.R.; Donis, R.; Hoffmann, E., et al. Generation of influenza A viruses entirely from cloned cDNAs. *Proc Natl Acad Sci U S A* **1999**, *96*, 9345-9350.
209. Pauly, M.D.; Lauring, A.S. Effective lethal mutagenesis of influenza virus by three nucleoside analogs. *J Virol* **2015**, *89*, 3584-3597, doi:10.1128/JVI.03483-14.
210. Hogue, I.B.; Grover, J.R.; Soheilian, F.; Nagashima, K.; Ono, A. Gag induces the coalescence of clustered lipid rafts and tetraspanin-enriched microdomains at HIV-1 assembly sites on the plasma membrane. *J Virol* **2011**, *85*, 9749-9766, doi:10.1128/JVI.00743-11.
211. Freeman, S.A.; Vega, A.; Riedl, M.; Collins, R.F.; Ostrowski, P.P.; Woods, E.C.; Bertozzi, C.R.; Tammi, M.I.; Lidke, D.S.; Johnson, P., et al. Transmembrane Pickets Connect Cyto- and Pericellular Skeletons Forming Barriers to Receptor Engagement. *Cell* **2018**, *172*, 305-317.e310, doi:10.1016/j.cell.2017.12.023.
212. Doud, M.B.; Lee, J.M.; Bloom, J.D. How single mutations affect viral escape from broad and narrow antibodies to H1 influenza hemagglutinin. *Nat Commun* **2018**, *9*, 1386, doi:10.1038/s41467-018-03665-3.
213. Harder, T.; Scheiffele, P.; Verkade, P.; Simons, K. Lipid domain structure of the plasma membrane revealed by patching of membrane components. *J Cell Biol* **1998**, *141*, 929-942.
214. Bubb, M.R.; Senderowicz, A.M.; Sausville, E.A.; Duncan, K.L.; Korn, E.D. Jasplakinolide, a cytotoxic natural product, induces actin polymerization and competitively inhibits the binding of phalloidin to F-actin. *J Biol Chem* **1994**, *269*, 14869-14871.
215. Schmitt, A.P.; Lamb, R.A. Influenza virus assembly and budding at the viral budozone. *Adv Virus Res* **2005**, *64*, 383-416, doi:10.1016/S0065-3527(05)64012-2.
216. Veit, M.; Thaa, B. Association of influenza virus proteins with membrane rafts. *Adv Virol* **2011**, *2011*, 370606, doi:10.1155/2011/370606.
217. Gunewardene, M.S.; Subach, F.V.; Gould, T.J.; Penoncello, G.P.; Gudheti, M.V.; Verkhusha, V.V.; Hess, S.T. Superresolution imaging of multiple fluorescent proteins with highly overlapping emission spectra in living cells. *Biophys J* **2011**, *101*, 1522-1528, doi:10.1016/j.bpj.2011.07.049.
218. Bourmakina, S.V.; García-Sastre, A. The morphology and composition of influenza A virus particles are not affected by low levels of M1 and M2 proteins in infected cells. *J Virol* **2005**, *79*, 7926-7932, doi:10.1128/JVI.79.12.7926-7932.2005.
219. Moreira, É.; Weber, A.; Bolte, H.; Kolesnikova, L.; Giese, S.; Lakdawala, S.; Beer, M.; Zimmer, G.; García-Sastre, A.; Schwemmle, M., et al. A conserved influenza A virus nucleoprotein code controls specific viral genome packaging. *Nat Commun* **2016**, *7*, 12861, doi:10.1038/ncomms12861.

220. Bui, M.; Whittaker, G.; Helenius, A. Effect of M1 protein and low pH on nuclear transport of influenza virus ribonucleoproteins. *J Virol* **1996**, *70*, 8391-8401.
221. Tobler, K.; Kelly, M.L.; Pinto, L.H.; Lamb, R.A. Effect of cytoplasmic tail truncations on the activity of the M(2) ion channel of influenza A virus. *J Virol* **1999**, *73*, 9695-9701.
222. Park, E.K.; Castrucci, M.R.; Portner, A.; Kawaoka, Y. The M2 ectodomain is important for its incorporation into influenza A virions. *J Virol* **1998**, *72*, 2449-2455.
223. Takeuchi, K.; Lamb, R.A. Influenza virus M2 protein ion channel activity stabilizes the native form of fowl plague virus hemagglutinin during intracellular transport. *J Virol* **1994**, *68*, 911-919.
224. Ciampor, F.; Bayley, P.M.; Nermut, M.V.; Hirst, E.M.; Sugrue, R.J.; Hay, A.J. Evidence that the amantadine-induced, M2-mediated conversion of influenza A virus hemagglutinin to the low pH conformation occurs in an acidic trans Golgi compartment. *Virology* **1992**, *188*, 14-24.
225. Madsen, J.J.; Grime, J.M.A.; Rossman, J.S.; Voth, G.A. Entropic forces drive clustering and spatial localization of influenza A M2 during viral budding. *Proc Natl Acad Sci U S A* **2018**, *115*, E8595-E8603, doi:10.1073/pnas.1805443115.
226. Martyna, A.; Gómez-Llobregat, J.; Lindén, M.; Rossman, J.S. Curvature Sensing by a Viral Scission Protein. *Biochemistry* **2016**, *55*, 3493-3496, doi:10.1021/acs.biochem.6b00539.
227. Schroeder, C.; Heider, H.; Möncke-Buchner, E.; Lin, T.I. The influenza virus ion channel and maturation cofactor M2 is a cholesterol-binding protein. *Eur Biophys J* **2005**, *34*, 52-66, doi:10.1007/s00249-004-0424-1.
228. Thaa, B.; Siche, S.; Herrmann, A.; Veit, M. Acylation and cholesterol binding are not required for targeting of influenza A virus M2 protein to the hemagglutinin-defined budozone. *FEBS Lett* **2014**, *588*, 1031-1036, doi:10.1016/j.febslet.2014.02.014.
229. Castrucci, M.R.; Hughes, M.; Calzoletti, L.; Donatelli, I.; Wells, K.; Takada, A.; Kawaoka, Y. The cysteine residues of the M2 protein are not required for influenza A virus replication. *Virology* **1997**, *238*, 128-134, doi:10.1006/viro.1997.8809.
230. Grantham, M.L.; Wu, W.H.; Lalime, E.N.; Lorenzo, M.E.; Klein, S.L.; Pekosz, A. Palmitoylation of the influenza A virus M2 protein is not required for virus replication in vitro but contributes to virus virulence. *J Virol* **2009**, *83*, 8655-8661, doi:10.1128/JVI.01129-09.
231. Stewart, S.M.; Wu, W.H.; Lalime, E.N.; Pekosz, A. The cholesterol recognition/interaction amino acid consensus motif of the influenza A virus M2 protein is not required for virus replication but contributes to virulence. *Virology* **2010**, *405*, 530-538, doi:10.1016/j.virol.2010.06.035.
232. Honigmann, A.; Sadeghi, S.; Keller, J.; Hell, S.W.; Eggeling, C.; Vink, R. A lipid bound actin meshwork organizes liquid phase separation in model membranes. *Elife* **2014**, *3*, e01671, doi:10.7554/eLife.01671.
233. Vogel, S.K.; Greiss, F.; Khmelinskaia, A.; Schwille, P. Control of lipid domain organization by a biomimetic contractile actomyosin cortex. *Elife* **2017**, *6*, doi:10.7554/eLife.24350.
234. Haggie, P.M.; Kim, J.K.; Lukacs, G.L.; Verkman, A.S. Tracking of quantum dot-labeled CFTR shows near immobilization by C-terminal PDZ interactions. *Mol Biol Cell* **2006**, *17*, 4937-4945, doi:10.1091/mbc.e06-08-0670.

235. Chen, Y.; Veracini, L.; Benistant, C.; Jacobson, K. The transmembrane protein CBP plays a role in transiently anchoring small clusters of Thy-1, a GPI-anchored protein, to the cytoskeleton. *J Cell Sci* **2009**, *122*, 3966-3972, doi:10.1242/jcs.049346.
236. Tinevez, J.Y.; Schulze, U.; Salbreux, G.; Roensch, J.; Joanny, J.F.; Paluch, E. Role of cortical tension in bleb growth. *Proc Natl Acad Sci U S A* **2009**, *106*, 18581-18586, doi:10.1073/pnas.0903353106.
237. Smith, A.S.; Nowak, R.B.; Zhou, S.; Giannetto, M.; Gokhin, D.S.; Papoin, J.; Ghiran, I.C.; Blanc, L.; Wan, J.; Fowler, V.M. Myosin IIA interacts with the spectrin-actin membrane skeleton to control red blood cell membrane curvature and deformability. *Proc Natl Acad Sci U S A* **2018**, *115*, E4377-E4385, doi:10.1073/pnas.1718285115.
238. Giner, D.; Neco, P.; Francés, M.e.M.; López, I.; Viniegra, S.; Gutiérrez, L.M. Real-time dynamics of the F-actin cytoskeleton during secretion from chromaffin cells. *J Cell Sci* **2005**, *118*, 2871-2880, doi:10.1242/jcs.02419.
239. Giner, D.; López, I.; Villanueva, J.; Torres, V.; Viniegra, S.; Gutiérrez, L.M. Vesicle movements are governed by the size and dynamics of F-actin cytoskeletal structures in bovine chromaffin cells. *Neuroscience* **2007**, *146*, 659-669, doi:10.1016/j.neuroscience.2007.02.039.
240. Jackson, D.; Lamb, R.A. The influenza A virus spliced messenger RNA M mRNA3 is not required for viral replication in tissue culture. *J Gen Virol* **2008**, *89*, 3097-3101, doi:10.1099/vir.0.2008/004739-0.
241. Nolen, B.J.; Tomasevic, N.; Russell, A.; Pierce, D.W.; Jia, Z.; McCormick, C.D.; Hartman, J.; Sakowicz, R.; Pollard, T.D. Characterization of two classes of small molecule inhibitors of Arp2/3 complex. *Nature* **2009**, *460*, 1031-1034, doi:10.1038/nature08231.
242. Isogai, T.; van der Kammen, R.; Innocenti, M. SMIFH2 has effects on Formins and p53 that perturb the cell cytoskeleton. *Sci Rep* **2015**, *5*, 9802, doi:10.1038/srep09802.
243. Yang, Q.; Zhang, X.F.; Pollard, T.D.; Forscher, P. Arp2/3 complex-dependent actin networks constrain myosin II function in driving retrograde actin flow. *J Cell Biol* **2012**, *197*, 939-956, doi:10.1083/jcb.201111052.
244. Bovellan, M.; Romeo, Y.; Biro, M.; Boden, A.; Chugh, P.; Yonis, A.; Vaghela, M.; Fritzsche, M.; Moulding, D.; Thorogate, R., et al. Cellular control of cortical actin nucleation. *Curr Biol* **2014**, *24*, 1628-1635, doi:10.1016/j.cub.2014.05.069.
245. Köster, D.V.; Mayor, S. Cortical actin and the plasma membrane: inextricably intertwined. *Curr Opin Cell Biol* **2016**, *38*, 81-89, doi:10.1016/j.ceb.2016.02.021.
246. Fujiwara, T.K.; Iwasawa, K.; Kalay, Z.; Tsunoyama, T.A.; Watanabe, Y.; Umemura, Y.M.; Murakoshi, H.; Suzuki, K.G.; Nemoto, Y.L.; Morone, N., et al. Confined diffusion of transmembrane proteins and lipids induced by the same actin meshwork lining the plasma membrane. *Mol Biol Cell* **2016**, *27*, 1101-1119, doi:10.1091/mbc.E15-04-0186.
247. Hiramoto-Yamaki, N.; Tanaka, K.A.; Suzuki, K.G.; Hirosawa, K.M.; Miyahara, M.S.; Kalay, Z.; Tanaka, K.; Kasai, R.S.; Kusumi, A.; Fujiwara, T.K. Ultrafast diffusion of a fluorescent cholesterol analog in compartmentalized plasma membranes. *Traffic* **2014**, *15*, 583-612, doi:10.1111/tra.12163.
248. Suzuki, K.; Ritchie, K.; Kajikawa, E.; Fujiwara, T.; Kusumi, A. Rapid hop diffusion of a G-protein-coupled receptor in the plasma membrane as revealed by single-molecule techniques. *Biophys J* **2005**, *88*, 3659-3680, doi:10.1529/biophysj.104.048538.

249. Rodgers, B.; Mims, C.A. Interaction of influenza virus with mouse macrophages. *Infect Immun* **1981**, *31*, 751-757.
250. Nicholls, J.M.; Chan, M.C.; Chan, W.Y.; Wong, H.K.; Cheung, C.Y.; Kwong, D.L.; Wong, M.P.; Chui, W.H.; Poon, L.L.; Tsao, S.W., et al. Tropism of avian influenza A (H5N1) in the upper and lower respiratory tract. *Nat Med* **2007**, *13*, 147-149, doi:10.1038/nm1529.
251. Landsman, L.; Jung, S. Lung macrophages serve as obligatory intermediate between blood monocytes and alveolar macrophages. *J Immunol* **2007**, *179*, 3488-3494.
252. Misharin, A.V.; Morales-Nebreda, L.; Reyfman, P.A.; Cuda, C.M.; Walter, J.M.; McQuattie-Pimentel, A.C.; Chen, C.I.; Anekalla, K.R.; Joshi, N.; Williams, K.J.N., et al. Monocyte-derived alveolar macrophages drive lung fibrosis and persist in the lung over the life span. *J Exp Med* **2017**, *214*, 2387-2404, doi:10.1084/jem.20162152.
253. Simons, K.; Sampaio, J.L. Membrane organization and lipid rafts. *Cold Spring Harb Perspect Biol* **2011**, *3*, a004697, doi:10.1101/cshperspect.a004697.
254. Sezgin, E.; Levental, I.; Mayor, S.; Eggeling, C. The mystery of membrane organization: composition, regulation and roles of lipid rafts. *Nat Rev Mol Cell Biol* **2017**, *18*, 361-374, doi:10.1038/nrm.2017.16.
255. Chichili, G.R.; Rodgers, W. Cytoskeleton-membrane interactions in membrane raft structure. *Cell Mol Life Sci* **2009**, *66*, 2319-2328, doi:10.1007/s00018-009-0022-6.
256. Winter, P.W.; Van Orden, A.K.; Roess, D.A.; Barisas, B.G. Actin-dependent clustering of insulin receptors in membrane microdomains. *Biochim Biophys Acta* **2012**, *1818*, 467-473, doi:10.1016/j.bbamem.2011.10.006.
257. Goswami, D.; Gowrishankar, K.; Bilgrami, S.; Ghosh, S.; Raghupathy, R.; Chadda, R.; Vishwakarma, R.; Rao, M.; Mayor, S. Nanoclusters of GPI-anchored proteins are formed by cortical actin-driven activity. *Cell* **2008**, *135*, 1085-1097, doi:10.1016/j.cell.2008.11.032.
258. Lillemeier, B.F.; Pfeiffer, J.R.; Surviladze, Z.; Wilson, B.S.; Davis, M.M. Plasma membrane-associated proteins are clustered into islands attached to the cytoskeleton. *Proc Natl Acad Sci U S A* **2006**, *103*, 18992-18997, doi:10.1073/pnas.0609009103.
259. Fontana, J.; Steven, A.C. At low pH, influenza virus matrix protein M1 undergoes a conformational change prior to dissociating from the membrane. *J Virol* **2013**, *87*, 5621-5628, doi:10.1128/JVI.00276-13.
260. Zhirnov, O.P. Isolation of matrix protein M1 from influenza viruses by acid-dependent extraction with nonionic detergent. *Virology* **1992**, *186*, 324-330.
261. Bruce, E.A.; Abbink, T.E.; Wise, H.M.; Rollason, R.; Galao, R.P.; Banting, G.; Neil, S.J.; Digard, P. Release of filamentous and spherical influenza A virus is not restricted by tetherin. *J Gen Virol* **2012**, *93*, 963-969, doi:10.1099/vir.0.038778-0.
262. Watanabe, R.; Leser, G.P.; Lamb, R.A. Influenza virus is not restricted by tetherin whereas influenza VLP production is restricted by tetherin. *Virology* **2011**, *417*, 50-56, doi:10.1016/j.virol.2011.05.006.
263. Agosto, L.M.; Zhong, P.; Munro, J.; Mothes, W. Highly active antiretroviral therapies are effective against HIV-1 cell-to-cell transmission. *PLoS Pathog* **2014**, *10*, e1003982, doi:10.1371/journal.ppat.1003982.
264. Jolly, C. Cell-to-cell transmission of retroviruses: Innate immunity and interferon-induced restriction factors. *Virology* **2011**, *411*, 251-259, doi:10.1016/j.virol.2010.12.031.

265. Sigal, A.; Kim, J.T.; Balazs, A.B.; Dekel, E.; Mayo, A.; Milo, R.; Baltimore, D. Cell-to-cell spread of HIV permits ongoing replication despite antiretroviral therapy. *Nature* **2011**, *477*, 95-98, doi:10.1038/nature10347.
266. Mori, K.; Haruyama, T.; Nagata, K. Tamiflu-resistant but HA-mediated cell-to-cell transmission through apical membranes of cell-associated influenza viruses. *PLoS One* **2011**, *6*, e28178, doi:10.1371/journal.pone.0028178.
267. Roberts, K.L.; Manicassamy, B.; Lamb, R.A. Influenza A virus uses intercellular connections to spread to neighboring cells. *J Virol* **2015**, *89*, 1537-1549, doi:10.1128/JVI.03306-14.
268. Kumar, A.; Kim, J.H.; Ranjan, P.; Metcalfe, M.G.; Cao, W.; Mishina, M.; Gangappa, S.; Guo, Z.; Boyden, E.S.; Zaki, S., et al. Influenza virus exploits tunneling nanotubes for cell-to-cell spread. *Sci Rep* **2017**, *7*, 40360, doi:10.1038/srep40360.
269. Bennett, A.E.; Narayan, K.; Shi, D.; Hartnell, L.M.; Gousset, K.; He, H.; Lowekamp, B.C.; Yoo, T.S.; Bliss, D.; Freed, E.O., et al. Ion-abrasion scanning electron microscopy reveals surface-connected tubular conduits in HIV-infected macrophages. *PLoS Pathog* **2009**, *5*, e1000591, doi:10.1371/journal.ppat.1000591.
270. Schneider, C.; Nobs, S.P.; Heer, A.K.; Kurrer, M.; Klinke, G.; van Rooijen, N.; Vogel, J.; Kopf, M. Alveolar macrophages are essential for protection from respiratory failure and associated morbidity following influenza virus infection. *PLoS Pathog* **2014**, *10*, e1004053, doi:10.1371/journal.ppat.1004053.
271. Tumpey, T.M.; García-Sastre, A.; Taubenberger, J.K.; Palese, P.; Swayne, D.E.; Pantin-Jackwood, M.J.; Schultz-Cherry, S.; Solórzano, A.; Van Rooijen, N.; Katz, J.M., et al. Pathogenicity of influenza viruses with genes from the 1918 pandemic virus: functional roles of alveolar macrophages and neutrophils in limiting virus replication and mortality in mice. *J Virol* **2005**, *79*, 14933-14944, doi:10.1128/JVI.79.23.14933-14944.2005.
272. Tate, M.D.; Pickett, D.L.; van Rooijen, N.; Brooks, A.G.; Reading, P.C. Critical role of airway macrophages in modulating disease severity during influenza virus infection of mice. *J Virol* **2010**, *84*, 7569-7580, doi:10.1128/JVI.00291-10.
273. Purnama, C.; Ng, S.L.; Tetlak, P.; Setiagani, Y.A.; Kandasamy, M.; Baalasubramanian, S.; Karjalainen, K.; Ruedl, C. Transient ablation of alveolar macrophages leads to massive pathology of influenza infection without affecting cellular adaptive immunity. *Eur J Immunol* **2014**, *44*, 2003-2012, doi:10.1002/eji.201344359.
274. Kopf, M.; Schneider, C.; Nobs, S.P. The development and function of lung-resident macrophages and dendritic cells. *Nat Immunol* **2015**, *16*, 36-44, doi:10.1038/ni.3052.
275. Morales-Nebreda, L.; Misharin, A.V.; Perlman, H.; Budinger, G.R. The heterogeneity of lung macrophages in the susceptibility to disease. *Eur Respir Rev* **2015**, *24*, 505-509, doi:10.1183/16000617.0031-2015.
276. Ettensohn, D.B.; Frampton, M.W.; Nichols, J.E.; Roberts, N.J. Human Alveolar Macrophages May Not Be Susceptible to Direct Infection by a Human Influenza Virus. *J Infect Dis* **2016**, *214*, 1658-1665, doi:10.1093/infdis/jiw413.
277. Pulendran, B.; Maddur, M.S. Innate immune sensing and response to influenza. *Curr Top Microbiol Immunol* **2015**, *386*, 23-71, doi:10.1007/82_2014_405.
278. Pang, I.K.; Iwasaki, A. Inflammasomes as mediators of immunity against influenza virus. *Trends Immunol* **2011**, *32*, 34-41, doi:10.1016/j.it.2010.11.004.

279. Kato, H.; Takeuchi, O.; Sato, S.; Yoneyama, M.; Yamamoto, M.; Matsui, K.; Uematsu, S.; Jung, A.; Kawai, T.; Ishii, K.J., et al. Differential roles of MDA5 and RIG-I helicases in the recognition of RNA viruses. *Nature* **2006**, *441*, 101-105, doi:10.1038/nature04734.
280. Pichlmair, A.; Schulz, O.; Tan, C.P.; Näslund, T.I.; Liljeström, P.; Weber, F.; Reis e Sousa, C. RIG-I-mediated antiviral responses to single-stranded RNA bearing 5'-phosphates. *Science* **2006**, *314*, 997-1001, doi:10.1126/science.1132998.
281. Rehwinkel, J.; Tan, C.P.; Goubau, D.; Schulz, O.; Pichlmair, A.; Bier, K.; Robb, N.; Vreede, F.; Barclay, W.; Fodor, E., et al. RIG-I detects viral genomic RNA during negative-strand RNA virus infection. *Cell* **2010**, *140*, 397-408, doi:10.1016/j.cell.2010.01.020.
282. Baum, A.; Sachidanandam, R.; García-Sastre, A. Preference of RIG-I for short viral RNA molecules in infected cells revealed by next-generation sequencing. *Proc Natl Acad Sci U S A* **2010**, *107*, 16303-16308, doi:10.1073/pnas.1005077107.
283. Te Velthuis, A.J.W.; Long, J.C.; Bauer, D.L.V.; Fan, R.L.Y.; Yen, H.L.; Sharps, J.; Siegers, J.Y.; Killip, M.J.; French, H.; Oliva-Martín, M.J., et al. Mini viral RNAs act as innate immune agonists during influenza virus infection. *Nat Microbiol* **2018**, *3*, 1234-1242, doi:10.1038/s41564-018-0240-5.
284. Vasilijevic, J.; Zamarreño, N.; Oliveros, J.C.; Rodriguez-Frandsen, A.; Gómez, G.; Rodriguez, G.; Pérez-Ruiz, M.; Rey, S.; Barba, I.; Pozo, F., et al. Reduced accumulation of defective viral genomes contributes to severe outcome in influenza virus infected patients. *PLoS Pathog* **2017**, *13*, e1006650, doi:10.1371/journal.ppat.1006650.
285. Vale-Costa, S.; Amorim, M.J. Clustering of Rab11 vesicles in influenza A virus infected cells creates hotspots containing the 8 viral ribonucleoproteins. *Small GTPases* **2016**, 1-7, doi:10.1080/21541248.2016.1199190.
286. Genoyer, E.; López, C.B. Defective viral genomes alter how Sendai virus interacts with cellular trafficking machinery leading to heterogeneity in the production of viral particles among infected cells. *J Virol* **2018**, doi:10.1128/JVI.01579-18.
287. Zebedee, S.L.; Lamb, R.A. Growth restriction of influenza A virus by M2 protein antibody is genetically linked to the M1 protein. *Proc Natl Acad Sci U S A* **1989**, *86*, 1061-1065.
288. Hirao, M.; Sato, N.; Kondo, T.; Yonemura, S.; Monden, M.; Sasaki, T.; Takai, Y.; Tsukita, S. Regulation mechanism of ERM (ezrin/radixin/moesin) protein/plasma membrane association: possible involvement of phosphatidylinositol turnover and Rho-dependent signaling pathway. *J Cell Biol* **1996**, *135*, 37-51.
289. Heiska, L.; Alfthan, K.; Grönholm, M.; Vilja, P.; Vaheri, A.; Carpén, O. Association of ezrin with intercellular adhesion molecule-1 and -2 (ICAM-1 and ICAM-2). Regulation by phosphatidylinositol 4, 5-bisphosphate. *J Biol Chem* **1998**, *273*, 21893-21900.
290. Zhang, M.; Bohlson, S.S.; Dy, M.; Tenner, A.J. Modulated interaction of the ERM protein, moesin, with CD93. *Immunology* **2005**, *115*, 63-73, doi:10.1111/j.1365-2567.2005.02120.x.
291. Kaufmann, S.; Käs, J.; Goldmann, W.H.; Sackmann, E.; Isenberg, G. Talin anchors and nucleates actin filaments at lipid membranes. A direct demonstration. *FEBS Lett* **1992**, *314*, 203-205.
292. Martel, V.; Racaud-Sultan, C.; Dupe, S.; Marie, C.; Paulhe, F.; Galmiche, A.; Block, M.R.; Albiges-Rizo, C. Conformation, localization, and integrin binding of talin depend

on its interaction with phosphoinositides. *J Biol Chem* **2001**, *276*, 21217-21227, doi:10.1074/jbc.M102373200.
293. Watson, M.J.; Lee, S.L.; Marklew, A.J.; Gilmore, R.C.; Gentzsch, M.; Sassano, M.F.; Gray, M.A.; Tarran, R. The Cystic Fibrosis Transmembrane Conductance Regulator (CFTR) Uses its C-Terminus to Regulate the A2B Adenosine Receptor. *Sci Rep* **2016**, *6*, 27390, doi:10.1038/srep27390.
294. Delaney, M.K.; Malikov, V.; Chai, Q.; Zhao, G.; Naghavi, M.H. Distinct functions of diaphanous-related formins regulate HIV-1 uncoating and transport. *Proc Natl Acad Sci U S A* **2017**, *114*, E6932-E6941, doi:10.1073/pnas.1700247114.
295. Dotson, D.; Woodruff, E.A.; Villalta, F.; Dong, X. Filamin A Is Involved in HIV-1 Vpu-mediated Evasion of Host Restriction by Modulating Tetherin Expression. *J Biol Chem* **2016**, *291*, 4236-4246, doi:10.1074/jbc.M115.708123.
296. Ménager, M.M. TSPAN7, effector of actin nucleation required for dendritic cell-mediated transfer of HIV-1 to T cells. *Biochem Soc Trans* **2017**, *45*, 703-708, doi:10.1042/BST20160439.
297. Usmani, S.M.; Murooka, T.T.; Deruaz, M.; Koh, W.H.; Sharaf, R.R.; Di Pilato, M.; Power, K.A.; Lopez, P.; Hnatiuk, R.; Vrbanac, V.D., et al. HIV-1 Balances the Fitness Costs and Benefits of Disrupting the Host Cell Actin Cytoskeleton Early after Mucosal Transmission. *Cell Host Microbe* **2019**, *25*, 73-86.e75, doi:10.1016/j.chom.2018.12.008.
298. Banerjee, I.; Miyake, Y.; Nobs, S.P.; Schneider, C.; Horvath, P.; Kopf, M.; Matthias, P.; Helenius, A.; Yamauchi, Y. Influenza A virus uses the aggresome processing machinery for host cell entry. *Science* **2014**, *346*, 473-477, doi:10.1126/science.1257037.
299. De Conto, F.; Fazzi, A.; Razin, S.V.; Arcangeletti, M.C.; Medici, M.C.; Belletti, S.; Chezzi, C.; Calderaro, A. Mammalian Diaphanous-related formin-1 restricts early phases of influenza A/NWS/33 virus (H1N1) infection in LLC-MK2 cells by affecting cytoskeleton dynamics. *Mol Cell Biochem* **2018**, *437*, 185-201, doi:10.1007/s11010-017-3107-9.
300. Delpeut, S.; Sisson, G.; Black, K.M.; Richardson, C.D. Measles Virus Enters Breast and Colon Cancer Cell Lines through a PVRL4-Mediated Macropinocytosis Pathway. *J Virol* **2017**, *91*, doi:10.1128/JVI.02191-16.
301. Dietzel, E.; Kolesnikova, L.; Maisner, A. Actin filaments disruption and stabilization affect measles virus maturation by different mechanisms. *Virol J* **2013**, *10*, 249, doi:10.1186/1743-422X-10-249.
302. Koga, R.; Sugita, Y.; Noda, T.; Yanagi, Y.; Ohno, S. Actin-Modulating Protein Cofilin Is Involved in the Formation of Measles Virus Ribonucleoprotein Complex at the Perinuclear Region. *J Virol* **2015**, *89*, 10524-10531, doi:10.1128/JVI.01819-15.
303. Wakimoto, H.; Shimodo, M.; Satoh, Y.; Kitagawa, Y.; Takeuchi, K.; Gotoh, B.; Itoh, M. F-actin modulates measles virus cell-cell fusion and assembly by altering the interaction between the matrix protein and the cytoplasmic tail of hemagglutinin. *J Virol* **2013**, *87*, 1974-1984, doi:10.1128/JVI.02371-12.
304. Aleksandrowicz, P.; Marzi, A.; Biedenkopf, N.; Beimforde, N.; Becker, S.; Hoenen, T.; Feldmann, H.; Schnittler, H.J. Ebola virus enters host cells by macropinocytosis and clathrin-mediated endocytosis. *J Infect Dis* **2011**, *204 Suppl 3*, S957-967, doi:10.1093/infdis/jir326.
305. Schudt, G.; Dolnik, O.; Kolesnikova, L.; Biedenkopf, N.; Herwig, A.; Becker, S. Transport of Ebolavirus Nucleocapsids Is Dependent on Actin Polymerization: Live-Cell

Imaging Analysis of Ebolavirus-Infected Cells. *J Infect Dis* **2015**, *212 Suppl 2*, S160-166, doi:10.1093/infdis/jiv083.